Vascularization in an orthotopic Pleural Mesothelioma model – Characteristics and targeted treatment

PhD thesis

Ildikó Kolarovszkiné Kovács

Semmelweis University Doctoral School

Károly Rácz Doctoral School of Clinical Medicine Division

Supervisor: Balázs Döme, MD, Ph.D

Official reviewers: Tamás Benkő, MD, Ph.D

Ákos Sávolt, MD, Ph.D

Head of the Complex Examination Committee: György Losonczy, MD, D.Sc

Members of the Complex Examination Committee: Nóra Bittner, MD, Ph.D

Marcell Szász A., MD, Ph.D

Budapest
2024

Table of Contents

List of Abbreviations 4

1. Introduction 7
1.1. Pleural mesothelioma 7
1.1.1. Epidemiology 7
1.1.2. Etiology 7
1.1.3. Asbestos-induced pathogenesis 9
1.1.4. Histopathology and classification 10
1.1.5. Treatment modalities 12
1.2. Tumor-associated angiogenesis 15
1.2.1. Vascular endothelial growth factor (VEGF) family 16
1.2.2. Mechanisms of tumor vascularization 17
1.2.3. Antivascular therapy 19
1.2.4. Angiogenesis in PM 20

2. Objectives 21

3. Methods 22
3.1. Cell lines 22
3.2. Animals 22
3.3. Orthotopic PM model 23
3.4. Immunofluorescence analysis: whole-mount samples 24
3.5. Immunofluorescence analysis: frozen sections 24
3.6. Electron Microscopy 25
3.7. Determination of the tumor cell proliferation index (PI) 25
3.8. ELISA 26
3.9. Spheroid formation 26
3.10. Endothelial sprouting anisotropy analysis 26
3.11. Invasion assays 27
3.12. RNA isolation, reverse transcription and real-time qPCR 28
3.13. Array comparative genomic hybridization (array CGH) 28
3.14. Chemosensitivity assays 29
3.15. Clonogenic assay 29

3.16. *In vitro* proliferation and apoptosis assays 29
3.17. Analysis of *in vitro* migratory activity 30
3.18. Immunohistochemical analysis of xenograft tumors 30
3.19. Magnetic Resonance Imaging (MRI) 30

4. Results 32
4.1. Tumor vascularization in PM 32
4.1.1. Early process of vascularization 32
4.1.2. Mechanisms of tumor-induced vascular plexus formation 33
4.1.3. Differences in the vascularization process of the two examined cell lines .. 36
4.1.4. Nutrition of avascular SCP111 nodules 41
4.1.5. The role of VEGF-A in vascular plexus formation 42
4.1.6. Interaction of PM cells with endothelial sprouting *in vitro* 44
4.1.7. 2D and 3D motility of PM cells *in vitro* 45
4.2. Effects of anti-angiogenic treatment in PM 46
4.2.1. RTK expression profiles and genomic characterization PM cell lines 46
4.2.2. Effects of nintedanib treatment *in vitro* 47
4.2.3. Effects of nintedanib treatment *in vivo* 52

5. Discussion 56

6. Conclusions 65

7. Summary 66

8. References 67

9. Bibliography of the candidate's publications 96
9.1. List of publications that served as a basis for the current thesis 96
9.2. Other publications 97

10. Acknowledgements 99

List of Abbreviations

Array CGH: Array comparative genomic hybridization

ARRIVE: Animal Research: Reporting of *In Vivo* Experiments

BAP1: BRCA1-associated protein 1

BAP1-TPDS: BAP1 tumor predisposition syndrome

BM: Basement membrane

BrdU: 5-bromo-2'-deoxyuridine

CDKN2A: Cyclin-dependent kinase inhibitor 2A

CDX: Cell-derived xenograft

ChT: Chemotherapy

CI: Combination index

CNT: Carbon nanotube

CRC: Colorectal cancer

CRCLM: Colorectal cancer liver metastasis

DMSO: Dimethyl sulfoxide

EC: Endothelial cell

ECM: Extracellular matrix

ELISA: Enzyme-linked immunosorbent assay

EMT: Epithelial-to-mesenchymal transition

EPC: Endothelial progenitor cell

EPD: Extended pleurectomy/decortication

EPP: Extrapleural pneumonectomy

ES: Endothelial sprouting

FBS: Fetal bovine serum

FGFR: Fibroblast growth factor receptor

FITC: Fluorescein isothiocyanate

GEM: Genetically engineered mouse

HGP: Histopathological growth pattern

HIF1: Hypoxia-inducible factor 1

HMGB1: High mobility group box 1

HUVEC: Human umbilical vein endothelial cells

IA: Intussusceptive angiogenesis

IC50: Inhibitory concentration 50

ICI: Immune checkpoint inhibitor

iMig: International Mesothelioma Interest Group

IP: Intraperitoneal

mAB: Monoclonal antibody

MCR: Macroscopic complete resection

mOS: Median overall survival

MPM: Malignant pleural mesothelioma

MRI: Magnetic resonance imaging

MVA: Microvessel area

MVD: Microvessel density

NCCN: National Comprehensive Cancer Network

NF2: Neurofibromatosis type 2

NF-κB: Nuclear factor kappa-light-chain-enhancer of activated B cells

NIH: National Institute of Health

OS: Overall survival

PBS: Phosphate buffered saline

PCR: Polymerase chain reaction

PDGFR: Platelet-derived growth factor receptor

PFS: Progression-free survival

PI: Proliferation index

PI3K: Phosphatidylinositol 3-kinase

PLA: poly-lactic acid

PlGF: Placental growth factor

PM: Pleural mesothelioma

PMA: Phorbol 12-myristate 13-acetate

PO: *Per os*

PS: Performance status

ROS: Reactive oxygen species

RR: Response rate

RTKI: Receptor tyrosine kinase inhibitor

SCID: Severe combined immunodeficiency

SETD2: SET domain containing 2

SMA: Smooth-muscle actin

SRB: Sulforhodamine B

SV-40: Simian virus 40

TAF: Tumor-angiogenesis factor

TNFα: Tumor necrosis factor α

TP53: Tumor protein P53

TSG: Tumor suppressor gene

TUNEL: Terminal deoxynucleotidyl transferase dUTP nick end labeling

VEGF: Vascular endothelial growth factor

VEGFR: Vascular endothelial growth factor receptor

VM: Vasculogenic mimicry

VPF: Vascular permeability factor

WHO: World Health Organization

1. Introduction

1.1. Pleural mesothelioma

1.1.1. Epidemiology

Mesothelioma is a relatively rare malignancy, accounting for less than 1% of all cancer incidence (1). Pleural mesothelioma (PM), or as often referred to, malignant pleural mesothelioma (MPM), is the most common form affecting 80-85% of all patients, followed by peritoneal mesothelioma with 10-15%. The other two localizations (pericardial and testicular) cover less than 5% of all mesothelioma cases (2).

The primary cause of PM is occupational or environmental exposure to asbestos (3). There is a long latency in the development of mesothelioma; 20-40 years can pass from asbestos exposure until the first symptoms appear (4-6).

The incidence of PM varies globally; however, it tends to be higher in industrialized countries with a history of heavy asbestos use. Worldwide the most affected regions are Northern Europe, Australia, and New Zealand. Meanwhile, the most documented cases in Europe are in the UK, Netherlands, Malta, and Belgium (7, 8). Although many countries have issued bans on asbestos usage, approximately 80% of the world's population still lives in countries where asbestos usage is not restricted (9, 10). Due to the continued mining and usage complicated by the long latency period between asbestos exposure and the onset of the disease, global PM incidence is still predicted to rise in the upcoming decades (11).

About three-quarters of the patients are male; this could be attributed to the differences in occupational asbestos exposure (1). However, non-occupational exposure is higher in women (12). Female PM patients have significantly longer survival, which might be linked to the supposed dose-dependent effects of asbestos exposure (13-15). This dose-dependent toxicity was confirmed by *in vitro* testing of mesothelial cell cultures exposed to asbestos fibers (16). At diagnosis, most patients are older than 65 years of age (17), whereas the median age is 73 years (1). Patients diagnosed younger than 40 years have significantly better overall survival (OS) (18).

1.1.2. Etiology

<u>Asbestos exposure</u>

PM is an aggressive malignancy arising from the serosal lining of the chest cavity. The connection between PM and asbestos exposure is well-established (19, 20). Asbestos is a

collective term for six variations of fibrous silicate minerals, which can be sorted into amphibole and serpentine. All six types are considered carcinogenic, although to a varying extent (21). Exposure to the straighter, needle-like, amphibole asbestos (crocidolite, amosite) holds a considerably higher risk of developing PM than serpentine (chrysotile) exposition (22, 23). Because of its excellent tensile strength, heat- and chemoresistance, and electricity-insulating attributes, asbestos was widely used in many industrial and household products, dating back to the Stone Age (24).

Non-asbestos related PM

Besides asbestos, other factors can also contribute to the pathogenesis of PM. Nevertheless, non-asbestos-related PMs are relatively rare (10-30% of all cases) (25). Exposure to mineral fibers that have similar properties to asbestos, like erionite, is suspected to be a risk of PM (26). Moreover, erionite showed more potent effects in rats than asbestos by inducing PM in all animals injected intrapleurally with erionite (27).

Evidence suggests that long and rigid multi-wall carbon nanotubes (CNTs) may cause PM in experimental animal models (28, 29). However, there is currently no evidence indicating that exposure to CNTs poses a risk of PM in humans (30). As CNTs can be biopersistent and share morphological similarities with asbestos, inhaled CNTs might lead to chronic inflammation and tissue damage in the pleura (31). Further studies are necessary to fully understand the potential risks associated with CNTs in PM.

The role of Simian virus 40 (SV-40) is highly controversial in the pathogenesis of PM. In hamsters, intrapleural SV-40 injection resulted in the development of PM in all animals (32). Meanwhile, SV-40-like DNA sequences were found in 60-80% of human PM tissue samples of French, American, and other origins (33-36). Still, in Turkish and Finnish human PM samples, the presence of any SV-40 sequences was not detectable (37, 38). In addition, *in vitro* studies suggest that SV-40 and asbestos are cofactors in the carcinogenesis of PM (16).

Exposure to ionizing radiation is a known carcinogen and risk factor for multiple cancers. Although extremely rare, evidence shows that PM can also develop in individuals who receive radiation therapy for lymphoma (39).

Genetic predisposition

A small percentage of PM is attributed to autosomal dominant germline mutations/deletion of the tumor suppressor gene (TSG) encoding BRCA1-associated

protein–1 (BAP1) (40, 41). The germline BAP-1 mutation is associated with the BAP1 tumor predisposition syndrome (BAP1-TPDS), which leads to the development of various tumoral entities including PM (42). Of note, PM patients carrying germline BAP1 mutations are mostly female (>60%) and are diagnosed at a younger age (43, 44).

1.1.3. Asbestos-induced pathogenesis

The neoplastic transformation of mesothelial cells is a complex process driven by multiple factors (45). The main components of asbestos-induced pathogenesis are summarized in Fig.1. Inhaled asbestos fibers migrate rapidly through the airway epithelium to the surface of the pleura (46). Since these fibers are biopersistent they stay in the pleura for decades thus inducing chronic inflammation that eventually leads to genomic instability and the development of PM (47). Moreover, asbestos fibers cause irritation, repeated tissue damage and impaired repair cycles. This constant irritation also leads to macrophage accumulation in the pleura and lungs (48). Asbestos provokes mesothelial cells to release inflammatory cytokines and growth factors, creating a pro-tumor microenvironment (49). Moreover, recruited macrophages release tumor necrosis factor α (TNFα), which stimulates mesothelial cells to proliferate and protects them from apoptosis by activating the NF-κB pathway (50). In addition, asbestos fibers can directly generate genomic aberrations by causing DNA damage through mechanical interference with chromosomes (47, 51, 52). Reactive oxygen species (ROS), released by macrophages and mesothelial cells, also lead to DNA damage (53). The high mobility group box 1 (HMGB1) release also contributes to the promotion of chronic inflammation through asbestos-induced macrophage and mesothelial cell necrosis (54).

The genetic landscape of PM is characterized by mutations in TSGs and subsequent loss of functions of tumor suppressor proteins (55, 56). The most common mutations affect the p53 DNA repair and PI3K-AKT signaling pathways. The most frequently mutated genes include BAP1 with up to 67%. The mutation of the cell cycle regulator gene, cyclin-dependent kinase inhibitor 2A (CDKN2A), which is also known as p16 is seen in 40-45% of the patients. The apoptosis regulator neurofibromatosis type 2 (NF2), is mutated in 20-50%, the TP53 in 5-8% and the histone methyltransferase encoding gene SETD2 is mutated in approximately 10% of PM patients (57-61). So far, no oncogenic driver mutation has been identified in PM (62).

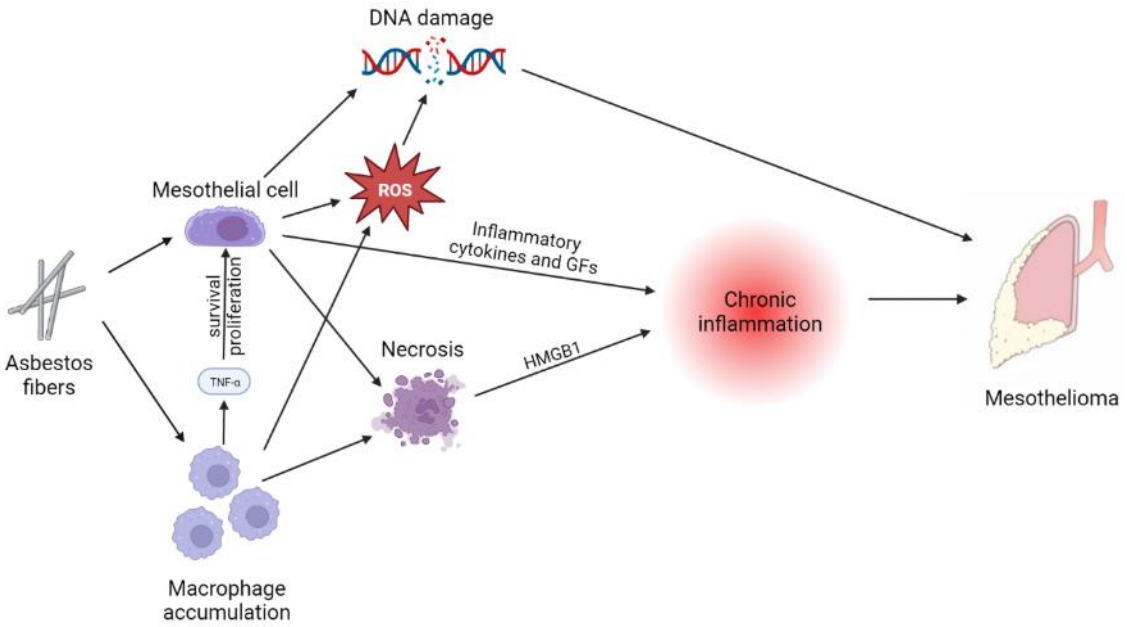

Figure 1. The main components of asbestos-induced PM pathogenesis

ROS: Reactive oxygen species, HMGB1: High mobility group box 1, TNF α: tumor necrosis factor α, GF: growth factors. Created with BioRender.com.

It has been determined that specific genetic changes can affect prognosis; mutated TP53 significantly decreases survival (55), while BAP1 loss is associated with improved outcomes (63). Currently, no biomarker is validated for PM screening or as a single diagnostic test (64).

1.1.4. Histopathology and classification

The mesothelium is the serosal membrane lining of the body cavities. In the thoracic cavity, this is called the pleura, and consists of two single-cell layers: the parietal pleura is attached to the surface of the chest wall, and the visceral pleura covers the lungs. PM can originate from either layer, although it more frequently arises from the parietal layer and then spreads to the visceral pleura (65). The pleura is a common site of metastasis and the differential diagnosis between PM and other cancer metastases is often challenging (66). Despite the improving tendency, approximately 14-50% of PM diagnosis turns out to be incorrect when further validated (67). Accordingly, the guidelines issued by the International Mesothelioma Interest Group (iMig) recommend the evaluation of at least two positive markers to confirm the mesothelial origin and two negative markers to exclude carcinomas. The recommended panel of markers and the frequency of their expressions in PM are summarized in Table 1. (68).

Table 1. Immunohistochemical markers and their frequency of expression (%) in PM for differential diagnosis recommended by iMig (68)			
Positive (mesothelial) markers		**Negative (carcinoid) markers**	
Wilms' tumor 1 (WT1)	70-95	Claudin 4 (CLDN4)	0
Cytokeratin 5 (CK5/6)	75-100	Thyroid transcription factor 1 (TTF-1)	0
Podoplanin (D2-40)	90-100	Carcinoembryonic antigen (CEA)	< 5
Calretinin (CALB2)	100	BerEp4	≤ 20
Mesothelin (MSLN)	100	Napsin A (NAPSA)	0
		MOC31	2-10
		BG8 (Lewis^y)	3-7

The WHO updated the classification of diffuse PM in 2021 (69). Three main histological subtypes were defined: epithelioid (50-70%), sarcomatoid (10-20%), and a transitional category, biphasic (10-20%) (70). Epithelioid tumors (Fig.2A) usually comprise of round epithelioid cells with eosinophilic cytoplasm and show low frequency of nuclear atypia and mitosis (68). Meanwhile, sarcomatoid PM (Fig.2C) is morphologically more heterogenous, composed of a haphazardly arranged sheet of elongated spindle-like cells within a fibrous stroma. Tumor cells display a significant range of morphological characteristics, exhibiting both plump and thin cytoplasm and varying degrees of nuclear atypia. Additionally, they may show a wide range of mitotic counts (68). The biphasic PK (Fig.2B) is characterized by both epithelioid and sarcomatoid components, each comprising a minimum of 10% of the tumor area (71).

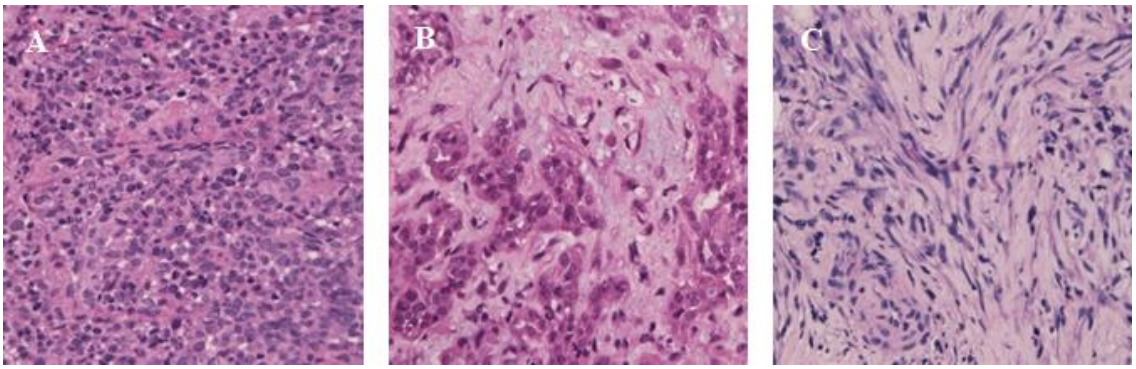

Figure 2. Representative images of the three main histological subtypes of PM
A. Epithelioid, B. Biphasic, C. Sarcomatoid. (Images were kindly provided by Karin Schelch.)

Survival time is greatly affected by tumor histology. Epithelioid tumors have the best prognosis with a median overall survival (mOS) of 14.4 months. For sarcomatoid and biphasic PMs, the mOS is 5.3 and 9.5 months, respectively (72). Non-epithelioid tumors

are considered more aggressive and also chemoresistant (73). Accordingly, the amount of sarcomatoid component in biphasic subtype tumors has a prognostic value; less than 20% or 50% spindle cell element means significantly longer survival (74, 75).

Appropriate histological subtyping of PM is crucial because it is a robust prognostic factor and determines treatment decisions (68). Unfortunately, this histological classification fails to accurately reflect the tumor diversity observed through molecular and clinical perspectives (76). Molecular classification based on large-scale omics and NGS studies raises the possibility of new types of classification (55, 59, 77-79).

1.1.5. Treatment modalities

PM is an aggressive and therapy-resistant cancer with a dismal prognosis (80). Unfortunately, the currently available treatment options are ineffective, and the mOS of unresectable patients remains between 8-14 months (81). Generally, the 5-year survival rate is 12% and the survival outcomes are poor even for stage I patients (16%) (82).

Most patients are diagnosed in an already advanced stage (49.8% of patients get diagnosed at stage IV) (1). The therapeutic options for these patients are limited; the backbone of the treatment is platinum-pemetrexed chemotherapy (ChT). In order to improve the clinical outcomes, first-line ChT is often complemented with the anti-angiogenic agent bevacizumab. Moreover, the role of immunotherapy in the treatment of PM is also increasing since several clinical trials suggests that immunotherapeutic agents might be efficient. Accordingly, the combination of nivolumab and ipilimumab constitutes an alternative option for first-line therapy (83). A recent retrospective study, based on 41,074 PM patients treated between 2004 and 2020 reported that 50.5% of included individuals received ChT, 27.6% underwent surgical resection, and 8.6% were treated with radiotherapy. Notably, only 5.4% of included patients received immunotherapy in the study period on average. Yet, the use of immunotherapy increased significantly between 2004 and 2020 (from 0.6% to 27%) (1).

The combination and sequence of treatment modalities are not standardized, and the role of multimodal therapy is debatable. The MARS randomized trial suggested that extrapleural pneumonectomy (EPP) may not provide any advantages as part of a trimodal therapy and could potentially harm patients (84). On the contrary, another study demonstrated OS improvement in patients who received multimodal therapy, including surgery and ChT (85). Nevertheless, the following factors should be taken into

consideration when designing treatment strategies for PM patients: stage, histology, age, performance status (PS), comorbidities, and the patient's preferences (86).

Surgery

Surgery has a role not only in the treatment but also in the diagnosis and palliative care of PM (86). Curative-intent surgery is controversial in PM since macroscopic complete resection (MCR) is hard to achieve. Therefore, treatment guidelines recommend surgery (as part of multimodal treatment) only for a highly selected group of patients with early-stage disease and non-sarcomatoid histology (87). Although surgery has been demonstrated to improve the 5-year survival for epithelioid patients by 10-15%, patients with non-epithelioid tumors may not benefit from this treatment modality (88-91). To enhance efficacy, surgery is recommended to be complemented by neoadjuvant or adjuvant ChT and, in some cases, radiotherapy (92).

In total, four surgical options are available for PM treatment; two of them have a curative intent (93). Extended pleurectomy/decortication (EPD) refers to the removal of the parietal and visceral pleura and the excision of all visible tumors, whereas EPP is the radical removal of the parietal and visceral pleura, and also parts of the diaphragm, pericardium, and lung (93). Based on a meta-analysis of 2903 patients treated surgically, the lung-sparing EPD showed favorable outcomes and a lower perioperative mortality rate; therefore, it is the preferred surgical approach (94). The other two procedures (pleurectomy/decortication, partial pleurectomy) are applied to improve symptom control and quality of life (95).

Systemic therapy

It is recommended to consider systemic ChT for all PM patients with PS scores of 0-2, as it is widely regarded as the best available treatment option (86). The standard first-line ChT for PM patients is a platinum agent (cisplatin or carboplatin) combined with the antimetabolite pemetrexed (96, 97). PM patients who received a combination of cisplatin and pemetrexed experienced a notable improvement in median survival although the benefit was only 3 months. The mOS for cisplatin monotherapy was 9.3 months and the combinational therapy was able to increased it to 12.1 months. This treatment also resulted in significantly higher response rates (RR) (96). Although the RR for cisplatin-pemetrexed ChT was 41% in this initial trial (96), a subsequent non-randomized study of 1704 patients revealed RRs of only at 26.3% (98). Another trial tested the efficacy of

antifolate raltitrexed in a similar setup and got similar results: raltitrexed improved mOS, progression-free survival (PFS), and RR compared to cisplatin monotherapy (99). For patients unfit to tolerate cisplatin's toxicity, the alternative is carboplatin, which demonstrated comparable RR and mOS (98). Unfortunately, the positive effects of systemic treatment do not last long; within 6 months, many patients experience disease progression (96, 99). Currently, no validated second-line treatment has been established (100).

Immunotherapy

The phase III CheckMate 743 study tested the efficacy of immune checkpoint inhibitors (ICIs) nivolumab and low-dose ipilimumab in treatment-naïve unresectable PM patients. The OS was significantly longer in the immunotherapy group compared to those receiving platinum-pemetrexed ChT, and the 3-year survival was also improved (23% vs. 15% in the ChT group). The benefit was comparable regardless of histotype, but there was no significant benefit in PFS (83). Based on these results, the nivolumab-ipilimumab regime is a newly approved first-line alternative, especially for non-epithelioid patients. Several other ICIs were tested for second- or subsequent-line treatments, with modest activity (101-104). Although therapeutic outcomes have improved, some data indicates that a particular group of patients may experience hyperprogression due to immunotherapy (105).

Targeted therapy

The phase III MAPS trial evaluated the efficacy of the combinational treatment of cisplatin-pemetrexed ChT and the anti-angiogenic agent bevacizumab in unresectable PM patients. A significant benefit in mOS was evident compared to the standard ChT group (16.1 months vs. 18.8 months) (106). Although bevacizumab is currently not included in the standard-of-care ChT, the National Comprehensive Cancer Network (NCCN) guideline recommends the combination of bevacizumab with cisplatin-pemetrexed ChT (92).

In preclinical studies, various anti-angiogenic agents demonstrated effective antineoplastic activity. However, the outcomes of subsequent clinical trials were controversial (106-110). As of now, there has not been any other anti-angiogenic drug that has shown a considerable increase in OS in phase III trials (111). This highlights the importance of further investigations of anti-angiogenic therapies in PM.

The advancements of multi-omics technologies explored many new possible therapeutic targets. Although some showed promising preliminary results, the clinical application of these drugs is yet to be established (112, 113).

Radiotherapy

Radiotherapy is often used after cytoreductive surgery as part of a multimodal therapeutic plan or as palliative care to manage chest pain. Due to its limited effectiveness, it is generally not recommended as a standalone treatment option (114). The diffuse nature of PM and the vicinity of vital organs in the thorax further complicates the application of radiotherapy (86).

1.2. Tumor-associated angiogenesis

The process of new blood vessel formation from the already existing ones is called angiogenesis. It is a physiological process during tissue development and wound healing, but it plays a fundamental role in the malignant transformation that leads to cancer (115). Tumor vascularization is a complex and multifactorial process that has substantial scientific literature. Due to the constraints of this thesis, only topics that closely relate to our findings will be briefly discussed.

Solid tumors rely on the formation of a complex vascular network to sustain their growth and metastatic potential. Moreover, tumor vascularization has an important role in therapy resistance mechanisms (116). Research indicates that solid tumors typically cease development once they reach a size of 2-3 mm and enter a dormant state, but rapid growth will occur once these dormant tumors are placed into a well-vascularized environment (117, 118).

The process of angiogenesis is tightly regulated by the dynamic interplay between pro- and anti-angiogenic factors (119). In tumor angiogenesis, the transcription factor hypoxia-inducible factor 1 (HIF1) is an essential inducer of pro-angiogenic cytokine production. Under hypoxic conditions, the dimerization of HIF1 subunits activates different signaling pathways (VEGF/VEGFR, Notch, PI3K/AKT/mTOR) to propagate angiogenesis through endothelial cell (EC) proliferation, migration, and survival (120, 121).

1.2.1. Vascular endothelial growth factor (VEGF) family

In 1971, Judah Folkman proposed his theory about the essential role of neovascularization in the growth of solid tumors (117). Folkman assumed that diffusion is insufficient for nutrient and oxygen supply for the growing tumors above a certain size. He also hypothesized that tumor cells secret tumor-angiogenesis factor (TAF) to communicate with blood vessels and induce angiogenesis (122). TAF was also referred to as vascular permeability factor (VPF), but later this cytokine was identified as VEGF (123, 124). Nowadays, VEGF is recognized as the most potent, hypoxia-dependent factor of angiogenesis induction (125).

The VEGF family consists of signaling molecules, VEGF-A, VEGF-B, VEGF-C, VEGF-D, and placental growth factor (PlGF), and the receptor tyrosine kinases VEGFR-1, VEGFR-2, and VEGFR-3. VEGF-A can bind to both VEGFR-1 and VEGFR-2 (Fig.3). VEGFR-1 has higher binding but lower kinase activity than VEGFR-2 (126). The VEGFR-1 receptor, exists in membrane-bound and soluble forms, the soluble form is a "trap receptor" (127). The primary role of VEGFR-1 in angiogenesis is the regulation of VEGFR-2 signaling (128). VEGF-B and PlGF can also bind to VEGFR-1 (Fig.3), but their role in angiogenesis regulation is less defined (129). The role of PlGF is controversial; some studies found PlGF to enhance angiogenesis (130), while others proved its anti-angiogenic potentials (131). VEGFR-2 is highly expressed on lymphatic and vascular ECs and also on tumor cells (132, 133). The main regulator of angiogenesis is the VEGF-A/VEGFR-2 axis; it mediates multiple signaling pathways (ERK/PI3K/Akt, FAK, NCK/p38/MAPK) to execute functions leading to sprouting angiogenesis through EC proliferation, migration, and survival (134-138). Additionally, VEGF-A acts as a vasodilator and enhances the permeability of microvessels (139). VEGF-C is also a mediator of angiogenesis through the binding to VEGFR-2, but its main function is the regulation of lymphangiogenesis through the high affinity binding to VEGFR-3 (Fig.3). VEGF-D also binds to VEGFR-3 (Fig.3) and regulates lymphangiogenesis (140).

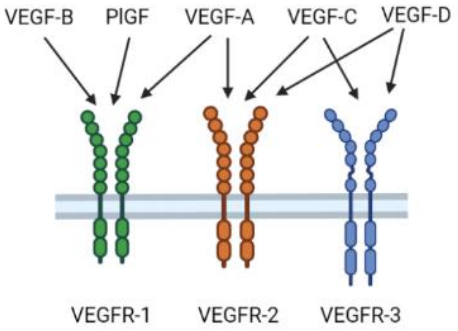

Figure 3. VEGF receptor and ligand binding schemes
Created with BioRender.com.

Research proved that VEGF is produced by both tumor and stromal cells, and its secretion is connected to tumor progression, elevated vessel density, invasiveness, metastasis, and tumor recurrence (141). VEGF receptor mutations and VEGF overexpression is directly linked to enhanced angiogenesis and tumor development (142-144).

1.2.2. Mechanisms of tumor vascularization

Previously, tumor vascularization was thought to be the result of the tumor-induced proliferation of host tissue capillaries by endothelial sprouting (ES). Since several other vascularization mechanisms were identified, these processes often occur concurrently in physiological and pathological angiogenesis (145).

Endothelial sprouting

The main events of ES are tip cell selection by lateral inhibition, sprout extension by EC proliferation and migration towards the VEGF gradient, and lumen formation by connecting the sprout's lumen to the parent vessel (146). Ausprunk and Folkmann described this series of events starting with the postcapillary venule dilation, the loss of cell-cell interactions, and basement membrane (BM) degradation resulting in vessel fenestrations. Then, ECs lose polarity and migrate toward the angiogenic stimuli. After the ECs form a tube and a lumen, new BM is synthesized and stabilized by pericytes (147). This model has been further developed by Paku and Paweletz. They described a model where the polarity of ECs and the BM of the sprouting vessels is maintained except for the tip of the sprout. During the sprouting, BM on the tip is continuously synthesized, and pericytes are recruited (148). This model offers a better explanation for some issues unexplained by the first model, like loss and regain of EC polarity and lumen formation before BM synthesis.

Intussusceptive angiogenesis

A lesser-known form of tumor network formation is called intussusceptive angiogenesis (IA). In this process, the insertion of connective tissue columns called pillars into the vessel lumen splits the vessel into two. IA increases the complexity of the intratumoral capillary network, thus providing additional space for ES. First, an intraluminal endothelial bridge is formed, and BM degradation allows the EC to attach to underlying collagen bundles. Then, the actin cytoskeleton pulls this collagen through the vessel lumen (149). This process does not require EC proliferation; therefore, it is faster than sprouting. Vessels going through IA are better stabilized and more resistant to the effects

of antivascular therapies. Therefore, it is a possibility that tumors can switch from ES to IA to evade the consequences of VEGF inhibition (150-152). VEGF-signaling is implied in the regulation of intussusception, but its exact role in controlling vessel sprouting versus intussusception is still not fully understood (153).

Vessel co-option

Vessel co-option refers to the incorporation of host tissue capillaries without disrupting its structure. This method frequently occurs in tissues with abundant vasculature, like lungs and liver (154). In these tissues, tumor cells invade normal tissue by growing along the existing vessels and hijacking the vasculature. Vascular co-option is emerging as an important factor associated with anti-angiogenic therapy resistance (155, 156). This process is also faster than ES and independent of EC proliferation.

Vasculogenic mimicry

Some aggressive tumors demonstrated the unique ability to form vessel-like structures to build their vascular network. In vasculogenic mimicry (VM), instead of ECs, the cancer cells *de novo* form vessel-like structures. When tumor cells undergo dedifferentiation, they can develop endothelial-like phenotypes and create channels that facilitate the transfer of nutrients and blood (157). Several molecular mechanisms, including the activation of epithelial-to-mesenchymal transition (EMT) pathways contribute to the establishment of VM (158).

It appears that none of the primary angiogenic cytokines including VEGF, takes part in the regulation of the creation of these vessel-like structures (157).

Glomeruloid angiogenesis

These structures consist of tightly associated capillary loops with differing BM thickness, resembling renal glomeruli hence the name. This type of microvascular proliferation is highly associated with glioblastoma multiforme (159). Glomeruloid angiogenesis does not require extensive EC proliferation since it is more like a re-organization of intratumoral capillaries rather than a form of true angiogenesis (160). The process's molecular mechanism remains unclear. Sundberg et al. suggests that VEGF plays a vital role in inducing glomeruloid body formation and maintaining these vessels (161). The vessels are able to supply enough oxygen and nutrients to prevent necrosis in tumors; therefore, it is considered a poor prognostic factor in some types of cancer (162).

Postnatal vasculogenesis

In postnatal vasculogenesis bone marrow-derived endothelial progenitor cells (EPCs) are incorporated into the EC layer of intratumoral vessels as a response to tumor-derived pro-angiogenic factors including VEGF, (163). After incorporation, EPCs differentiate into EC and secrete pro-angiogenic factors to attract additional EPCs to the scene.

1.2.3. Antivascular therapy

The idea of targeting tumor vascularization to impair tumor progression and metastasis was raised along with the establishment of the basic principles of tumor-associated angiogenesis (117). Given the crucial role of tumor vascularization in cancer progression, antivascular therapies have been explored to disrupt oxygen and nutrient supplies to block tumor development and metastasis (160). The majority of antivascular therapies target VEGF or other growth factor-dependent vascularization methods, although it seems to be insufficient to hamper tumor progression effectively. Research found that VEGF inhibition induced apoptosis only in the developing capillaries but not in the already-established vascular networks (164). Moreover, tumors are able to switch to alternative vascularization mechanisms to bypass the effects of the blockade of a single pathway, further reducing the effectiveness of such drugs (145).

Bevacizumab

Bevacizumab (Avastin) is a recombinant humanized monoclonal anti-VEGF antibody (mAB) and is the first-ever approved antivascular drug for treating colorectal cancer (CRC) (165). Today, besides CRC, it is used to treat various types of solid tumors including non-small cell lung cancer, and renal-, ovarian- and cervical cancers. Notably, since 2016 it is also recommended for the treatment of PM in combination with standard ChT (106).

Nintedanib

Nintedanib is an oral small molecule receptor tyrosine kinase inhibitor (RTKI) with activity against the tyrosine kinase receptors VEGFR-1 - 3, PDGFR α, β, and FGFR-1 - 3 (166). Nintedanib has demonstrated preclinical and clinical anticancer potential and has been approved for the second-line treatment of lung adenocarcinoma and idiopathic pulmonary fibrosis (167, 168).

Vessel normalization theory

The abnormal vasculature in tumors contributes to hypoxia, inadequate drug delivery, and increased interstitial pressure, which can hinder the effectiveness of the applied treatments. The vessel normalization theory proposes that restoring the balance of tumor blood vessels can improve drug delivery, reduce metastasis, and enhance the overall efficacy of anticancer therapies (169). Tumors often exhibit a chaotic and disorganized vascular network characterized by tortuous, leaky, and irregularly shaped blood vessels (146). These vessels are functionally compromised leading to poor blood flow, and thus to uneven distribution of oxygen, nutrients and therapeutic agents. The abnormal vasculature also promotes the extravasation of cancer cells into the bloodstream facilitating metastasis. According to this theory, the normalization process helps to restore vessel integrity, improve blood flow, reduce vessel leakiness, and enhance oxygenation within the tumor microenvironment. Moreover, increased immune cell infiltration enables a more robust antitumor immune response (170). Preclinical research demonstrated that propagating vessel normalization could improve cancer therapy by increasing blood flow and oxygenation to tumors, making conventional treatments more effective and reducing the risk of metastasis (171, 172).

1.2.4. Angiogenesis in PM

Evidence suggests that angiogenesis is important in PM development (173). A study found 2-3 folds higher serum levels of VEGF in PM patients compared to other cancer patients and healthy individuals (174). PM patients had higher levels of serum VEGF than individuals with documented asbestos exposure but without PM (175). Moreover, PM patients' tumor tissue samples showed higher microvessel density (MVD) than other cancers, and higher MVD correlates with poor survival (176). Besides VEGF, many other pro-angiogenic factors are known for their role in angiogenesis regulation; platelet-derived growth factor (PDGF) is proven to be a crucial autocrine stimulator and has an importance in the pathogenesis of PM (177, 178). Fibroblast growth factors (FGFs) were also implicated in PM pathogenesis, with their role in stimulating proliferation and migration (179). High FGF-2 expression correlates with increased tumor aggressiveness and poor prognosis (180).

Notably, two prognostic factors are linked to angiogenesis in PM: high circulating VEGF levels and increased MVD are both negative prognosticators (175, 181).

2. Objectives

PM is a rare but fast-growing thoracic malignancy characterized by rapid progression and poor prognosis (182). The vasculature plays an essential role in the advancement of solid tumors and in hypoxia-mediated chemo- and radiotherapy resistance (183). Tumor vasculature can be very diverse in appearance and in formation (184). Besides sprouting angiogenesis, the most well-known way of tumor vascularization, several alternative vascularization methods are known today. One of these mechanisms is called vascular co-option. In this process, the tumors gain vasculature without neo-angiogenesis by incorporating the already existing vascular network of the host tissues (145). Combining antivascular agents with ChT can improve cancer treatment effectiveness. Based on previous research, it has been concluded that angiogenesis is a crucial factor in the biology of PM (173). So far, bevacizumab (anti-VEGF antibody) is the only molecular-targeted therapy available for treatment of PM (86). However, bevacizumab is anticipated to be effective only in tumors expressing high levels of VEGF (107). Effective personalized treatment methods for PM require further exploration of key vascularization mechanisms and the development of novel anti-angiogenic approaches.

Our research aimed to assess the microanatomical steps of PM vascularization by investigating the vascularization processes of orthotopically implanted human PM nodules and their protein- and gene expression backgrounds. We also assessed the *in vitro* characteristics of the PM cells according to their motility, invasion potential, and interaction with ECs in spheroid co-cultures. Moreover, we analyzed the role of secreted VEGF-A in tumor-induced vascular plexus formation. Finally, we studied the antitumor and antivascular effects of two anti-angiogenic drugs (bevacizumab and nintedanib) *in vitro* and in orthotopic human PM xenograft models. We compared the effectiveness of these agents in monotherapies and in combinations with conventional ChT regimes.

All animal experiments were performed following the ARRIVE guidelines and were approved by the Animal Care and Use Committee of Semmelweis University in compliance with National Institute of Health (NIH) guidelines for the care and use of animals.

3. Methods

3.1. Cell lines

In total 20 PM cell lines, one immortalized mesothelial cell line, and three normal mesothelial cell cultures were used in our studies. SPC111, SPC212, and M38K cells were established from human biphasic PMs and kindly provided by Prof. R. Stahel (SPC111 and SPC212, University of Zurich) and by Prof. V.L. Kinnula (M38K, University of Helsinki). The epithelioid cell lines P31 and I2 were kindly provided by Prof. K. Grankvist (P31, University of Umea) and Prof. A. Catania (I2, University of Milano). The VMC and Meso PM cell lines were established at the Medical University of Vienna. The non-malignant mesothelial cell line Met5A (ATCC CRL-9444) was purchased from the American Type Culture Collection. The NP normal mesothelial cell cultures were established from pleura tissue samples of patients operated on for spontaneous pneumothorax. HUVEC primary endothelial cells were purchased from Lonza and maintained in EGM2 medium. PM and mesothelial cells were maintained in RPMI-1640 or DMEM supplemented with 10% Fetal Bovine Serum (FBS) and 1% penicillin-streptomycin solution. All cell lines were maintained at 37°C in a humidified incubator with 5% CO2.

We also studied VEGF-A overexpressing SPC111 (SPC111-RFP-VEGF-A), SPC111-RFP, SPC111-mCherry and P31-mCherry cells. These transgenic cell lines were generated by infection with replication incompetent pseudotyped retroviruses and subsequent antibiotic selection. For that, the open reading frames of mCherry, RFP or VEGFA121 were subcloned into the retroviral expression plasmids pQCXIP or pQCXIN from Clontech. The retroviral expression plasmids were then co-transfected into HEK293 cells with the helper plasmids pVSV-G and p-gag-pol-gpt to generate viral particles. Viral particles were harvested after 72 hours and used for infection of target cells without enrichment. PM cells stably expressing the transgenes from the pQCXIP or pQCXIN constructs were selected by treatment with puromycin (0.8 μg/ml) or G-418 (500 μg/ml), respectively, for two weeks.

3.2. Animals

For the *in vivo* experiments eight-week-old male SCID mice were used. All animal experiments were carried out in accordance with the ARRIVE guidelines (185) and with the animal welfare regulations of the host institutes.

According to the institutional animal welfare guidelines, all mice were maintained on a daily 12-h light/12-h dark cycle and were housed under pathogen-free conditions in microisolator cages with laboratory chow and water ad libitum. Body weights were monitored every other day, and animals demonstrating severe stress or 20% of weight loss were euthanized.

3.3. Orthotopic PM model

Under anesthesia (Ketamine-Xylazine, 80:12 mg/kg,), a midline incision was made on the chest of the mice, muscles on the right side were separated and cells ($2x10^6$ SCP111 cells or $1x10^6$ P31 cells) were injected between the 2^{nd} and 3^{rd} ribs. Before the tumor cell inoculation, the analgesic, butorphanol (0,4 mg/kg) were administered intramuscularly. To study the vascularization of PM nodules, animals were sacrificed at 5, 7, 12, 21, 24, 29, 31 and 35 days after SPC111 cell injection, 4, 42 and 52 days after P31 cell injection and 3, 4 and 7 days after SPC111-RFP-VEGF-A cell injection.

In the next set of experiments, we studied the *in vivo* effects of nintedanib treatment. Once PM nodules reached a macroscopically visible size (28 days after tumor implantation), mice (n=9/group) were randomized into treatment and control groups. For the survival experiments, animals with human P31 PM growing in the thoracic cavity received 1. nintedanib per os (PO, 50 mg/kg), 2. nintedanib intraperitoneally (IP, 50 mg/kg), 3. solvent PO or 4. solvent IP. Animals were weighed three times a week and euthanized when they showed significant morbidity. Nintedanib was dissolved either in methylcellulose (PO treatment) or in DMSO (IP treatment).

For the tumor growth experiment, P31 or SPC111 tumor-bearing animals were randomized into the following groups (n=9/group): 1. solvent IP, 2. cisplatin (3 mg/kg, dissolved in 0.9% NaCl IP) and pemetrexed IP (30 mg/kg, dissolved in 0.9% NaCl), 3. nintedanib IP (50 mg/kg, dissolved in DMSO), 4. bevacizumab IP (10 mg/kg), 5. cisplatin and pemetrexed in combination with nintedanib IP, 6. cisplatin and pemetrexed in combination with bevacizumab IP.

The treatments started 21 and 12 days after P31 and SPC111 tumor cell inoculation, respectively. In both sets of experiments, cisplatin was applied once weekly, pemetrexed and nintedanib were administered five times a week on consecutive days, while bevacizumab was injected twice weekly. Body weight was checked thrice a week. The experiments were terminated on the 28th day (P31 tumors) and 16th day (SPC111 tumors)

of treatments due to signs of distress in the control groups. Two hours before the mice were sacrificed, 500 mg/kg 5-bromo-2'-deoxyuridine (BrdU) in 0.9% NaCl was injected IP. Tumor nodules were harvested, weighed, and frozen in liquid nitrogen.

For comparing two groups, Mann-Whitney U tests were applied. One-way ANOVA with Tukey's multiple comparison test was used for the comparison of more than two groups. The correlations between different parameters were calculated by Spearman correlation test. Kaplan-Meier curves for animals' survival were evaluated and the log-rank test was used to establish the significance of the difference. All statistical analysis was performed by using GraphPad Prism 5.0 software. P values are given as two-sided and were considered statistically significant below 0.05.

3.4. Immunofluorescence analysis: whole-mount samples

After euthanizing the mice diaphragms were fixed by injecting 2% paraformaldehyde (4 ºC) into the abdomen (2 ml) and into the thorax (1 ml). After 15 minutes, the diaphragm was removed and washed in phosphate buffered saline (PBS). The sample was permeabilized with 1.25% Triton-X 100 (15 min, RT). After washing, samples were incubated overnight with CD31 antibody. After 8 hours of washing in PBS, samples were incubated overnight with the appropriate secondary antibody. After another 8-hour washing, samples were put onto slides, covered (Fluorescence mounting medium), and analyzed by confocal laser scanning microscopy using the Bio-Rad MRC-1024 system.

3.5. Immunofluorescence analysis: frozen sections

The diaphragm was removed, then tumors were cut out and embedded into cryomatrix as follows: Cryomolds were filled half full with cryomatrix and were frozen in isopentane chilled with liquid nitrogen. Cut-out diaphragms with tumors were put onto a teflon card and were frozen to ensure that the samples remained flat. The frozen samples were put on the top of the frozen cryomatrix and the mold was filled with cryomatrix and quickly frozen. Frozen sections cut perpendicular to the surface of the diaphragm (15 μm) were fixed in methanol (at -20 ºC) for 10 minutes and incubated at room temperature for 1 hour with a mixture of primary antibodies (Table 2.). After washing, sections were incubated for 30 minutes with appropriate secondary antibodies. Samples were analyzed by confocal laser scanning microscopy using the Bio-Rad MRC-1024 system.

Table 2. Antibodies and fluorescent dyes used for immunofluorescence		
Antibody	**Species**	**Dilution**
CD31	Rat monoclonal	1:50
Laminin	Rabbit polyclonal	1:200
PanCK	Rabbit polyclonal	1:100
BrdU	Mouse monoclonal	1:50
SMA	Mouse monoclonal	1:200
Fibronectin	Rabbit polyclonal	1:200
Human Collagen type I	Rabbit polyclonal	1:50
Collagen type I	Rabbit polyclonal	1:50
Lyve-1	Rabbit polyclonal	1:200
Alexa Fluor 488	Donkey-anti-rat	1:400
Alexa Fluor 488	Donkey-anti-mouse	1:400
Alexa Fluor 555	Donkey-anti-mouse	1:400
Alexa Fluor 555	Donkey-anti-rabbit	1:400
DAPI (100µg/ml)		1:50
TOTO-3 (1 mM)		1:500

3.6. Electron Microscopy

Tumor-bearing animals were anesthetized as mentioned above and perfused via the left ventricle with PBS for 10 minutes and with a mixture of 4% paraformaldehyde and 1% glutaraldehyde in PBS for 15 minutes at room temperature. Diaphragms with tumors were removed, cut into 1-2 mm pieces, and immersed in the same fixative for an additional 2 hours. Pieces were post-fixed in 1% OsO4 and 0.5% K-ferrocyanide in PBS for 2 hours, dehydrated in a graded series of acetone and embedded in Spurr's mixture. Samples were analyzed on semithin sections stained by 0.5% toluidine blue (pH 8.5). Ultrathin sections, cut by an RMC MT-7 ultramicrotome, were contrasted with uranyl-acetate and lead citrate and analyzed using a Philips CM10 electron microscope.

3.7. Determination of the tumor cell proliferation index (PI)

Animals received 200 mg/kg BrdU 1 hour prior to termination. Immunolabeled (PanCK, BrdU, DAPI) and scanned (Pannoramic Scanner) frozen sections of SPC111 tumor colonies were divided into four quarters according to the supply of the nutrients (Q1: area of the tumor facing the lung, Q2: area of the tumor facing the diaphragm, Q3, Q4: area of the tumor facing the vascular proliferations located at the two sides of the sectioned tumor colonies. Proliferating (BrdU labeled) and all tumor cells (DAPI) were counted (Pannoramic Viewer software). The PI was defined according to the next formula: PI (%)

= (number of proliferating cells/number of all cells) x 100. The presence of vascular proliferations and lack of intratumoral vessels was monitored by appropriate serial sections (CD31, laminin) from at least 4 different depths of the tumor nodules. Samples containing intratumoral vessels were omitted. The average size of the examined tumors was 1034±255 x 355±77 μm.

3.8. ELISA

PM cells were seeded in the appropriate culture medium. On the next day, the medium was replaced with serum-free medium and cells were incubated for 24 hours. Adherent cells were lysed in RIPA buffer and protein concentration was determined using the Pierce BCA kit. VEGF-A was measured in the supernatant by ELISA (DVE00) and secretion was calculated as pg VEGF-A/ml.

3.9. Spheroid formation

For endothelial sprout growth assay, HUVEC, P31 and SPC111 spheroid aggregates were created by seeding cells in aggregation chambers that do not support cell adherence. The chambers were then incubated in EGM-2 medium for 1 day allowing cells to self-organize into spheroid aggregates. These aggregates were collected and embedded in 3 mg/ml fibrin gel prepared as described earlier (186). Briefly, 3 mg/ml human fibrinogen was combined with 200 U/ml aprotinin, 2 U/ml human thrombin, 2.5 mM CaCl2 and 2 U/ml human factor XIII, then HUVEC and P31 or SPC111 aggregates were added and the solution was transferred and allowed to gelate in circular wells. These 6 mm diameter circular open wells of 50 μl volume were created by filament-deposition ("3D") printing (Ultimaker V2) of poly-lactic acid (PLA) well walls in 35-mm tissue culture dishes using a customized technique described recently (187). Fibrin gels containing the two types of spheroid aggregates were covered with 3 ml EGM-2 medium supplemented with 40 ng/ml bFGF, 40 ng/ml VEGF, 80 nM PMA, and 50 μg/ml ascorbic acid as described earlier (188) and they were kept at 37 ºC in a humidified incubator with 5% CO2 atmosphere. Spheroid size ranged between 300 and 400 μms in diameter.

3.10. Endothelial sprouting anisotropy analysis

Anisotropy of the sprout arbor growing from endothelial (HUVEC) aggregates in contact with PM spheroids in fibrin gel co-cultures was measured on the basis of sprout morphology and by using a modified Sholl analysis (189) developed earlier (190). The

algorithm's source code is shared at https://github.com/gulyasmarton/SproutAnalysis/. Brightfield z-stack images with z-steps of 20 μm were collected from the sprouting cell aggregates fixed with 4% paraformaldehyde and stained with toluidine-blue. The ImageJ software was used to segment the images for individual sprout identification. Based on the binarized 2D images and the optical system's depth-of-field parameter (10 microns), we generated voxels and created a 3D reconstruction of the entire volume of the sprout arbor.

Next, we inserted concentric cylinders separated with a radial distance of 20 μm into the reconstructed volume and identified areas where sprout segments traversed the cylinder surfaces. We applied the ImageJ particle detection algorithm (191) to identify individual sprouts. We used these identified sprout segments to create vectors pointing from the center to a given cylinder. Vectors were then normalized into the unit range and averaged to yield the anisotropy value for each sprout arbor. Thus, the value 0 corresponds to a fully isotropic arbor morphology while 1 corresponds to a fully anisotropic arbor where all sprouts extend in the same direction. The sprout anisotropy measure was calculated for several sprout arbors and the pooled data were subjected to statistical analysis.

Four radii of invaded area around of each aggregate were measured using ImageJ. Average values were determined, then each average radius was normalized by the average radius of original aggregates (R/R0). At least 7 aggregates were measured and averaged for each substrate and each cell line. Statistical analyses were performed using Student's unpaired t-test.

3.11. Invasion assays

Spheroids of SPC111 or P31 cells were transferred onto TC plastic or fibronectin-coated (5 μg/ml) surfaces. Other spheroids were embedded in collagen type I gels (1.7 mg/ml) and were prepared following the manufacturer's instructions. Finally, some aggregates were embedded in combined collagen/fibronectin gels, which was produced by mixing fibronectin (10 μg/ml final concentration), human factor FXIII (2 U/ml) and thrombin (0.2 U/ml) to 1.7 mg/ml collagen type I gel.

Gels were made and kept in 6 mm diameter PLA wells, 3D printed on 35-mm culture dishes (187). First, 30 μl gel solution was poured into the wells and was allowed to form a 0.5 mm thick gel (measured at the center of the well) at 37ºC for 30 minutes. Then to each well, a few spheroids were added within an additional 30 μl of gel solution, which

was layered on the surface of the already solid hydrogel. After gelation at 37ºC, for 30 minutes the 1 mm thick spheroid-containing gel sandwiches were submerged in DMEM medium supplemented 10% FBS. Multi-field phase-contrast mosaic images of the aggregates were taken after seeding and after 48 hours by using a Leica DM IRB inverted microscope equipped with a motorized stage (Marzhauser SCAN-IM), a 10X HC-PLAN objective (NA 0.25, working distance 11.0 mm), and an Olympus DP70 CCD camera.

3.12. RNA isolation, reverse transcription and real-time qPCR

Isolation of total RNA from cell lines was performed using TRIzol Reagent. Contaminating DNA was removed with TURBO DNA-free kit. One μg total RNA per sample was reverse-transcribed with a high-capacity cDNA reverse transcription kit as recommended by the supplier.

Real-time qPCR was performed by the ABI 7500 Fast Real-time PCR system, the following ABI TaqMan assays were used according to the manufacturer's instructions: COL1A1 (Hs00164004_m1), PDGFRA (Hs00183486_m1), PDGFRB (Hs00387364_m1), FGFR1 (Hs00915134_g1), FGFR2 (Hs00256527_m1), FGFR3 (Hs00179829_m1), VEGFR1 (Hs01052961), VEGFR2 (Hs00911700_m1) and VEGFR3 (Hs01047677_m1). GAPDH (Assay ID: Hs02786624_g1) was used as endogenous control. The relative gene expression was calculated using the ΔΔC(T) method described by Livak and Schmittgen (192).

3.13. Array comparative genomic hybridization (array CGH)

Isolation of genomic DNA and array CGH analysis were performed as described previously (193) using 4x44K human whole genome oligonucleotide-based arrays (Agilent). Labeling and hybridization procedures were performed according to the instructions provided by Agilent using the SureTag DNA Labeling Kit. Slides were scanned with a G2505B Micro Array Scanner (Agilent). Feature extraction and data analysis were carried out using the Feature Extraction and Agilent Genomic Workbench software, respectively. Gene dose was categorized into normal, gain, amplification (ampl), loss, and deletion (del). This was done by calculating the mean signal (log2 ratio) of the respective number of oligonucleotides present on the microarry for each gene (2 oligonucleotides for VEGFR2, 3 for PDGFRA, 5 for PDGFRB, 5 for FGFR1, 1 for BAP1, 3 for CDKN2A, 4 for NF2). Borders for gain or loss were set to +0.2 or -0.2, and for

amplification or deletion to +1 or -1. In case of partial gene loss or deletion, mean signals for each part of the gene were calculated.

3.14. Chemosensitivity assays

To determine cell viability, sulforhodamine B (SRB) assay was performed as published (194). PM cells were seeded in 96-well plates 24 hours prior to drug exposure and then treated with different cisplatin and nintedanib concentrations for 72 hours. In order to study drug interactions, combination indices (CI) were calculated according to Chou and Talalay (195) with the CalcuSyn software (Biosoft). CI values <0.9, from 0.9 to 1.1, or >1.1 represented synergism, additive effects or antagonism between nintedanib and cisplatin, respectively.

3.15. Clonogenic assay

Cells were seeded into 6-well plates at densities of $1x10^3$ to $2x10^3$ cells/well 24 hours before treatment. Medium containing fresh drugs was added every 4 days. After 7 and 14 days, cells were washed with PBS, fixed with the mixture of methanol and acetic acid and stained with crystal violet as published (179). Plates were scanned with TissueFaxs. Cell colonies were then destained and clonogenicity was quantified by a plate reader.

3.16. *In vitro* proliferation and apoptosis assays

For the BrdU incorporation assay, cells ($1.5x10^4$ per well) were plated on cover slips in a 24 well plate in cell culture medium containing 10% FBS. After 24 hours, cells were treated with different concentrations of nintedanib. 48 hours later the slides were incubated with 10 μM BrdU for 2 h at 37°C, washed with PBS and fixed with Histofix for 10 minutes. For BrdU staining, cells were permeabilized with Triton X, DNA was denatured with 2N HCl for 15 minutes, blocked with 2% non-fat dry milk for 20 minutes and then incubated with a BrdU antibody (mouse, 1:50 in PBS) for 60 minutes, followed by appropriate secondary antibody and DAPI and finally covered in Prolong Gold Antifade reagent. Images were taken with an LSM 700 laser scanning microscope. The ratio of BrdU and DAPI-positive nuclei were counted in at least 2000 cells in total to determine the percentage of proliferation.

For the TUNEL (terminal deoxynucleotidyl transferase dUTP nick end labeling) assay, cells were plated and treated as described above. After 2 days of incubation with

nintedanib, slides were fixed in Histofix and TUNEL staining was performed using *an in-situ* cell death detection kit according to the manufacturer`s instructions.

3.17. Analysis of *in vitro* migratory activity

2D videomicroscopy measurements were carried out as described previously (196). Briefly, cells were plated on 24-well plates and incubated overnight in cell culture medium supplemented with 10% FBS. For measurements, culture medium was changed to CO_2-independent medium supplemented with 10% FBS. Cells were cultured in a custom designed incubator built around an inverted phase-contrast microscope (World Precision Instruments). Images were taken every 5 minutes from 3 neighboring microscopic fields. Nintedanib was added after 24 hours of observation and cells were followed for an additional 24 hours. The captured pictures were analyzed with a cell-tracking program and the migrated distance was determined as described earlier (196).

3.18. Immunohistochemical analysis of xenograft tumors

Consecutive 10 μm frozen sections were prepared and fixed in methanol (for hematoxylin, CD31 and BrdU staining) or 4.5% Histofix (for cleaved caspase-3 staining). For microvessel labeling, the slides were incubated with rat monoclonal anti-mouse CD31 antibody (dilution 1:50) followed by Alexa 555-conjugated anti-rat IgG. To detect apoptotic cells, sections were incubated with cleaved caspase-3 antibody (dilution 1:400) and anti-rabbit FITC. To determine the proliferation rate of tumor cells, anti-BrdU mAB (dilution 1:50) and FITC-conjugated anti-mouse IgG were applied. Nuclei were stained with DAPI. Slides were scanned by TissueFAXS (TissueGnostics) and ImageJ was used to analyze the images as described recently (197). Relative microvessel areas (MVAs) were calculated by counting the number of CD31-positive pixels in the total tumor area. The percentages for cleaved caspase-3 and BrdU-positive pixels were also determined.

3.19. Magnetic Resonance Imaging (MRI)

For MRI imaging, terminated mice without thoracotomy were placed in a 50 ml falcon tube head first and fixed in 10% formaldehyde. Tubes were inserted in a small volume resonator for MRI on a 9.4 Tesla Scanner (Biospec 94/30). T2- weighted imaging of the mouse thorax was carried out in axial, sagittal and coronal planes with the following sequence parameters: time of echo = 25.58 ms, time of repetition = 1904.86 ms, flip angle = 90°, FOV = 30.720x30.720 mm, number of averages = 9, RARE factor = 8, slice

thickness = 0.6 mm, slice number = 23, matrix size = 256x256 (coronal and sagittal) and 320x320 (axial). The overall examination time was approximately 30 minutes per sample. For assessment of images the in-built software Paravision 6.0 was used.

4. Results

4.1. Tumor vascularization in PM

4.1.1. Early process of vascularization

To better understand the mechanisms of tumor vascularization in PM, human PM cell lines were injected orthotopically into the pleural cavity of immunodeficient mice. Then, intrathoracic tumors were allowed to grow until the animals became moribund. Animals injected with SPC111 cells showed severe distress after 28-35 days, while it took 42-45 days for animals injected with P31 cells to reach this state. At this time, PM nodules, 1-3 mm in size, were observable all over the chest cavity, including the diaphragmatic (Fig.4A) and costal (Fig.4B) surfaces of the parietal pleura. We found that the early process of tumor vascularization is identical in the two orthotopic PM models we examined. Upon macroscopical examination, the two cell lines displayed similar dissemination patterns and morphological characteristics. However, SPC111 nodules reached this state slightly faster, explaining why the mice became moribund more quickly than the ones inoculated with P31 cells.

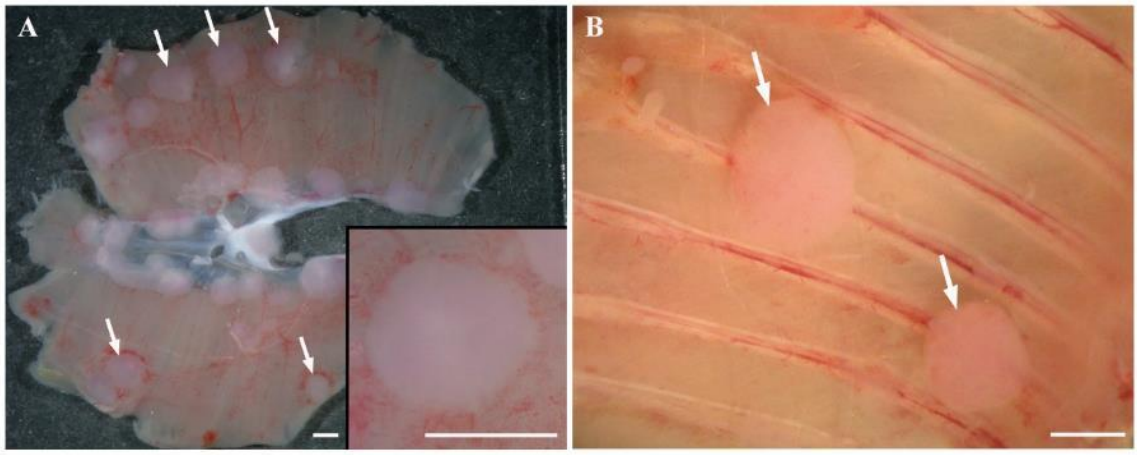

Figure 4. PM nodules on the surfaces of the chest cavity
A. SPC111 nodules scattered on the entire surface of the diaphragm 24 days after injection of tumor cells. Inset shows a single nodule surrounded by a highly vascularized area of abundant dilated vessels. **B.** P31 nodules located on the costal surface of the parietal pleura, 42 days after orthotopic injection. Arrows point at representative nodules. Scale bars: 1 mm

The diaphragms were removed whole, and analyzed by confocal (whole-mount preparation and frozen sections) and electron microscopy. The results showed that both PM cell lines induced dense, tortuous vascular proliferations that bulged into the pleural space and covered large areas of the diaphragm. The vessels of these vascular

proliferations were dilated and arranged irregularly; in contrast, the normal vessels of the diaphragm are narrow and run parallelly (Fig.5A-B). PM nodules stimulated pleural angiogenesis peritumorally and also distant from the tumor site. Regardless of the duration of the experiment, the vascular proliferations were not confined to regions covered by tumors but were found throughout the surface of the diaphragm. This tumor-independent capillary plexus growth on the pleural surface was observed in both groups, and these vascular deposits were homogenous between cell lines.

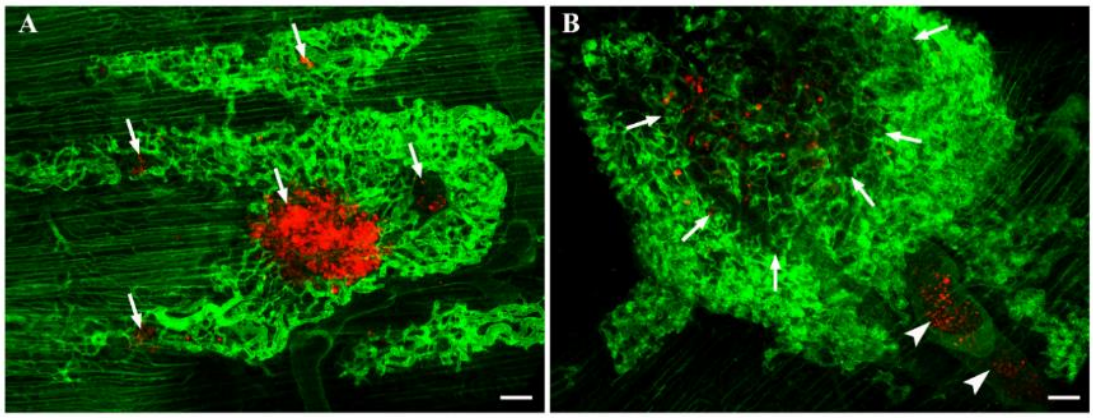

Figure 5. Whole-mount immunostaining of PM nodules on the surface of the diaphragm

A. Vascular proliferations (CD31, green) surround small SPC111 colonies (mCherry, red, arrows) on the surface of the diaphragm, 21 days after tumor cell injection. **B.** Immunostaining of CD31 (green), and P31 tumor cells (mCherry, red), 52 days after tumor cell injection. Arrows point at the periphery of the nodule. The mCherry expression of P31 cells in this colony is low. Vascular proliferations are present around and inside the nodule. Tumor cells are also visible in the efferent lymphatic vessel (arrowheads). Scale bar (A, B): 100 μm

4.1.2. Mechanisms of tumor-induced vascular plexus formation

We thoroughly examined the vascular plexuses to gain a deeper understanding of PM-induced angiogenesis. Our findings suggest that both ES and IA contribute to the formation of PM-induced vascular plexus. The growing capillary plexuses elevated above the original diaphragmatic surface while remained covered by the mesothelium (Fig.6A). We used 3D reconstruction of CD31 stained samples and observed numerous blind endothelial sprouts and intraluminal pillars of different sizes within these capillary plexuses (Fig.6B-C).

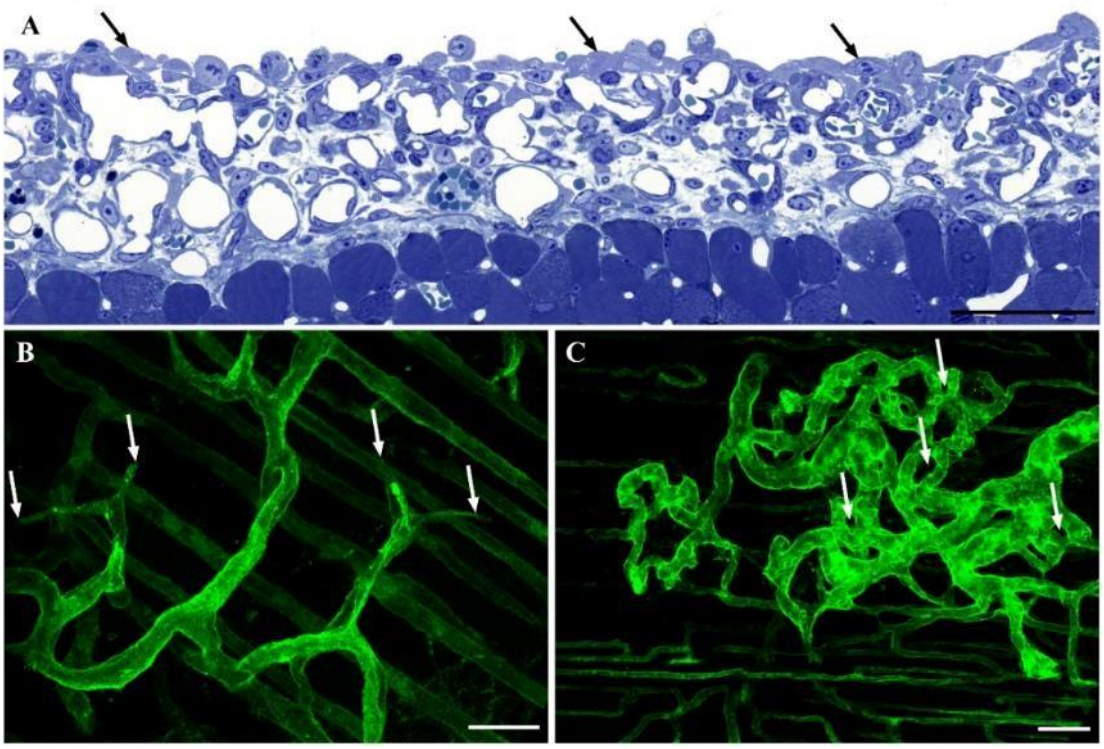

Figure 6. Early-stage capillary plexus proliferations on the surface of the diaphragm

A. Semi-thin cross-section of a capillary plexus elevated above the surface of the diaphragm 35 days after SPC111 tumor cell injection. Arrows point at the mesothelial cover. Scale bar: 50 µm **B.** Horizontal view of a whole mount sample 12 days after SPC111 tumor cell injection. CD31 (green) staining shows numerous endothelial sprouts (arrows) located above the diaphragm's original vasculature. Scale bar: 25 µm **C.** CD31 (green) staining 5 days after SPC111 tumor cell injection. Pillars of different sizes (hallmarks of intussusceptive angiogenesis) appear as black holes (arrows) within the tortuous vascular plexus. Scale bar: 50 µm

The first step and a distinctive feature of IA is the formation of transluminal pillars within the vessel lumens (149). By electron microscopic analysis, close to the original surface of the diaphragm, we found that the pillars contained collagen bundles, which are basal components of these structures (149) (Fig.7A). However, higher above the diaphragmatic surface, these pillars, consisted of fibronectin-rich amorphous extracellular matrix (ECM), instead of the collagen bundles (Fig.7B). Accordingly, at this level, a loose fibronectin-containing matrix is concentrated around the microvessels, embedding capillaries. This provisional matrix showed signs of maturation as collagen fibers appeared around the vessels.

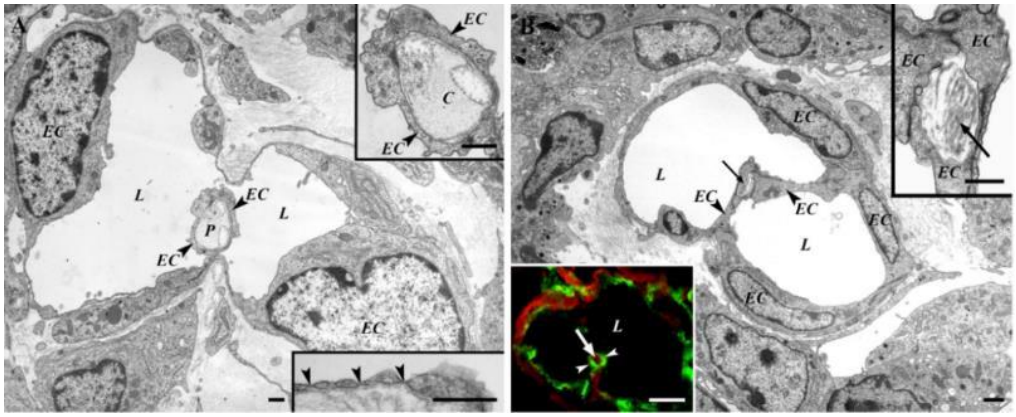

Figure 7. Electron micrographs of tumor-induced vessel proliferations

A. A vessel close to the level of the original surface of the diaphragm. Cross section of a pillar (P) is visible within the vessel lumen (L). Right upper inset: the pillar is composed of a collagen core (C) covered by endothelial cells (EC). Right lower inset: the endothelium of the vessels undergoing intussusceptive angiogenesis contains fenestrations (arrows). Scale bar: 1 μm **B.** A vessel above the original surface of the diaphragm containing a pillar (arrow). Right upper inset: higher magnification endothelial cells (EC) cover amorphous material in the core of the pillar (arrow). Left lower inset: immunohistochemical staining shows that in a capillary lumen (L), fibronectin (red) is located in the core of a pillar (arrow) which is surrounded by CD31 (green) positive endothelial cells (arrowheads). Scale bar: 2 μm (B), 1 μm (right upper inset), 10 μm (left lower inset)

The endothelium of the proliferating capillaries had fenestrations (Fig.7A right lower inset). Alpha-smooth muscle actin (SMA)-positive pericytes surrounded the capillaries of the vascular plexuses. In contrast, pericytes of the capillaries situated deeper in the diaphragm were negative for SMA. In late-stage tumor nodules, SMA-positive myofibroblasts were embedded in fibronectin and collagen type I matrix (Fig.8A-B).

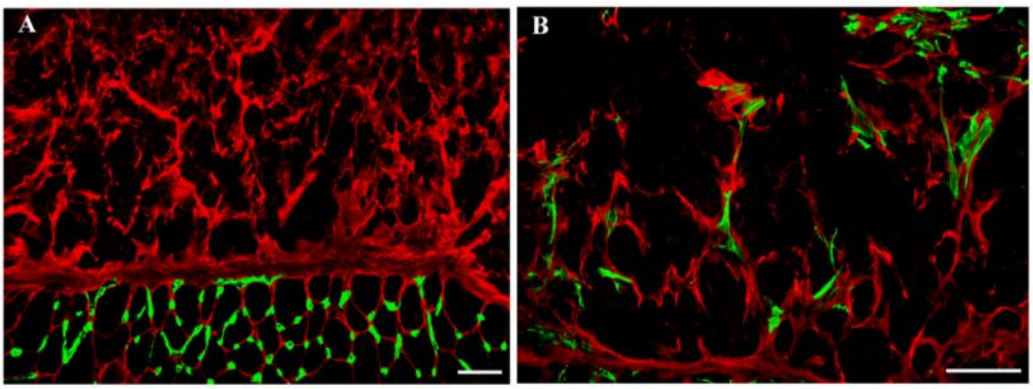

Figure 8. Maturation of capillary plexuses

A. Avascular SPC111 tumor sample on day 21, CD31 (green) and fibronectin (red). The ECM of the tumor contains fibronectin. At the lower part of the micrograph, fibronectin covers the regularly arranged muscle fibers (appear black). Scattered capillaries are visible among the muscle fibers. **B.** Late-stage (35 days) SPC111 sample, SMA (green), and collagen type I (red). The high-power micrograph shows that the SMA-positive myofibroblasts are embedded in collagen type I containing matrix. A-B Scale bar: 50 μm

4.1.3. Differences in the vascularization process of the two examined cell lines

Although the early vascularization of the two cell lines was uniform, we found significant differences in tumor vascularization during later stages. To be able to analyze the relationship between the developing vasculature and the growing tumor nodules from the earliest stage, the tumor cells were labeled by a red fluorescent protein, mCherry. At a very early stage (4-5 days following inoculation), a few tumor cells were located within small vascular proliferations (Fig.9A-B). However, the growing SPC111 colonies pushed away capillary proliferations and remained avascular for up to 2-4 weeks (Fig.9C-D).

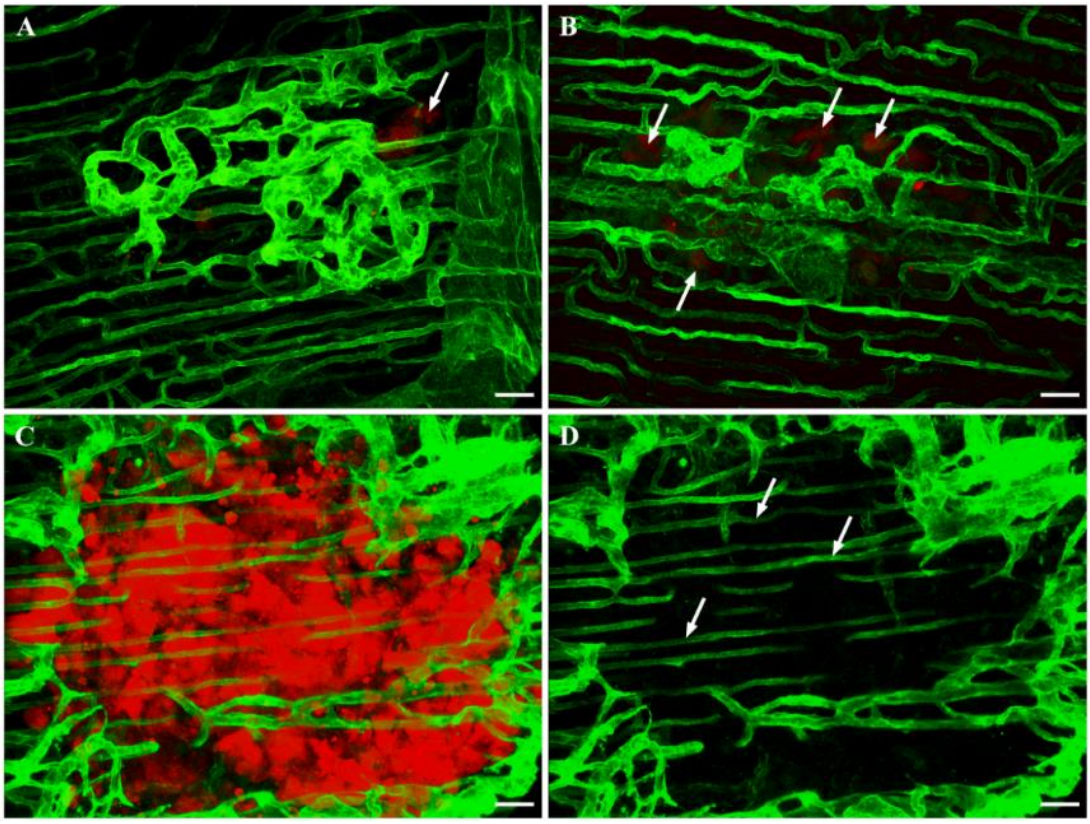

Figure 9. Early vascularization of PM nodules

A. Small vascular proliferation above the original vasculature of the diaphragm. A low number of tumor cells (mCherry, red, arrow) can be observed 5 days after inoculation of SPC111 tumor cells. Whole mount sample stained for CD31 (green). **B.** A low number of P31 tumor cells (mCherry, red, arrows) can be observed within and around the small vascular proliferation 4 days after tumor cell inoculation. Whole mount sample stained for CD31 (green). **C-D.** SPC111 nodule (mCherry, red) 21 days after tumor inoculation on the surface of the diaphragm. Vascular proliferations (CD31, green) were pushed away by the SPC111 colony (red). For clarity, the green (CD31) channel shows that there are no vessels within the SPC111 nodule shown in C. Under the nodule, normally parallelly arranged vessels of the diaphragm are visible (arrows). Scale bars: 25 μm

In SPC111 tumors, microvessels appeared only at a later stage of development, around 5 weeks after inoculation. The first step of SPC111 tumor vascularization is a desmoplastic reaction underneath the tumor nodule. The deposition of desmoplastic connective tissue at the base of the tumor colonies, mainly at the center, preceded SPC111 vascularization. The tumor subsequently invaded this desmoplastic matrix, as malignant cells appeared between the layers of the ECM (Fig.10A). The aforementioned process resulted in the incorporation of an ECM network into the avascular tumors forming connective tissue paths (Fig.10A). This matrix consisted of collagen type I, fibronectin, and myofibroblasts (Fig.10B). Using species-specific antibodies, we were able to establish the mouse origin of this matrix (Fig.10B).

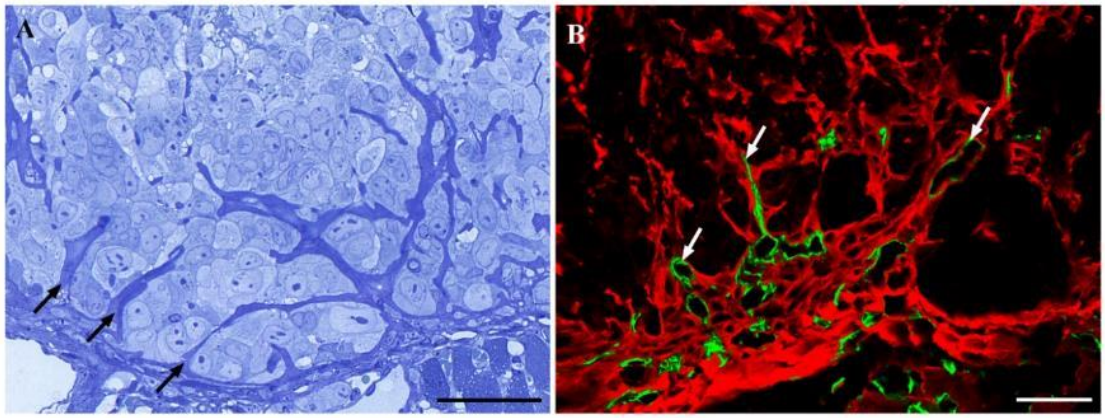

Figure 10. Connective tissue deposition in SPC111 tumor nodules

A. Semi-thin section of an SPC111 tumor shows the separated and elevated layers of the desmoplastic matrix (arrows) at the basal part of the tumor colony as a result of the invasion and growth of the tumor cells. **B.** SPC111 sample on day 29 stained for CD31 (green) and mouse-specific collagen type I (red). The vessels are located at the center of the tumor base and are embedded into collagen type I containing desmoplastic matrix of mouse origin. The vessels follow the connective tissue paths toward the inner part of the nodule (arrowheads). Scale bar: 50 μm

During the process of tumor vascularization, first, small capillaries originating from the vessels of the diaphragm appeared in the desmoplastic connective tissue beneath the colonies (Fig.11A). Subsequently, these vessel proliferations sprouted further into the tumor through the engulfed connective tissue paths (Fig.11B-C) and remained confined to this compartment. (Fig.10B). With the help of 3D reconstruction, we concluded that connective tissue layers form a continuous network and layers become elevated by tumor cells which penetrate between the layers of the matrix.

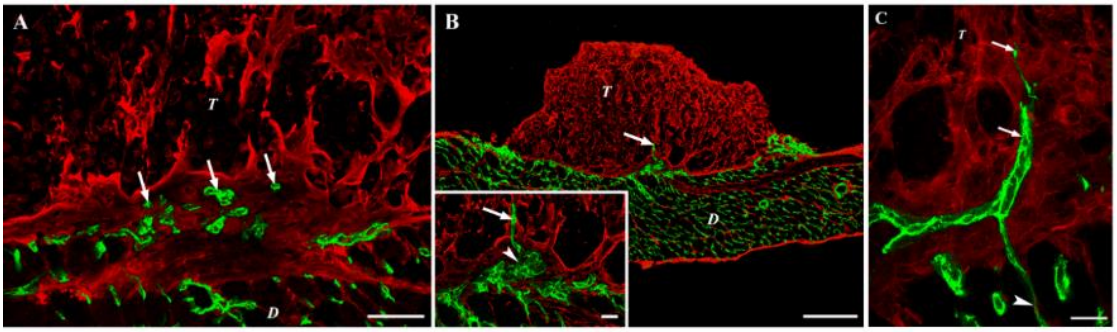

Figure 11. Sprouting angiogenesis in SPC111 nodules

A. The base of an SPC111 tumor nodule on day 29. Vessels are labeled by CD31 (green), the matrix is stained by collagen type I (red). The initial phase of vascularization of the tumor nodule shows the appearance of the vessels (arrows) in a collagen-containing desmoplastic matrix located beneath the tumor nodule. Diaphragm *(D)*, tumor *(T)*. Scale bar: 50 μm **B.** Section of a 29-day-old SPC111 tumor nodule, CD31 (green) and fibronectin (red). Fibronectin highlights the SPC111 tumor nodule *(T)* and the diaphragm *(D)*. One vessel sprouts towards the tumor center from the desmoplastic matrix at the base of the tumor nodule (arrow). Inset: the sprouting vessel (CD31, green, arrow) is continuous with the vessels located in the desmoplastic tissue (arrowhead). Scale bar: 200 μm (B), 25 μm (inset) **C**. The high-power micrograph shows a sprout (CD31, green, arrows) oriented toward the tumor center *(T)*. The sprout is embedded in collagen type I containing connective tissue (red). Note that the sprout is continuous with the vascular network of the diaphragm (arrowhead). Scale bar: 25 μm

In contrast, P31 tumor nodules developed into well-vascularized tumors from an early stage, as the P31 cells continuously invaded and incorporated the network of the proliferating vessels (Fig.12). As for the ECM composition of P31 tumors, we observed large amounts of collagen type I and fibronectin scattered among the tumor cells. Fluorescent staining of frozen sections of late-stage P31 tumors showed high amounts of fibronectin deposited evenly in the nodule and vessels are regularly arranged within the fibronectin matrix trunks.

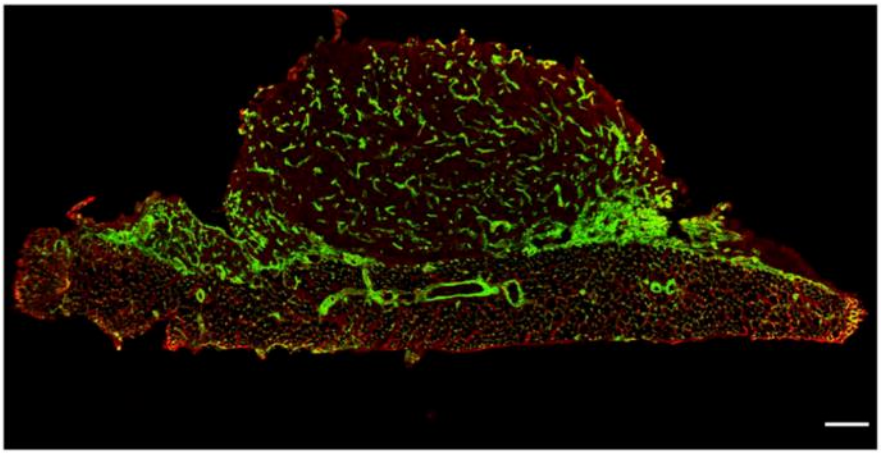

Figure 12. Vascularized late-stage P31 nodule

P31 nodule on day 42 is well-vascularized according to CD31 (green) labeling. Laminin (red) reveals the borders of the diaphragm and the tumor nodule. Scale bar: 200 μm

ECM deposition plays a crucial role during tumor vascularization. With immunofluorescent staining, we found significantly higher collagen type I accumulation in P31 tumors (Fig.13B). Interestingly, our studies using species-specific collagen type I antibodies revealed that in P31 tumors, the majority of collagen type I was of human origin, concentrated in the center of the tumors (Fig.13B). On the other hand, SPC111 tumors were almost entirely negative for human-specific collagen type I staining (Fig.13A). To confirm this finding at the mRNA level, we analyzed the expression of the human COL1A1 gene with real-time PCR in both cell lines. We found that the relative expression levels of the COL1A1 were significantly higher in the P31 compared to SPC111. (Fig. 14).

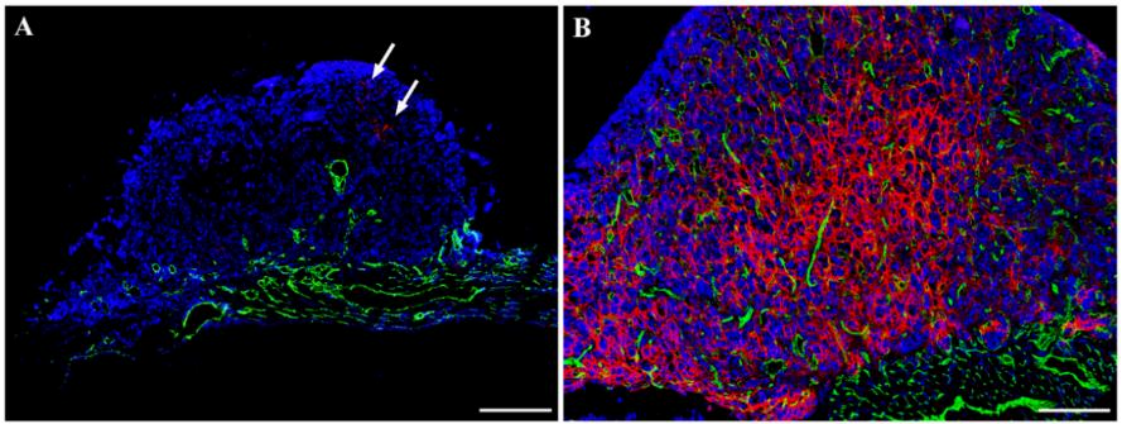

Figure 13. Distribution of collagen type I of human origin in PM nodules

A. Late-stage SPC111 tumor nodule (35 days) stained for CD31 (green), human-specific collagen type I (red) and TOTO-3 (blue). The tumor is mainly negative for human-specific collagen type I (red). Only a small amount of deposited human collagen type I is present (arrows). **B.** P31 tumor nodule (42 days) stained for CD31 (green), human-specific collagen type I (red) and TOTO-3 (blue). The nodule contains a large amount of collagen type I (red) of human origin scattered throughout the tumor. The collagen staining shows higher intensity in the central part of the tumor. Note that the diaphragm is negative for the human-specific collagen. Scale bar (A, B): 200 μm

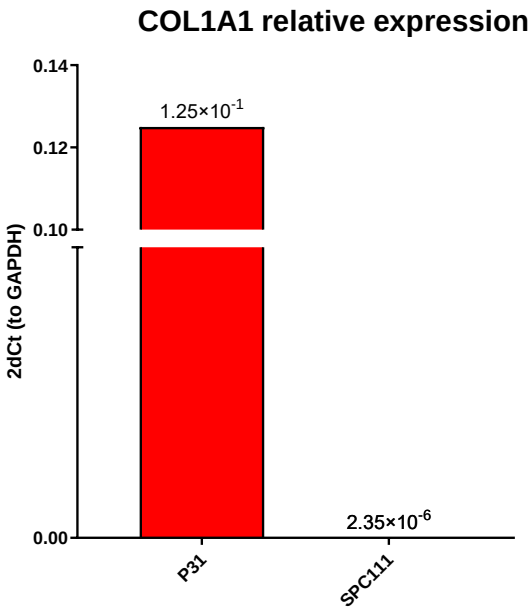

Figure 14. Real-time PCR shows that the relative expression level of COL1A1 is significantly higher in the P31 cell line.

4.1.4. Nutrition of avascular SCP111 nodules

We used BrdU incorporation assay to reveal the role of vascular proliferations in the nutrition of the avascular SPC111 nodules. According to the supply of nutrition, we divided frozen sections of SPC111 tumor colonies into four quarters: Q1: area of the tumor facing the lung, Q2: area of the tumor facing the diaphragm, Q3, Q4: area of the tumor facing the vascular proliferations located at the two sides of the sectioned tumor colonies (Fig.15). Based on the PIs, our analysis showed that the vasculature of the diaphragm provided the highest level of nutrients to the avascular tumors through diffusion (Q2). Below this were the BrdU counts of tumor areas next to the vascular plexuses located at the periphery of the tumor colonies (Q3-Q4). Interestingly, the lowest proliferation rate was detected at the area closest to the lungs (Q1) (Fig.15).

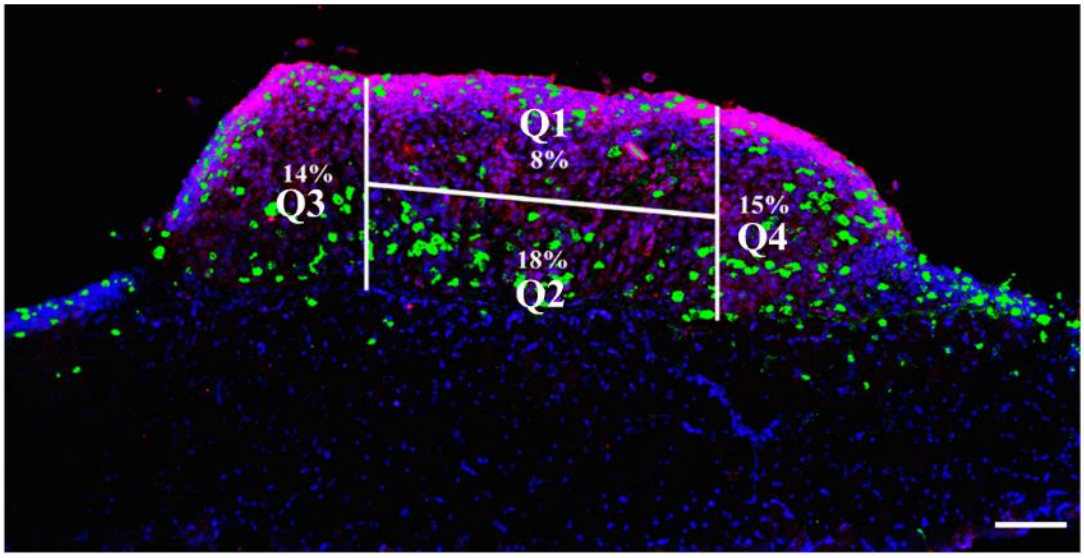

Figure 15. BrdU staining of a frozen section of an SPC111 nodule on day 29.
To determine the proliferation rates of the different regions of the tumors, the nodules were divided into four quarters (Q1-Q4). Samples were stained for BrdU (proliferating cells, green), panCK (tumor cells, red) and TOTO-3 (all cell nuclei, blue). Scale bar: 100 μm

4.1.5. The role of VEGF-A in vascular plexus formation

Our investigation involved studying how VEGF-A expression in PM cells affects vascularization. The baseline VEGF-A expression profiles of our two investigated cell lines differed greatly. P31 cells express a much higher level of VEGF-A than SPC111 cells (Fig.16).

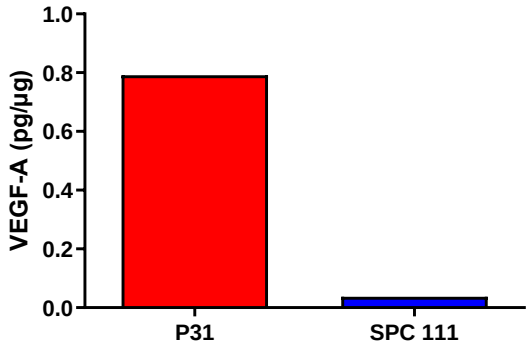

Figure 16. ELISA detection of secreted VEGF-A in conditioned medium from P31 and SPC111 cell cultures

To reveal the role of VEGF-A in PM vascularization, we stably transduced SPC111 cells with retroviral constructs to overexpress VEGF-A. We concluded that VEGF-A is an important promoter of vascular plexus proliferation in PM. As expected, compared to the control SPC111-RFP cells, the transfected SPC111-RFP-VEGF-A cells secreted a significantly higher amount (1.97 pg/ml versus 10750.47 pg/ml, respectively) of VEGF-A (Fig.17A). The increased production of VEGF-A by PM cells resulted in accelerated capillary plexus formation. The process was observable from day 4 after tumor cell injection and increased rapidly by day 7 (Fig.17B-C). This ultimately led to the coverage of the entire surface of the diaphragm by vascular proliferations, leading to the death of the animals by day 7, even without the appearance of macroscopic tumor colonies.

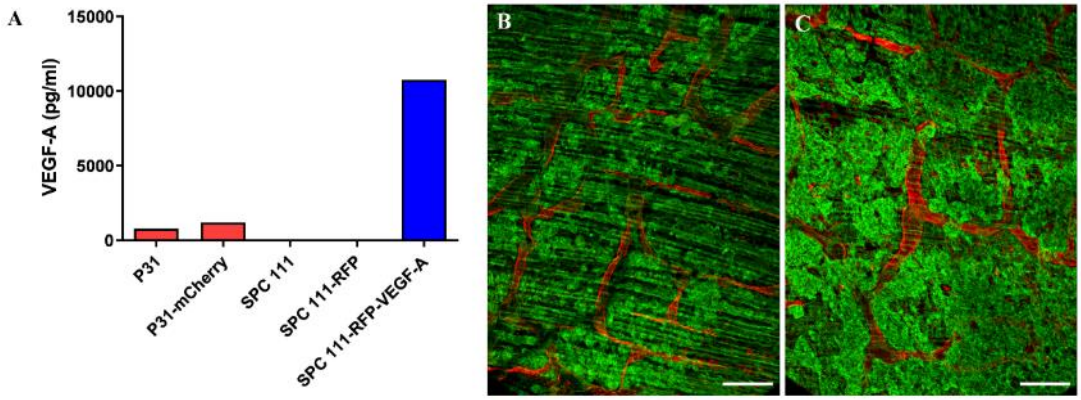

Figure 17. VEGF-A overexpression in the SPC111 cell line

A. VEGF-A ELISA shows that compared with the control SPC111-RFP cells, SPC111-RFP-VEGF-A cells secreted 5.5 x 10^3-fold the amount of this key angiogenic factor. **B**. Whole mount sample 4 days after injection of vascular endothelial growth factor A (VEGF-A) overexpressing SPC111 tumor cells. CD31 (green) labeling shows the appearance of the capillary plexuses throughout the whole surface of the diaphragm. Lymph vessels (Lyve-1, red) show normal morphology. **C.** Whole mount sample 7 days after injection of VEGF-A overexpressing SPC111 tumor cells. CD31 (green) labeling shows a high density of the capillary plexuses above the surface of the diaphragm. Lymph vessels (Lyve-1, red) show normal morphology. Scale bar (B, C): 200 μm

4.1.6. Interaction of PM cells with endothelial sprouting *in vitro*

To investigate the influence of PM cells on the growth of endothelial sprouts *in vitro*, we created a co-culture assay of sprout-forming aggregates of HUVEC cells and spheroids of P31 or SPC111 PM cells. The presence of the two PM cell lines caused significant differences in the spatial structure of multicellular HUVEC sprout arbors in these co-culture assays. To quantify our findings, we calculated anisotropy index values ranging from 0 to 1, where the anisotropy of a symmetric sprout arbor is close to 0, whereas a heavily distorted arbor is characterized by an anisotropy index close to 1. SPC111 spheroids displayed significantly higher endothelial sprout arbor anisotropy compared to P31 spheroids ($p<0.05$, Fig.18A). P31 spheroids allowed HUVEC sprouts to grow with minimal spatial distortion, whereas SPC111 spheroids repealed endothelial sprouts resulting in a highly anisotropic sprout arborization (Fig.18B).

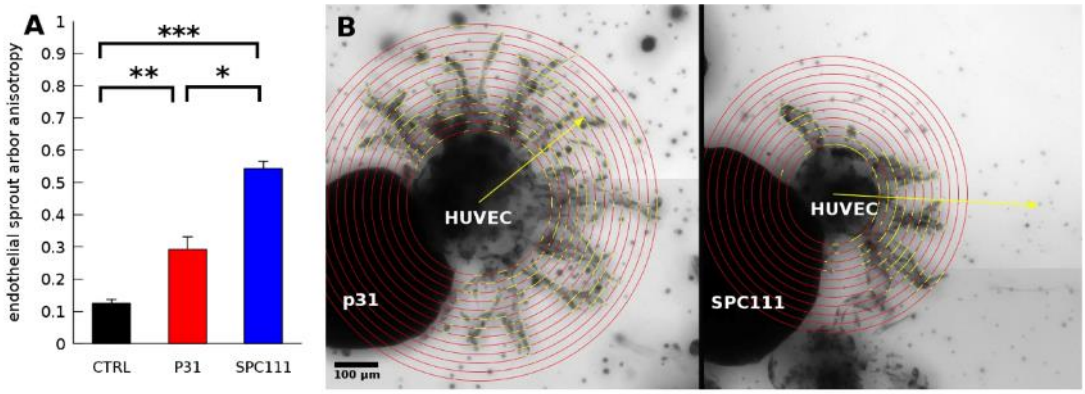

Figure 18. Interaction of PM cells with endothelial sprouting *in vitro*

A. *In vitro* endothelial sprouting morphology is influenced by the presence of PM spheroids. Quantitative sprout arbor anisotropy analysis. Columns are mean anisotropy values (±SEM) of endothelial sprout arbors in the presence of P31 (n=5) or SPC111 (n=3) PM spheroids. * indicate significant difference by Student's t-test ($p^*=1.07\times10^{-5}$, $p^{**}=7.8\times10^{-4}$, $p^{***}= 3.1\times10^{-13}$). **B**. Representative HUVEC aggregates with different sprout arbors developed when co-cultured for 4 days in fibrin gel with P31 (left) or SPC111 (right) PM spheroids. Sprout anisotropy vectors (yellow arrows) indicate the distortion of developing sprout arbors by the proximity of PM cells. Yellow segments of red circles indicate extending sprouts. Scale bar: 100 µm

4.1.7. 2D and 3D motility of PM cells *in vitro*

We conducted additional *in vitro* tests to better understand the background of the differences seen in the vascularization of SPC111 and P31 tumors. We examined the migratory and invasive capacity of the PM cell lines and also analyzed the motile and invasive activity of spheroid-forming P31 and SPC111 cells. Our results were consistent with our previous *in vivo* findings; P31 cells demonstrated significantly higher spreading (motility) on plastic and fibronectin-coated plastic surfaces. Moreover, we saw higher invasive capacity in collagen type I and collagen type I plus fibronectin containing gels of the P31 cells (Fig.19).

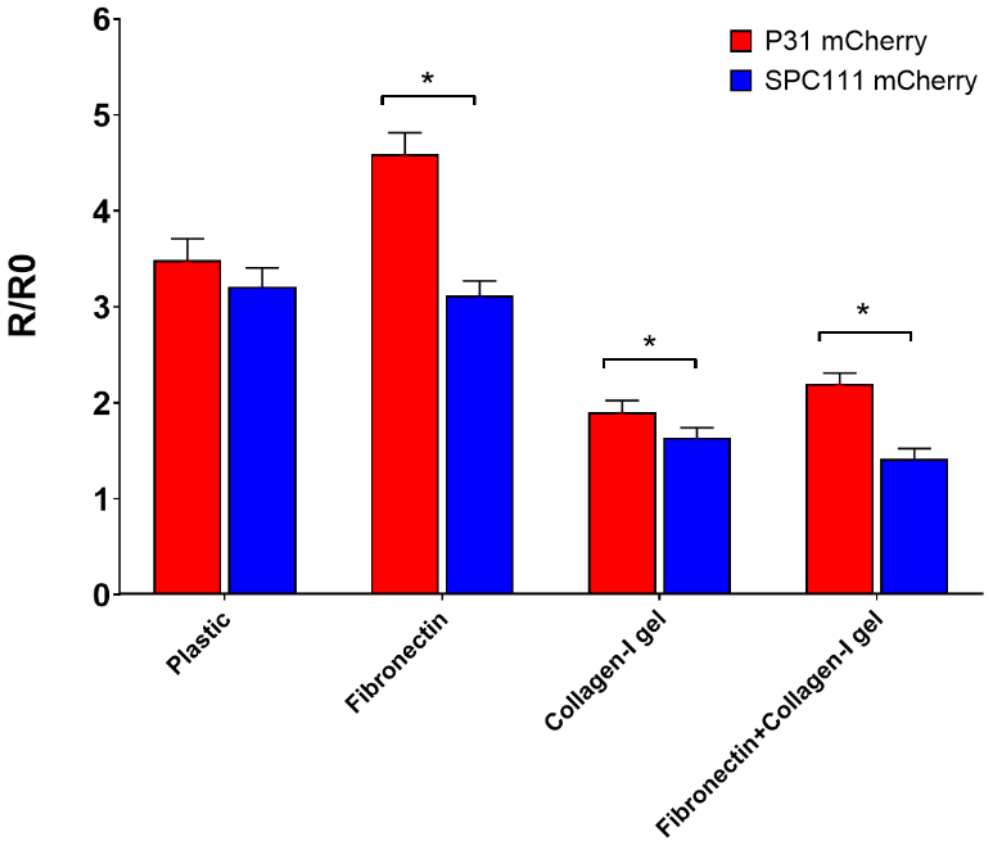

Figure 19. Spreading ability of SPC111 and P31 cell spheroids

SPC111 and P31 spheroids spreading on plastic or fibronectin coated surfaces (first four columns). Invasive activity of the spheroids in collagen type I and fibronectin/collagen type I mixed gels (second four columns). Average values were determined, then each average radius (R) was normalized by the average radius of original aggregates (R0). Significant differences are marked by * ($p < 0.05$).

4.2. Effects of anti-angiogenic treatment in PM

The role of anti-angiogenic therapies in PM is already established, and multiple drugs showed preclinical potential, but sadly no clinical benefit came out of these results except for bevacizumab. We tested the multitarget RTKI, nintedanib against PM *in vitro* and *in vivo*, in mono- and combinational therapies.

4.2.1. RTK expression profiles and genomic characterization PM cell lines

In order to more accurately predict the effectiveness of nintedanib in PM cell lines *in vitro*, we determined the transcript levels of the key target molecules of nintedanib in 20 PM cell lines (listed in Table 3.). For controls, an immortalized mesothelial cell line (Met5a) and three primary mesothelial cell cultures (NP1, NP2, NP3) were used.

PDGFRA, VEGFR-1 - 3, FGFR-2, and FGFR-3 were expressed only by some cell lines and at relatively low levels. PDGFRB and FGFR-1 mRNAs could be detected in each tumor cell line and in most of the non-malignant control cell lines, although with varying expression levels (Fig.20). Importantly, all of the examined PM cell lines were double positive for PDGFRB and FGFR-1. Moreover, we found that PM cells had elevated FGFR-1 expressions compared to the control cells (Fig.20; $p<0.05$).

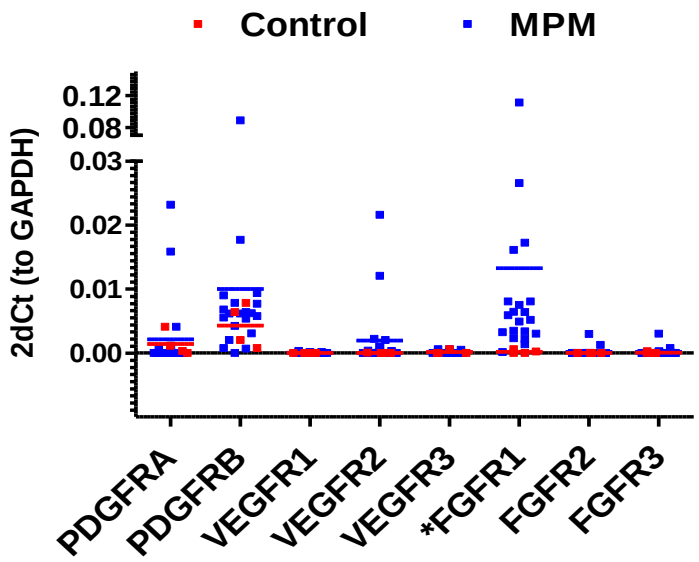

Figure 20. Target RTKs of nintedanib in control mesothelial and in PM cells

mRNA levels of PDGFRA and -B, VEGFR-1 - 3, and FGFR-1 - 3 in three normal mesothelial cell lines (red dots), in the immortalized Met5A cell line (red dots) and in PM cells (blue dots; n=20). Horizontal lines represent mean. FGFR-1 mRNA levels are significantly higher in the PM cell lines (*P<0.05; vs. controls).

We analyzed if there is an association between the histological subtypes of PM and the mRNA levels of PDGFRB, FGFR-1, or other RTKs. No correlation was found between any receptor expression profiles and the tumor histotypes. While sarcomatoid and biphasic PM cells showed similar expression patterns, the epithelioid group was more heterogeneous. Regarding the cell lines used for the *in vivo* vascularization experiments (P31 and SPC111), the FGFR-1 expression levels were similar, while the PDGFRB transcript level was higher in P31 cells. The other target RTKs of nintedanib cannot be detected on the mRNA level in either cell line.

Genomic profiling of PM cells revealed that specific TSGs are frequently mutated in PM. In our PM cell lines, we identified the most common mutations in BAP1, NF2, and CDKN2A TSGs. We could not find any association between the mutational status or the copy number changes and nintedanib sensitivity (Table 3.).

4.2.2. Effects of nintedanib treatment *in vitro*

First, we determined IC50 values for nintedanib and cisplatin in all 20 PM cell lines (Table 3.). PM cells were exposed to different concentrations of nintedanib for 72 hours. Cell viability was determined by SRB assay, and dose-response curves were plotted to determine IC50 values for each cell line. IC50 values for control cell lines differed between 1.1 μM (Met5a) and 4.1 μM (NP3). PM cells also showed a wide range of sensitivity with IC50 varying from 1.6 μM to 5.9 μM (Table 3.). Regarding the IC50s, no association was found with the histological subtype (Fig.21) or mRNA expression profile of target RTKs.

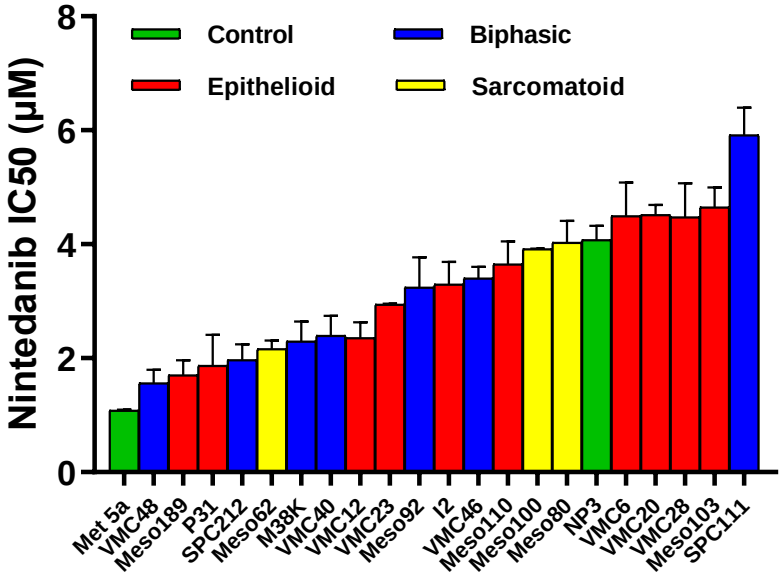

Figure 21. IC50 values of nintedanib in control and PM cell lines

Mesothelial control (n=2) and PM cells (n=20) were incubated for 72 hours with different concentrations of nintedanib, then viability was determined with SRB assay. IC50 values are shown as mean+SD. Colors green, red, blue and yellow indicate control mesothelial, epithelioid, biphasic, and sarcomatoid PM cells, respectively.

In long-term growth assays, P31 and SPC111 cell lines, nintedanib was able to effectively inhibit clonogenicity at much lower concentrations than their IC50 values (Fig.22). For clonogenic survival analysis, PM cells were seeded at low densities, treated with different concentrations of nintedanib and incubated for 10 days than clonogenicities were determined. Crystal violet was dissolved, and intensity was quantified to determine clonogenicity.

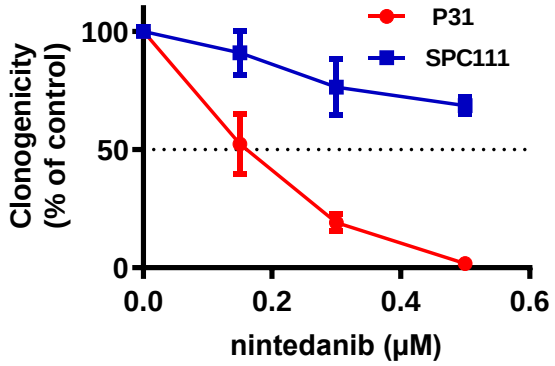

Figure 22. Clonogenic survival analysis of P31 and SPC111 cells

PM cells were treated with different concentrations of nintedanib and incubated for 10 days. Data (mean±SD) is taken from three independent experiments.

Table 3. Histological subtypes, drug sensitivity data, and copy number changes of target RTKs in PM cell lines

Cell line	Histological subtype	Nintedanib IC50 (μM)	Cisplatin IC50 (μM)	copy number							
				VEGFR-2		*PDGFRA*		*PDGFRB*		*FGFR-1*	
				log2 ratio	status	log2 ratio	status	log2 ratio	status	log2 ratio	status
P31	epithelioid	1.9	4.3	-0.13	normal	-0.24	loss	0.03	normal	-0.41	loss
I2	epithelioid	3.3	3.8	-0.00	normal	0.28	gain	-0.08	normal	-0.09	normal
VMC6	epithelioid	4.5	3.0	-0.09	normal	-0.85	loss	0.49	gain	0.18	normal
VMC12	epithelioid	2.4	1.1	-0.48	loss	-0.18	normal	0.39	gain	0.00	normal
VMC20	epithelioid	4.5	1.1	-0.49	loss	-0.16	normal	0.11	normal	0.01	normal
VMC23	epithelioid	2.9	6.4	-0.38	loss	-0.28	loss	-0.01	normal	0.32	gain
VMC28	epithelioid	4.5	4.2	-0.22	loss	-0.85	loss	0.55	gain	0.09	normal
Meso103	epithelioid	4.7	3.1	-0.21	loss	-0.27	loss	-0.45	loss	0.30	gain
Meso110	epithelioid	3.7	10	-0.83	loss	-0.62	loss	0.05/ -0.56	normal /loss	0.58	gain
Meso189	epithelioid	1.7	2.2	0.03	normal	-0.07	normal	0.23	gain	0.20	gain
Meso62	sarcomatoid	2.2	4.1	-0.12	normal	-0.17	normal	-0.49	loss	0.04	normal
Meso80	sarcomatoid	4.0	0.6	-0.12	normal	-0.01	normal	-0.03	normal	-0.66	loss
Meso100	sarcomatoid	3.9	1.9	-0.48	loss	-0.16	normal	-0.69	loss	0.08	normal
SPC111	biphasic	5.9	0.7	0.47	gain	0.36	gain	-0.01	normal	-0.36	loss
SPC212	biphasic	2.0	1.9	-0.49	loss	-0.63	loss	0.06	normal	0.54	gain
M38K	biphasic	2.3	1.8	0.32	gain	0.24	gain	-0.36	loss	0.17	normal
VMC40	biphasic	2.4	3.7	-0.23	loss	-0.28	loss	0.15	normal	0.52	gain
VMC46	biphasic	3.4	0.4	-0.92	loss	-0.66	loss	0.15	normal	-0.64	loss
VMC48	biphasic	1.6	1.2	-0.11	normal	-0.31	loss	0.86/ -0.33	gain /loss	-0.12	normal
Meso92	biphasic	3.2	1.9	0.00	normal	-0.06	normal	1.10	ampl.	-0.02	normal

Several studies suggest that RTKs targeted by nintedanib can interfere with ChT in other malignancies (198-200). To investigate nintedanib's impact on ChT, P31 and SPC111 cells were treated with different concentrations of nintedanib and cisplatin, alone or in combination. P31 cells are relatively responsive to nintedanib (IC50: 1.9 μM) but insensitive to cisplatin (IC50: 4.3 μM). SPC111 cells proved to be more resistant to nintedanib (IC50: 5.9 μM) than P31 cells (Table 3.). On the other hand, P31 is more resistant to cisplatin than SPC111 (IC50s are 4.3 μM vs. 0.7 μM, respectively; Table 3.). Notably, an additive effect between nintedanib and cisplatin was observed at certain concentrations in both cell lines (Fig.23). However, no synergism between nintedanib and

cisplatin was evident in either cell line (Fig.23). Furthermore, there was no correlation found between cisplatin and nintedanib sensitivities in our panel of 20 human PM cell lines (Table 3.).

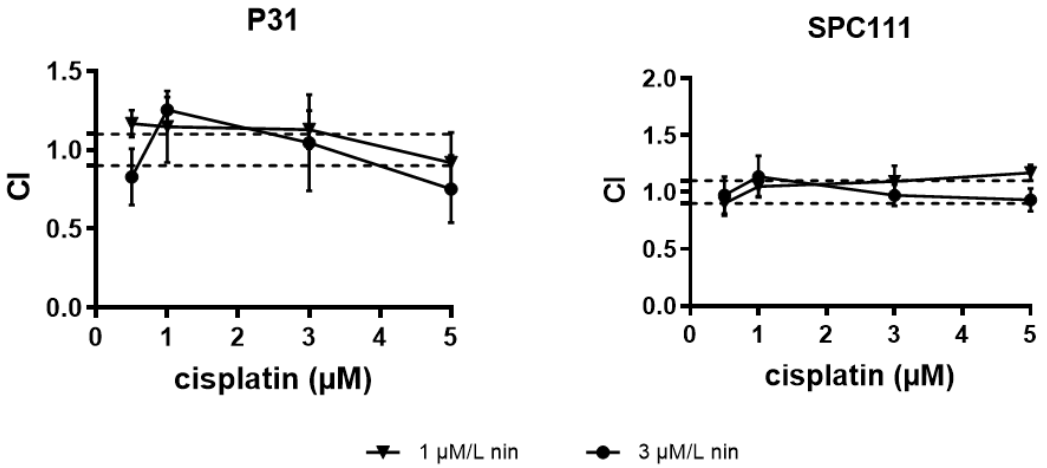

Figure 23. Viability after 72 hours of treatment with different concentrations of nintedanib and cisplatin alone or in combination

Viabilities were measured with SRB assay and combination indices (CI) were calculated. CI values <0.9, from 0.9 to 1.1, or >1.1 represent synergism, additive effects or antagonism between nintedanib and cisplatin, respectively. Data (mean ± SD) from three independent experiments are shown.

To investigate the effects of nintedanib on tumor cell proliferation, we performed BrdU incorporation assays in five different PM cell lines. Nintedanib exhibited a significant antiproliferative effect in a dose-dependent manner in each investigated PM cell line (Fig.24A). To study the apoptosis inductive ability of nintedanib, TUNEL assays were performed (Fig.24B). The TUNEL assay was developed to detect DNA fragmentation during apoptosis. Apoptosis rates were significantly elevated upon nintedanib treatment only in two cell lines (SPC212, VMC40) (Fig.24B).

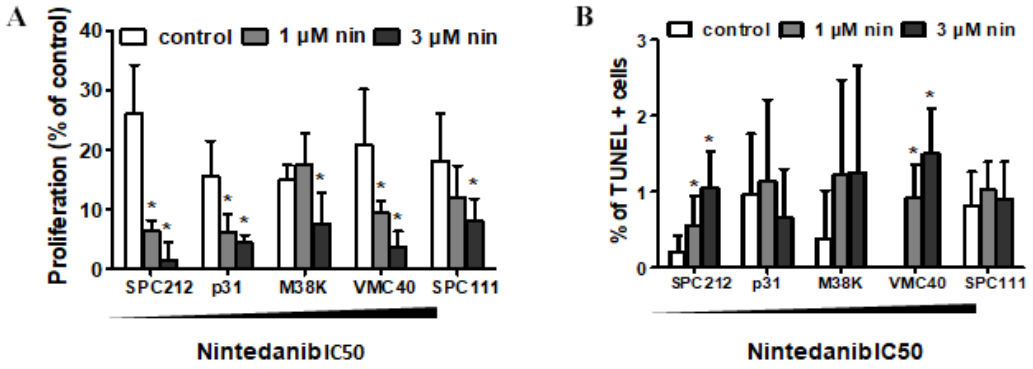

Figure 24. Effects of nintedanib on PM cell proliferation and apoptosis

A. PM cells were treated with nintedanib for 48 hours, and the proliferation rate was measured by BrdU assay. A significant reduction of cell proliferation could be observed upon nintedanib treatment in all five PM cultures. Columns, mean for three experiments; bars, SEM. *p≤0.05. **B.** To measure the ratio of apoptotic cells in PM cultures TUNEL staining was performed, and cultures were exposed for 48 hours to increasing concentrations of nintedanib. Columns, mean for three experiments; bars, SEM. * p≤0.05.

To test the anti-migratory effects of nintedanib, five human PM cell lines were chosen with different nintedanib sensitivities based on the IC50 values (Table 3.). Cell cultures were treated with nintedanib (1µM or 3µM) or solvent in a CO2-independent medium with 10% FBS for 24 hours and cell migration was analyzed with videomicroscopy. Nintedanib treatment in both tested concentrations was able to significantly reduce the migratory activity of each cell line (Fig.25).

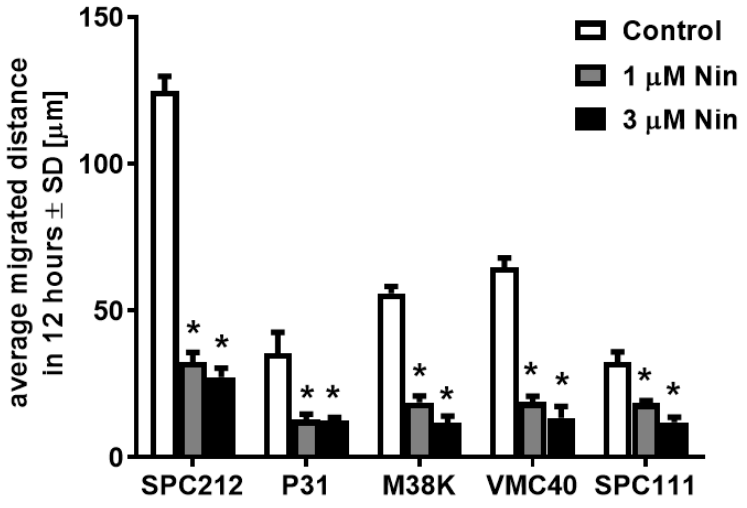

Figure 25. Impact of nintedanib treatment on the migration of PM cells *in vitro*

Nintedanib showed a significant anti-migratory potential at both concentrations in all tested cell lines (*p≤0.0001 versus control).

4.2.3. Effects of nintedanib treatment *in vivo*

After the promising results of the *in vitro* experiments, we wanted to test the *in vivo* efficacy of nintedanib in the treatment of PM. We used the same cell lines (P31, SPC111) in the same orthotopic PM model as in the vascularization experiments. In two sets of experiments, PM cells were injected intrapleurally, into the thoracic cavity of SCID mice.

Effects of nintedanib treatment on the survival of orthotopic tumor-bearing animals

In the first set of experiments, nintedanib was administered either PO or IP at 50 mg/kg concentration. The therapy started on the 21st day after tumor cell inoculation because, at this time, macroscopic tumor nodules are already present on the pleural surfaces. For this set of experiments, P31 cells were chosen because P31 cells highly express PDGFRB and FGFR-1 receptors and are relatively sensitive to nintedanib and resistant to cisplatin (Table 3.).

During the treatment period nintedanib was well tolerated by the animals, without any signs of toxicity. To further corroborate the antitumor effects of nintedanib, *in vivo* PM growth was also examined by MR imaging. 25 days after tumor implantation, the control animals had significant intrathoracic tumor burden, and the considerable reduction of tumor mass in nintedanib-treated animals was evident (Fig.26).

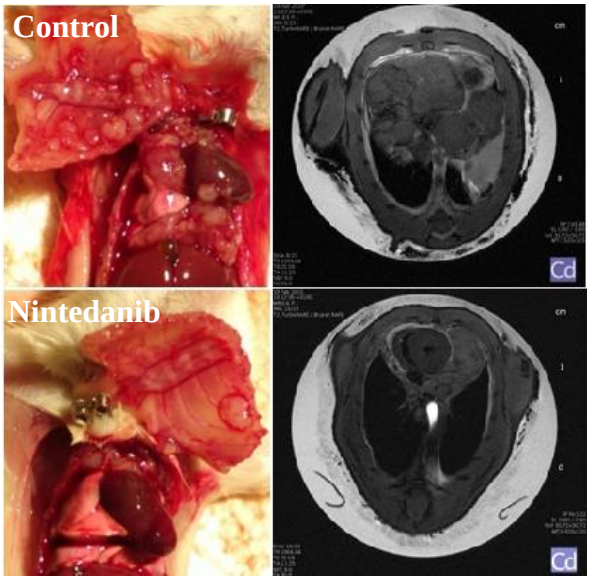

Figure 26. Representative images of orthotopically growing human PM nodules

Representative macroscopic (upper panel) and MR (lower panel) images of orthotopically growing human PM nodules (day 25) in control and nintedanib (IP) treated mice. In MR images, arrows mark the tumor rims.

We assessed the effects of nintedanib on the survival of animals with orthotopic human P31 tumors. Although the survival of PO-treated animals showed a favorable trend, no significant benefit was proven (P=0.059; vs. PO control; Fig.27A). However, nintedanib was able to significantly prolong the survival of mice when it was administered IP (p=0.0008; Fig.27A). Moreover, IP administered nintedanib was also able to significantly inhibit the relative weight loss of the animals (P=0.0337, Fig.27B). In accordance we observed a better overall condition at the end of the experiment of these animals. Our interpretation of these data is that IP administered nintedanib not only prolongs the survival of mice with orthotopically growing human PM but also interferes with PM-induced cachexia.

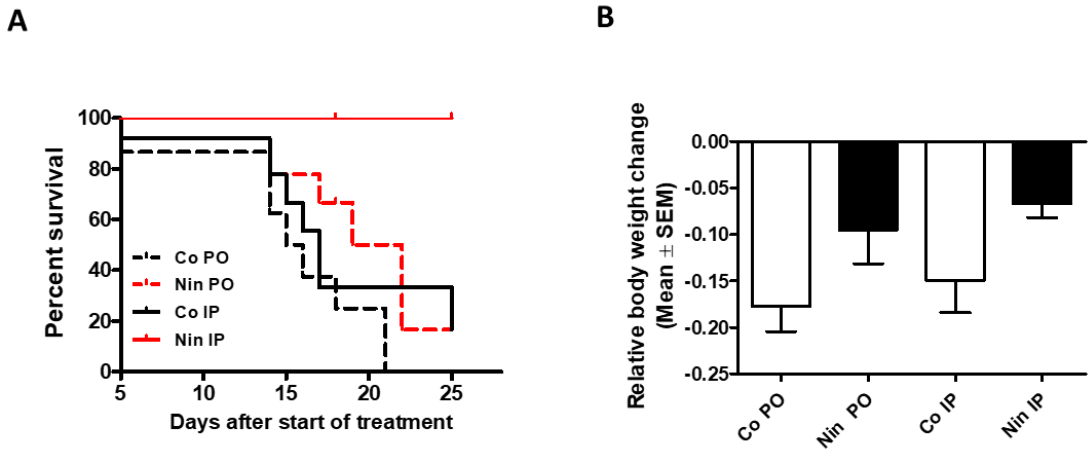

Figure 27. Nintedanib prolongs survival of mice bearing orthotopically growing PM

A. Kaplan-Meier curves for the survival of human PM-bearing mice treated with nintedanib, according to the route of drug administration. Animals treated with nintedanib IP had significantly longer survival times than those treated with vehicle (Co) IP only (P=0.0008). **B.** Relative body weight changes of human PM-bearing mice. *P=0.0337 versus IP controls.

Effects of nintedanib treatment on *in vivo* tumor growth

In the second set of experiments, we investigated the efficacy of nintedanib, combined with standard-of-care ChT, in P31 and SPC111 orthotopic xenografts. The animals were treated IP, as in the aforementioned set of *in vivo* experiments this route of administration proved to be superior to PO treatment. Besides the control group, the animals were assigned to the following treatment groups: cisplatin-pemetrexed, nintedanib or bevacizumab in monotherapy, and combination therapy of cisplatin-pemetrexed with either nintedanib or bevacizumab. In both cell models, mice treated with cisplatin/pemetrexed ChT alone or nintedanib alone, significantly reduced tumor burden

was evident (versus untreated controls) (Fig.28). Combined chemo- and anti-angiogenic regimens (either nintedanib or bevacizumab) also demonstrated significant *in vivo* tumor growth-inhibitory potential in both cell models when compared to untreated control tumors (Fig.28). In accordance with the previous finding of Li Q et al. (107), bevacizumab was effective only against P31 tumors (versus control) with high baseline VEGF-A levels (Fig.16). Bevacizumab monotherapy could not provide therapeutic benefit in the SPC111 model where tumor cells had markedly low baseline VEGF-A levels (Fig.16, Fig.28). Another key observation in this set of experiments is, that combining nintedanib with standard ChT produces significantly higher responses than ChT alone. These responses were comparable (P31) or superior (SPC111) to those achievable by combination of bevacizumab and ChT (Figure 25). Moreover, in contrast to bevacizumab, nintedanib monotherapy proved to be a more effective inhibitor of *in vivo* tumor growth than standard ChT in P31 tumors (Fig.28).

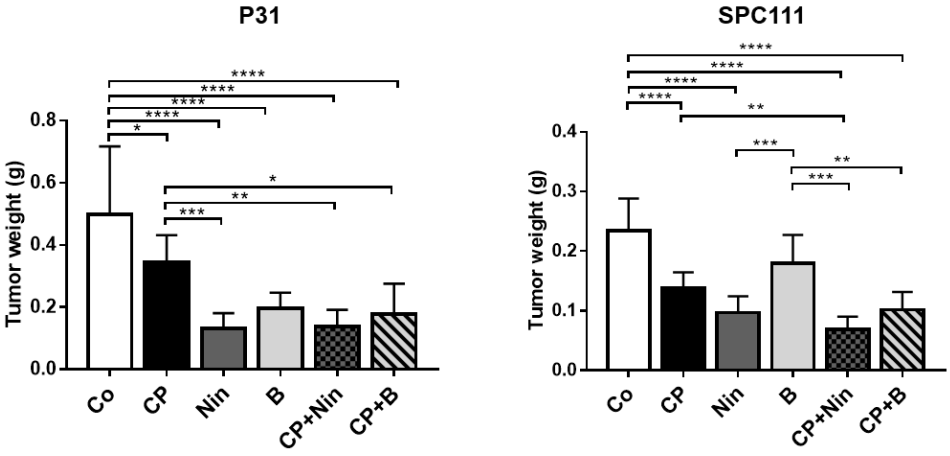

Figure 28. Effects of different mono- or combined chemo- and anti-angiogenic therapies on *in vivo* PM tumor-growth

Nintedanib inhibits the growth of orthotopically growing PM more effectively than standard-of-care ChT or bevacizumab. Total tumor weight of P31 (left panel) and SPC111 (right panel) xenografts in each mouse was determined. Columns, means for ten mice per group; bars, SD; *p≤0.05, **p≤0.005, ***p≤0.0005, ****p≤0.0001. **Co**: control; **CP**: cisplatin/pemetrexed; **Nin**: nintedanib; **B**: bevacizumab; **CP+Nin**: cisplatin/pemetrexed + nintedanib; **CP+B**: cisplatin/pemetrexed + bevacizumab

Effects of nintedanib treatment on angiogenesis

We also examined the antivascular and antitumoral effects of nintedanib treatment. Morphometric analysis using the endothelial marker CD31 revealed a strong tendency for increased MVAs in control P31 tumors with high baseline VEGF-A expression as compared with untreated SPC111 tumors with low baseline VEGF-A (2.7±1.2% vs.

1.2±0.8%, respectively; P=0.067). In accordance with the potent *in vivo* PM growth inhibitory effect of nintedanib, significantly lower MVAs were present in tumors treated with nintedanib (alone or in combination) in both models (vs. controls; Fig.29A). Interestingly, though, no significant reduction was found in MVAs of either model treated with bevacizumab with or without ChT (Fig.29A). The robust antivascular effects of nintedanib were accompanied by increased intratumoral necrosis in both models. This was most prominent in the combined nintedanib-ChT groups (Fig.29B). Nintedanib monotherapy was able to significantly increase PM cell apoptosis compared with controls (P=0.0317; Fig.29C) and also decreased proliferation in P31 tumors (P=0.0341; Fig.29D). However, no other treatment caused significant changes in tumor cell apoptosis and proliferation rates. Furthermore, we failed to identify any obvious associations between PM cell apoptosis and proliferation and the net *in vivo* tumor growth inhibitory effect of nintedanib presented in Figure 28.

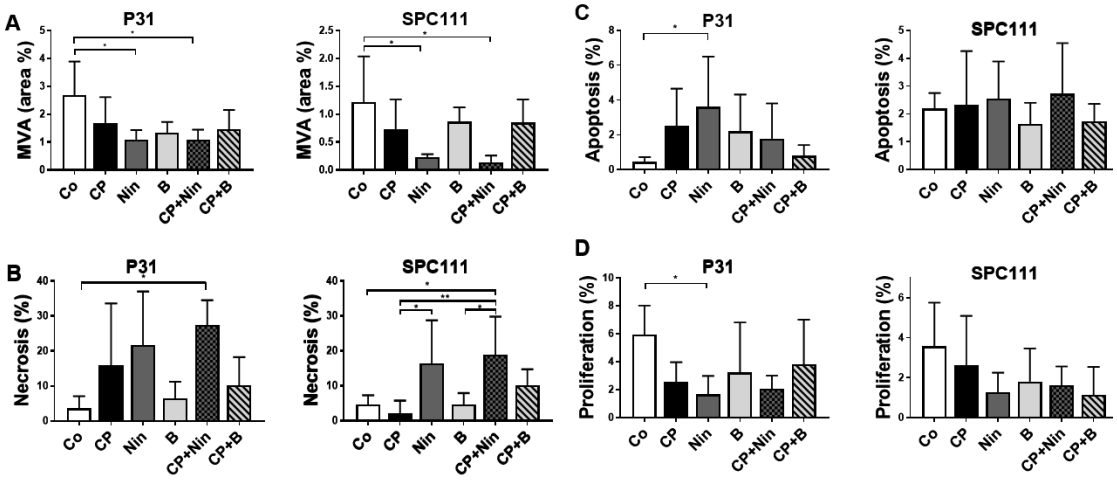

Figure 29. Antivascular and antitumor effects of nintedanib and bevacizumab

For quantifications of **A**. angiogenesis, **B**. tumor necrosis, **C**. apoptosis and **D**. proliferation, MVDs (vessel areas per total areas) and percentages of necrotic tumor regions and the ratios of apoptotic and proliferating PM cells were determined across the entire areas of P31 and SPC111 tumor sections. Columns, means for 10 mice per group; bars, SD *P≤0.05, **P≤0.005 **A**. Frozen tissue sections were labeled with the endothelial marker CD31. **B**. Necrotic area ratios are shown in the percentage of the whole tumor section. **C**. The apoptotic rate is expressed as the percentage of cleaved caspase-3-positive cells. **D**. The ratio of proliferating PM cells was assessed by BrdU labeling. **Co**: control; **CP**: cisplatin/pemetrexed; **Nin**: nintedanib; **B**: bevacizumab; **CP+Nin**: cisplatin/pemetrexed + nintedanib; **CP+B**: cisplatin/pemetrexed + bevacizumab

5. Discussion

In the studies discussed here, human PM cell lines were implanted orthotopically into the thoracic cavity of immunodeficient mice to examine the process of tumor vascularization and the effects of anti-angiogenic treatments. In mesothelioma research, orthotopic tumor cell implantation is not a commonly used method due to the complexity of the implantation technique and the challenges in monitoring tumor development and therapy response (201). The histological subtyping of PM has a substantial prognostic and possibly predictive value (202). Therefore, we implanted cells derived from two distinct histological subtypes to analyze the vascularization processes and the impact of nintedanib treatment. To establish orthotopic tumor models, we engrafted an epithelioid (P31) and a biphasic (SPC11) PM cell line intrapleurally into SCID mice.

After tumor cell implantation, animals were sacrificed at specific time points to study the progress of tumor development. The diaphragms, along with the tumor nodules sitting on the surface of the diaphragms, were removed and fixed in formalin. By analyzing these whole-mount samples, we were able to examine the tumor-induced vascularization thoroughly. At the very early stages, intact diaphragmatic lymphatic vessels were present in both of our *in vivo* models below the mesothelium but above the blood vessels. During the development of vascular proliferations, blood vessels elevated above lymphatics but remained covered by the mesothelium. Baluk et al. (203) described a similar vascular growth phenomenon in airways, with a tet-on inducible transgenic system producing VEGF. They found that induced VEGF expression caused ES and vessel proliferation. Moreover, this neovasculature elevated above the BM of the epithelium, protruding into the airway lumens. In this study, the authors described a fenestrated endothelium of the vessels due to VEGF-induced angiogenesis; this finding was also collaborated by several other studies (204-206). In accordance, a fenestrated endothelium was observed in the neovasculature in our models.

Although the initial stages of tumor nodule formation were similar, our two models exhibited notable differences in the subsequent vascularization processes. Interestingly, tumor-induced capillary plexuses did not seem to impact significantly SPC111 tumor expansion. The progressing SPC111 nodules pushed away the surrounding neovasculature and remained avascular for several weeks. The SPC111 cells in spheroid-forming assays demonstrated a higher cohesive strength *in vitro;* this could explain the

inability of tumor cells to invade the induced vasculature and simply displace it while growing.

In contrast, P31 tumors continuously assimilated the surrounding tumor-induced vasculature into the growing nodules. Moreover, P31 cells deposited a high amount of ECM within the tumor nodules, providing an appropriate environment for vascular sprouting. We observed that a compelling amount of collagen type I of human origin was scattered throughout the nodule. To further support this observation, mRNA expression levels were measured by qPCR. P31 cells expressed significantly higher levels of COL1A1 compared to SPC111 cells. Previous studies proved that mesothelial cells produce many fibrous components in humans, including collagen, which forms a thin layer of connective tissue under the pleura (207-209). Moreover, a study found evidence of subtype-specific ECM production in PM and that ECM differences are able to influence the migratory ability of tumor cells (210). Another study demonstrated *in vivo* PM tumor-growth reduction after collagen inhibitor treatment, suggesting the importance of collagen in PM growth and proposing a potential therapeutic target (211).

The tumor nodules of SPC111 began to vascularize only in the later stages of development. The first and most crucial step in the vascularization process was the accumulation of a desmoplastic matrix at the base of the nodules. Then this matrix, accompanied by myofibroblasts, became incorporated into the tumor mass layer-by-layer, perhaps by its contractile nature (212). This incorporated connective tissue provides suitable space for vessels of the diaphragm to sprout into the tumor nodules. Interestingly, in contrast to P31 tumors, the SPC111 nodules were highly negative for collagen type I of human origin confirmed by species-specific antibody immunofluorescence staining. In SPC111, most of the accumulated ECM is of mouse origin, proving that activated fibroblasts and not the tumor cells deposited it. The importance of host tissue fibroblast in the development of tumor stroma has been established by several studies (213).

Similar tumor growth patterns and the possible role of vessel co-option in anti-angiogenic therapy resistance mechanisms were described previously in other tumor types (184). In liver metastasis of colorectal cancer (CRCLM), three main categories of histopathological growth pattern (HGP) are recognized (214). In the desmoplastic type HGP, tumor tissue is surrounded by a well-defined rim of fibroblasts and immune cells separating it from the host tissue. In the pushing HGP, tumor cells do not infiltrate the host tissue, but instead

push it away as the tumor progresses. In these HGP types, the primary method of vascularization is through sprouting angiogenesis. On the other hand, in the replacement HGP, tumor cells replace the host tissue hepatocytes, and sinusoidal vessels are co-opted by the tumor to ensure their blood supply (184). In CRCLM, HGP has a prognostic value and it might also have therapeutic implications (184).

The central region at the base of the SPC111 colonies demonstrated the most pronounced infiltration and incorporation of the ECM, leading to a radial arrangement of the connective tissue inside the nodules. This area has been in contact with the underlying tissue for the longest time. The microenvironment in this area supports invasiveness by allowing ES from the diaphragm.

VEGF-A plays a crucial role in both physiological and pathological vascularization processes (215). VEGF-A secretion measured by ELISA was significantly lower in SPC111 cells than in P31 cells. Therefore, to analyze the effects of VEGF-A secretion, we significantly increased the VEGF-A expression of SPC111 cells with the help of an RFP-VEGF-A-coding retroviral construct. The VEGF-A overexpression of tumor cells caused rapid vascular proliferation development, which elevated above the diaphragmatic surface. Ultimately, tortuous microvascular structures covered the whole surface of the diaphragm but without the presence of macroscopic tumor nodules. Furthermore, these vascular proliferations were present not only in the vicinity of tumor colonies but further away on the surface of the diaphragm. This highlights the key role of secreted VEGF-A in tumor-induced capillary development. Previous studies have shown that VEGF plays a major role in regulating cytokines and promoting angiogenesis in solid tumors (146, 216). Unfortunately, the early death (after 7 days) of VEGF-A overexpressing SPC111 tumor-bearing mice made it impossible to further study the impact of increased VEGF-A levels on tumor vascularization patterns.

The essential role of VEGF-A in angiogenic processes made it a well-established target for antitumor treatments (217). Currently, the standard first-line systemic therapy for the treatment of PM patients is often supplemented with the anti-angiogenic drug bevacizumab, based on the evidence of the MAPS trial. In this phase 3 study, the addition of bevacizumab to the standard systemic therapy significantly increased the OS of unresectable PM patients from 16.1 to 18.8 months (106). Likewise, cediranib (a small-molecule RTKI) in combination with pemetrexed-cisplatin ChT prolonged the PFS of PM

patients in a phase 2 randomized trial (218). These results suggest that combinational anti-angiogenic therapy has the potential to improve the survival of PM patients. Therefore, with the help of *in vitro* and *in vivo* PM models, we examined nintedanib's antitumor and antivascular activity. Nintedanib is a small molecule RTKI targeting VEGFR-1 - 3, FGFR-1 - 3, and PDGFR α, β signaling (166).

First, we analyzed the expression profiles of nintedanib's target receptors by qPCR in 20 human PM cell lines. For control, we used an immortalized mesothelial cell line and three primary mesothelial cell cultures. The results showed that all PM cell lines express relatively high levels of FGFR-1 and PDGFRB, although only the FGFR-1 expression was significantly elevated in PM cell lines compared with control cells. PDGFRA and VEGFR-2 expressions were also measurable in certain cell lines, while the expressions of the other target RTKs were negligible in all of the tested cell cultures and cell lines. This is in line with the findings of several previous studies (177, 179, 219).

The importance of PDGFRA and VEGFR-2 signaling in PM is implicated by a retrospective study that analyzed samples of advanced-stage mesothelioma patients. They observed mutations in nintedanib target genes in approximately one-third of PM patients (60). Although other studies in the genomics of PM failed to confirm these results. (55, 56).

It is assumed that with FGF, PDGF, and VEGF secretion, PM cells can promote their growth and survival through distinct autocrine signaling loops. In accordance, a study demonstrated that VEGF is able to induce PM growth *in vitro* through the phosphorylation of VEGFR-1 and -2 (220). The same research concludes that molecules of the VEGF/VEGFR axis are expressed in human PM tissues. VEGF or VEGFR-2 neutralizing antibody treatment can effectively reduce tumor cell proliferation. Numerous studies established the autocrine growth-promoting impacts of PDGF/PDGFR and FGF/FGFR pathways in PM (177, 179, 180) and in different solid tumors (221). Based on these reports and our observations, it can be concluded that nintedanib has a direct antitumor effect *in vitro* in parallel to its anti-angiogenic potential. This is also supported by the dose-dependent inhibition of PM growth following nintedanib treatment.

A previous study reported that PM cells possess a significantly high capacity for migration, surpassing even the migratory potential of malignant cells found in highly metastatic tumors like lung cancer or melanoma (196). Our results proved that nintedanib

can effectively inhibit *in vitro* PM cell migration. Besides, there is evidence that nintedanib can impair the movement of fibroblasts in patients with idiopathic pulmonary fibrosis (222).

Various studies have previously explored the efficacy and interactions of anti-angiogenic agents in combination regimens. Several studies demonstrated that FGFR-1 inhibition is able to increase the effectiveness of ChT in PM (179) and breast cancer (223). Moreover, PDGFR inhibition showed synergistic effects with paclitaxel and doxorubicin treatment in breast cancer, both *in vitro* and *in vivo* (199). In lung cancer cells, the overexpression of VEGFR-2 resulted in platinum resistance, and this induced resistance decreased when VEGFR-2 signaling was suppressed with the help of small interfering RNAs. This suggests that blocking VEGFR-2 may help reduce platinum resistance in cancer (198). Our results concluded that the combined use of nintedanib and cisplatin has an additive antineoplastic effect on human PM cells *in vitro*.

The robust *in vivo* antitumor effects of nintedanib were also evident from our results. When administered IP, nintedanib monotherapy was able to significantly prolong the survival time and reduce the body weight loss of mice in the orthotopic P31 mesothelioma model. The survival times of PO-treated animals were also prolonged, but this benefit was not statistically significant. A possible explanation for this observation is that the intrathoracic concentration of nintedanib could have been higher following IP administration. It has been reported that the lymphatic capillary system of the diaphragm directly connects the peritoneal and thoracic cavities both in mice and humans (224, 225). Further investigation is required to determine the mechanism and effectiveness of this trans-diaphragmal drug transfer. However, our results suggest that administering nintedanib IP could produce a more potent antitumor effect in PM, despite being approved for oral administration in the clinic.

Because of its superior efficacy, all drugs were administered IP in the subsequent experiments. In our murine model, we observed a significant advantage in combining standard ChT with nintedanib. The anti-angiogenic agents, nintedanib and bevacizumab showed similar potential in reducing *in vivo* tumor growth in tumors with high levels of VEGF-A expression. Our results suggest that nintedanib is just as effective as bevacizumab, which is currently used as the standard angiogenesis inhibitor in clinical settings (92, 226). Furthermore, we observed that nintedanib surpasses the effectiveness

of bevacizumab in inhibiting the growth of human PM nodules with low baseline VEGF-A expression. Bevacizumab monotherapy was only effective in high VEGF-A-expressing P31 tumors but did not provide any therapeutic advantage in the SPC111 model with low VEGF-A expression. Therefore, our findings suggest that combining nintedanib with ChT could be a better choice of treatment for PM patients with low VEGF-A expression. Consistent with this, previous research demonstrated that bevacizumab effectively suppressed the orthotopic growth of PM cells with a high level of VEGF-A expression (EHMES-10); however, it did not have the same impact on the MSTO-211H PM cells that produced low levels of VEGF (107). It is important to consider that the initial levels of VEGF detected in our PM cell lines may have undergone changes through *in vivo* tumor progression. Therefore, validated VEGF-A-related biomarkers or other indicators are needed to predict the effectiveness of anti-angiogenic treatment before the patients can benefit from these findings (227).

Including ours, several preclinical results provided a rationale for the concept of LUME-Meso trials to evaluate the therapeutic potentials of nintedanib in combination with cisplatin/pemetrexed ChT for patients with unresectable PM. Unfortunately, nintedanib treatment was unable to meet the expectations and is no longer considered for further exploration in combination with cisplatin and pemetrexed ChT for the treatment of PM patients (111). The results of the phase 2 part of the LUME-Meso trials were promising; nintedanib prolonged the PFS of patients compared to the placebo group. The median OS was 18.3 months versus 14.2 months (228). Unfortunately, in the confirmatory phase 3 trial, the results failed to meet the primary endpoint, and the addition of nintedanib to standard ChT did not improve the PFS (111). The only major change in the protocol between the two phases was that in phase 3, only patients with epithelioid subtype were included because the observed benefits were more prominent in this subgroup of patients in phase 2 setting (111). Otherwise, the reasons behind the inconsistency between the trials are undetermined.

Accompanying the direct *in vivo* antitumor effects of nintedanib, notable anti-angiogenic effects were observed in our research. Our research indicates that nintedanib exhibits more potent anti-angiogenic and antineoplastic effects than bevacizumab. In both cell lines, a significant reduction in vascularization of nintedanib-treated tumors (vs. control) was evident, regardless of the presence of concurrent ChT. However, in bevacizumab-

treated animals, the same effect was only observable in P31 tumors with high baseline VEGF-A levels, where the results suggested a strong tendency for reduced vascularization.

The IC50 values of nintedanib found in our *in vitro* assays are higher than the pharmacologically achievable tissue concentrations in mammals, which ranges from 200-450 nmol/L (166). This suggests that the antivascular potential of nintedanib is the key component in its *in vivo* tumor growth-inhibiting effects. Further supporting this conclusion, in a previous study, nintedanib's IC50 values in EC cultures were about one order of magnitude lower than the IC50s we experienced for PM cells (166).

Interestingly, anti-angiogenic RTKIs have both antivascular and direct antitumor effects, but these actions may partially contradict each other regarding tumor progression. There is evidence that RTKI treatment can destroy the tumor microvasculature; this capillary reduction can lead to insufficient RTKI penetration into the tumor tissue, resulting in limited drug delivery and reduced efficacy (197).

Our study reveals that nintedanib exhibits similar levels of effectiveness as a single agent and in combination with cisplatin/pemetrexed ChT in human PM xenografts. Although nintedanib and ChT demonstrated additive effects *in vitro*, the combination of nintedanib does not enhance PM growth inhibition *in vivo*. These findings align with the results of a previous research, which demonstrated that while nintedanib synergizes with gemcitabine in pancreatic cancer *in vitro* and exhibits potent antitumor effects *in vivo*, the combination of nintedanib and gemcitabine does not result in synergistic tumor growth reduction in mice bearing human pancreas cancer xenografts (221). However, in other studies of human pancreas and lung cancer xenografts, nintedanib significantly enhanced the activity of ChT (229). Moreover, nintedanib "normalized" the vasculature in human A549 lung cancer xenografts (230) and in an *in vivo* model of pulmonary fibrosis (231).

At the moment, it remains uncertain whether anti-angiogenic medication can enhance the performance of ChT. Based on Jain and colleagues' vessel normalization theory, bevacizumab can "normalize" the erratic tumor vasculature, which may result in enhanced delivery of chemotherapeutic agents (232). Contrary to this, clinical data has raised serious concerns about the effects of bevacizumab on the uptake of ChT in solid tumors, as it appears to have a reducing rather than improving effect (233). In addition, a study by Kutluk-Cenik and colleagues demonstrated that nintedanib therapy reduced the

pericyte coverage in capillaries and decreased the delivery of doxorubicin in human pancreatic cancer xenografts (229). These results contradict the vessel normalization concept. It is possible that anti-angiogenic therapy disrupts the vasculature instead of normalizing, thereby compromising drug delivery by eliminating the pericyte coverage of tumor capillaries. This is due to the vital role of the PDGF/PDGFR axis in pericytes and the pericyte layer's crucial contribution to vessel wall stability (232).

There is some important translational relevance in our findings. The differences in the vascularization patterns might contribute to the inconsistent therapeutic effects of the tested anti-angiogenic agents. Insufficient penetration of anticancer agents into the tumor nodules might lead to reduced efficacy in PM neoplasms with avascular, "pushing" growth patterns compared to well-vascularized tumors exhibiting invasive growth patterns. Additionally, our data support the idea that anti-angiogenic therapy in PM may not be universally suitable for every patient or setting. Predictive biomarkers and advanced patient selection methods are crucial to increase patient outcomes.

Our results have a few possible limitations. First, there are some known differences in the anatomy of the human and mouse diaphragm. The sub-mesothelial connective tissue layer in mice is almost unrecognizable (234, 235). In contrast, in humans, a vascularized, thick collagen layer under the mesothelium is probably blocking the development and elevation of vascular proliferations on the surface of the diaphragm, as seen in mouse models. Thus, the findings in murine models might not accurately replicate pathogenesis in humans. It is possible that similar to late-SPC111 tumors, the collagen layer could be integrated into the tumor and form pathways of connective tissue that aid the growth of tumor vasculature.

Another potential limitation of this study is the use of human PM cell lines in immunodeficient mice. Cell-derived xenografts (CDXs) are standard models in cancer research, including PM, because of their high reproducibility (236). However, extended culture conditions can lead to karyotypic changes and genomic instability, compromising their ability to accurately replicate human tissue and disease (237, 238). Moreover, immunodeficient mouse models lack the immunological aspects of tumorigenesis. Therefore, it is necessary to validate our findings in immunocompetent models, specifically in asbestos-induced or genetically engineered mouse (GEM) models.

Finally, the connection between histological subtypes and tumor vascularization in PM has yet to be established (181, 239). Additional research is necessary to reveal potential connections between histological features, diverse vascularization patterns, and treatment outcomes in PM.

6. Conclusions

To the best of our knowledge, our study was the first to report two distinct vascularization patterns in orthotopic xenografts of human PM. Moreover, we were the first to test the *in vivo* efficacy of the triple angiokinase inhibitor nintedanib in these orthotopic PM xenograft models. Our findings most likely bear translational relevance and can assist in developing new therapeutic approaches for this deadly malignancy.

We showed that the two tumor models we investigated use significantly different mechanisms to develop intratumoral vasculature. In the invasive growth pattern (P31), tumor nodules vascularize from an early stage by the invasion and co-option of the peritumoral capillary plexuses. On the contrary, in the pushing/desmoplastic growth pattern (SPC111), tumor nodules remain avascular for an extended period of time. Then, the vascularization process starts with the deposition of a desmoplastic matrix underneath the tumor nodules. This matrix enables the endothelial ingrowth from the diaphragmatic vessels to develop a nutritive vasculature.

Significant differences were also seen in the *in vitro* characteristics of the two cell lines. The epithelioid P31 cell line was significantly more invasive, motile, and also less repellent to HUVEC sprouts in co-cultures than the biphasic SPC111 cell line.

Secreted VEGF-A has an important role in the regulation of capillary plexus formation on the diaphragmatic surface, as proved by the results obtained from the VEGF-A overexpressing SPC111 transfected model.

Our preclinical testing on the potential of nintedanib as a treatment for PM yielded promising results. We determined that the target receptors of nintedanib are co-expressed on human PM cells. Furthermore, nintedanib inhibits PM cell growth, proliferation, and migration *in vitro*. Moreover, we showed that nintedanib potently reduces tumor growth and vascularization in mice with orthotopically growing human PM xenografts. Interestingly, these *in vivo* antivascular and antineoplastic effects of nintedanib are more robust in tumors with low baseline VEGF-A expression than the effects of bevacizumab. Our findings offer valuable insights into the formation and vascularization of PM nodules and provide evidence that nintedanib has the potential to inhibit angiogenesis and tumor growth in PM, both *in vitro* and *in vivo*. These results can potentially form the foundation for personalized therapeutic approaches and future biomarker studies in PM patients.

7. Summary

PM is a rare and aggressive cancer that remains challenging to treat since no truly effective treatment option has been yet established. Tumor vasculature plays a vital role in the progression and therapy resistance mechanisms of solid tumors, making it a potential therapeutic target. Previous studies proved that PM is an angiogenic tumor, and based on the benefits of bevacizumab treatment, anti-angiogenic therapy plays an essential role in the care of PM patients. Understanding how PM vascularizes may provide insights into potential targets for therapeutic interventions. We studied vascularization and anti-angiogenic therapy responses of PM nodules using human PM cell lines from different subtypes. Epithelioid (P31) and biphasic (SPC111) cells were orthotopically implanted into the thoracic cavity of immunodeficient mice to establish orthotopic tumor colonies. By analyzing the tumor nodules growing on the surface of the diaphragm, we found significant differences between the vascularization processes of the two cell lines. The P31 tumors grow well-vascularized nodules from early stages of development, while the SPC111 tumors remained avascular for weeks. The initial step of SPC111 tumor vascularization is a desmoplastic matrix deposition at the base of the nodules. Then the layer-by-layer incorporation of this matrix by the tumors facilitate the vascular ingrowth from the sprouting of diaphragmatic vessels. On the molecular level, significant differences were found in COL1A1 mRNA expression and VEGF-A protein secretion; both are overexpressed in the well-vascularized P31 cell line. The crucial role of VEGF-A in the development of vessel proliferations was confirmed by the extensive diaphragmatic capillary growth induced by the orthotopically implanted VEGF-A overexpressing xenografts. Significant differences were also observed in the *in vitro* behavior of the cell lines. Accordingly, P31 was more invasive, motile, and less repellent toward HUVEC sprouts in co-cultures. Our *in vivo* PM xenograft study was the first preclinical study that analyzed the preclinical therapeutic efficiency of nintedanib in PM. We examined the expression of nintedanib's target receptor tyrosine kinases in 20 PM and 4 control cell lines and showed that they are (co)expressed in PM cells. Nintedanib effectively decreases PM proliferation and migration *in vitro*. Our findings also indicate that nintedanib demonstrates significant VEGF-A expression-independent PM growth inhibition *in vivo*, ultimately leading to reduced tumor burden and longer survival rates for PM-bearing animals.

8. References

1. Bou-Samra, P., A. Chang, F. Azari, G. Kennedy, A. Segil, E. Guo, M. Marmarelis, C. Langer, and S. Singhal, *Epidemiological, therapeutic, and survival trends in malignant pleural mesothelioma: A review of the National Cancer Database.* Cancer Med, 2023.
2. Shavelle, R., K. Vavra-Musser, J. Lee, and J. Brooks, *Life Expectancy in Pleural and Peritoneal Mesothelioma.* Lung Cancer Int, 2017. **2017**: p. 2782590.
3. Krowczynska, M. and E. Wilk, *Environmental and Occupational Exposure to Asbestos as a Result of Consumption and Use in Poland.* Int J Environ Res Public Health, 2019. **16**(14).
4. Woolhouse, I., L. Bishop, L. Darlison, D. De Fonseka, A. Edey, J. Edwards, C. Faivre-Finn, D.A. Fennell, S. Holmes, K.M. Kerr, A. Nakas, T. Peel, N.M. Rahman, M. Slade, J. Steele, S. Tsim, and N.A. Maskell, *British Thoracic Society Guideline for the investigation and management of malignant pleural mesothelioma.* Thorax, 2018. **73**(Suppl 1): p. i1-i30.
5. Frost, G., *The latency period of mesothelioma among a cohort of British asbestos workers (1978-2005).* Br J Cancer, 2013. **109**(7): p. 1965-73.
6. Selikoff, I.J., E.C. Hammond, and H. Seidman, *Latency of asbestos disease among insulation workers in the United States and Canada.* Cancer, 1980. **46**(12): p. 2736-40.
7. Bianchi, C. and T. Bianchi, *Global mesothelioma epidemic: Trend and features.* Indian J Occup Environ Med, 2014. **18**(2): p. 82-8.
8. Huang, J., S.C. Chan, W.S. Pang, S.H. Chow, V. Lok, L. Zhang, X. Lin, D.E. Lucero-Prisno, 3rd, W. Xu, Z.J. Zheng, E. Elcarte, M. Withers, M.C.S. Wong, and A.o.P.R.U. Ncd Global Health Research Group, *Global Incidence, Risk Factors, and Temporal Trends of Mesothelioma: A Population-Based Study.* J Thorac Oncol, 2023. **18**(6): p. 792-802.
9. Marsili, D., B. Terracini, V.S. Santana, J.P. Ramos-Bonilla, R. Pasetto, A. Mazzeo, D. Loomis, P. Comba, and E. Algranti, *Prevention of Asbestos-Related Disease in Countries Currently Using Asbestos.* Int J Environ Res Public Health, 2016. **13**(5).

10. Roe, O.D. and G.M. Stella, *Malignant pleural mesothelioma: history, controversy and future of a manmade epidemic.* Eur Respir Rev, 2015. **24**(135): p. 115-31.
11. Zhai, Z., J. Ruan, Y. Zheng, D. Xiang, N. Li, J. Hu, J. Shen, Y. Deng, J. Yao, P. Zhao, S. Wang, S. Yang, L. Zhou, Y. Wu, P. Xu, L. Lyu, J. Lyu, R. Bergan, T. Chen, and Z. Dai, *Assessment of Global Trends in the Diagnosis of Mesothelioma From 1990 to 2017.* JAMA Netw Open, 2021. **4**(8): p. e2120360.
12. Liu, B., M. van Gerwen, S. Bonassi, E. Taioli, and F. International Association for the Study of Lung Cancer Mesothelioma Task, *Epidemiology of Environmental Exposure and Malignant Mesothelioma.* J Thorac Oncol, 2017. **12**(7): p. 1031-1045.
13. Taioli, E., A.S. Wolf, M. Camacho-Rivera, and R.M. Flores, *Women with malignant pleural mesothelioma have a threefold better survival rate than men.* Ann Thorac Surg, 2014. **98**(3): p. 1020-4.
14. Sirri, E., J. Kieschke, C. Vohmann, A. Katalinic, A. Nennecke, M. Ressing, A. Eberle, B. Holleczek, L. Jansen, H. Brenner, and G.C.S.W. Group, *Survival of malignant mesothelioma and other rare thoracic cancers in Germany and the United States: A population-based study.* Int J Cancer, 2020. **147**(6): p. 1548-1558.
15. Luberto, F., D. Ferrante, S. Silvestri, A. Angelini, F. Cuccaro, A.M. Nannavecchia, E. Oddone, M. Vicentini, F. Barone-Adesi, T. Cena, D. Mirabelli, L. Mangone, F. Roncaglia, O. Sala, S. Menegozzo, R. Pirastu, D. Azzolina, S. Tunesi, E. Chellini, L. Miligi, P. Perticaroli, A. Pettinari, V. Bressan, E. Merler, P. Girardi, L. Bisceglia, A. Marinaccio, S. Massari, C. Magnani, and g. working, *Cumulative asbestos exposure and mortality from asbestos related diseases in a pooled analysis of 21 asbestos cement cohorts in Italy.* Environ Health, 2019. **18**(1): p. 71.
16. Bocchetta, M., I. Di Resta, A. Powers, R. Fresco, A. Tosolini, J.R. Testa, H.I. Pass, P. Rizzo, and M. Carbone, *Human mesothelial cells are unusually susceptible to simian virus 40-mediated transformation and asbestos cocarcinogenicity.* Proc Natl Acad Sci U S A, 2000. **97**(18): p. 10214-9.
17. Boffetta, P., M. Malvezzi, E. Pira, E. Negri, and C. La Vecchia, *International Analysis of Age-Specific Mortality Rates From Mesothelioma on the Basis of the*

International Classification of Diseases, 10th Revision. J Glob Oncol, 2018. **4**: p. 1-15.

18. Thomas, A., Y. Chen, T. Yu, A. Gill, and V. Prasad, *Distinctive clinical characteristics of malignant mesothelioma in young patients.* Oncotarget, 2015. **6**(18): p. 16766-73.
19. McDonald, J.C. and A.D. McDonald, *The epidemiology of mesothelioma in historical context.* Eur Respir J, 1996. **9**(9): p. 1932-42.
20. Wagner, J.C., C.A. Sleggs, and P. Marchand, *Diffuse pleural mesothelioma and asbestos exposure in the North Western Cape Province.* Br J Ind Med, 1960. **17**: p. 260-71.
21. Yano, E., *Adverse health effects of asbestos: solving mysteries regarding asbestos carcinogenicity based on follow-up survey of a Chinese factory.* Environ Health Prev Med, 2018. **23**(1): p. 35.
22. Hodgson, J.T. and A. Darnton, *The quantitative risks of mesothelioma and lung cancer in relation to asbestos exposure.* Ann Occup Hyg, 2000. **44**(8): p. 565-601.
23. Gilham, C., C. Rake, G. Burdett, A.G. Nicholson, L. Davison, A. Franchini, J. Carpenter, J. Hodgson, A. Darnton, and J. Peto, *Pleural mesothelioma and lung cancer risks in relation to occupational history and asbestos lung burden.* Occup Environ Med, 2016. **73**(5): p. 290-9.
24. Malcolm Ross, R.P.N., *History of asbestos discovery and use and asbestos-related disease in context with the occurrence of asbestos within ophiolite complexes.* Geological Society of America Special Papers, 2003. **373**: p. 447-470.
25. Attanoos, R.L., A. Churg, F. Galateau-Salle, A.R. Gibbs, and V.L. Roggli, *Malignant Mesothelioma and Its Non-Asbestos Causes.* Arch Pathol Lab Med, 2018. **142**(6): p. 753-760.
26. Panou, V., M. Vyberg, U.M. Weinreich, C. Meristoudis, U.G. Falkmer, and O.D. Roe, *The established and future biomarkers of malignant pleural mesothelioma.* Cancer Treat Rev, 2015. **41**(6): p. 486-95.
27. Wagner, J.C., J.W. Skidmore, R.J. Hill, and D.M. Griffiths, *Erionite exposure and mesotheliomas in rats.* Br J Cancer, 1985. **51**(5): p. 727-30.

28. Ryman-Rasmussen, J.P., M.F. Cesta, A.R. Brody, J.K. Shipley-Phillips, J.I. Everitt, E.W. Tewksbury, O.R. Moss, B.A. Wong, D.E. Dodd, M.E. Andersen, and J.C. Bonner, *Inhaled carbon nanotubes reach the subpleural tissue in mice.* Nat Nanotechnol, 2009. **4**(11): p. 747-51.
29. Nagai, H., Y. Okazaki, S.H. Chew, N. Misawa, Y. Yamashita, S. Akatsuka, T. Ishihara, K. Yamashita, Y. Yoshikawa, H. Yasui, L. Jiang, H. Ohara, T. Takahashi, G. Ichihara, K. Kostarelos, Y. Miyata, H. Shinohara, and S. Toyokuni, *Diameter and rigidity of multiwalled carbon nanotubes are critical factors in mesothelial injury and carcinogenesis.* Proc Natl Acad Sci U S A, 2011. **108**(49): p. E1330-8.
30. Nel, A., *Carbon nanotube pathogenicity conforms to a unified theory for mesothelioma causation by elongate materials and fibers.* Environ Res, 2023. **230**: p. 114580.
31. Dong, J. and Q. Ma, *Integration of inflammation, fibrosis, and cancer induced by carbon nanotubes.* Nanotoxicology, 2019. **13**(9): p. 1244-1274.
32. Cicala, C., F. Pompetti, and M. Carbone, *SV40 induces mesotheliomas in hamsters.* Am J Pathol, 1993. **142**(5): p. 1524-33.
33. Carbone, M., H.I. Pass, P. Rizzo, M. Marinetti, M. Di Muzio, D.J. Mew, A.S. Levine, and A. Procopio, *Simian virus 40-like DNA sequences in human pleural mesothelioma.* Oncogene, 1994. **9**(6): p. 1781-90.
34. Galateau-Salle, F., P. Bidet, Y. Iwatsubo, E. Gennetay, A. Renier, M. Letourneux, J.C. Pairon, S. Moritz, P. Brochard, M.C. Jaurand, and F. Freymuth, *SV40-like DNA sequences in pleural mesothelioma, bronchopulmonary carcinoma, and non-malignant pulmonary diseases.* J Pathol, 1998. **184**(3): p. 252-7.
35. Rotondo, J.C., E. Mazzoni, I. Bononi, M. Tognon, and F. Martini, *Association Between Simian Virus 40 and Human Tumors.* Front Oncol, 2019. **9**: p. 670.
36. Testa, J.R., M. Carbone, A. Hirvonen, K. Khalili, B. Krynska, K. Linnainmaa, F.D. Pooley, P. Rizzo, V. Rusch, and G.H. Xiao, *A multi-institutional study confirms the presence and expression of simian virus 40 in human malignant mesotheliomas.* Cancer Res, 1998. **58**(20): p. 4505-9.

37. De Rienzo, A., M. Tor, D.H. Sterman, F. Aksoy, S.M. Albelda, and J.R. Testa, *Detection of SV40 DNA sequences in malignant mesothelioma specimens from the United States, but not from Turkey.* J Cell Biochem, 2002. **84**(3): p. 455-9.
38. Hirvonen, A., K. Mattson, A. Karjalainen, T. Ollikainen, L. Tammilehto, T. Hovi, H. Vainio, H.I. Pass, I. Di Resta, M. Carbone, and K. Linnainmaa, *Simian virus 40 (SV40)-like DNA sequences not detectable in finnish mesothelioma patients not exposed to SV40-contaminated polio vaccines.* Mol Carcinog, 1999. **26**(2): p. 93-9.
39. Teta, M.J., E. Lau, B.K. Sceurman, and M.E. Wagner, *Therapeutic radiation for lymphoma: risk of malignant mesothelioma.* Cancer, 2007. **109**(7): p. 1432-8.
40. Carbone, M., L.K. Ferris, F. Baumann, A. Napolitano, C.A. Lum, E.G. Flores, G. Gaudino, A. Powers, P. Bryant-Greenwood, T. Krausz, E. Hyjek, R. Tate, J. Friedberg, T. Weigel, H.I. Pass, and H. Yang, *BAP1 cancer syndrome: malignant mesothelioma, uveal and cutaneous melanoma, and MBAITs.* J Transl Med, 2012. **10**: p. 179.
41. Testa, J.R., M. Cheung, J. Pei, J.E. Below, Y. Tan, E. Sementino, N.J. Cox, A.U. Dogan, H.I. Pass, S. Trusa, M. Hesdorffer, M. Nasu, A. Powers, Z. Rivera, S. Comertpay, M. Tanji, G. Gaudino, H. Yang, and M. Carbone, *Germline BAP1 mutations predispose to malignant mesothelioma.* Nat Genet, 2011. **43**(10): p. 1022-5.
42. Masoomian, B., J.A. Shields, and C.L. Shields, *Overview of BAP1 cancer predisposition syndrome and the relationship to uveal melanoma.* J Curr Ophthalmol, 2018. **30**(2): p. 102-109.
43. Baumann, F., E. Flores, A. Napolitano, S. Kanodia, E. Taioli, H. Pass, H. Yang, and M. Carbone, *Mesothelioma patients with germline BAP1 mutations have 7-fold improved long-term survival.* Carcinogenesis, 2015. **36**(1): p. 76-81.
44. Hassan, R., B. Morrow, A. Thomas, T. Walsh, M.K. Lee, S. Gulsuner, M. Gadiraju, V. Panou, S. Gao, I. Mian, J. Khan, M. Raffeld, S. Patel, L. Xi, J.S. Wei, M. Hesdorffer, J. Zhang, K. Calzone, A. Desai, E. Padiernos, C. Alewine, D.S. Schrump, S.M. Steinberg, H.L. Kindler, M.C. King, and J.E. Churpek, *Inherited predisposition to malignant mesothelioma and overall survival following platinum chemotherapy.* Proc Natl Acad Sci U S A, 2019. **116**(18): p. 9008-9013.

45. Asciak, R., V. George, and N.M. Rahman, *Update on biology and management of mesothelioma.* Eur Respir Rev, 2021. **30**(159).
46. Bernstein, D.M., R.A. Rogers, R. Sepulveda, P. Kunzendorf, B. Bellmann, H. Ernst, O. Creutzenberg, and J.I. Phillips, *Evaluation of the fate and pathological response in the lung and pleura of brake dust alone and in combination with added chrysotile compared to crocidolite asbestos following short-term inhalation exposure.* Toxicol Appl Pharmacol, 2015. **283**(1): p. 20-34.
47. Yang, H., Z. Rivera, S. Jube, M. Nasu, P. Bertino, C. Goparaju, G. Franzoso, M.T. Lotze, T. Krausz, H.I. Pass, M.E. Bianchi, and M. Carbone, *Programmed necrosis induced by asbestos in human mesothelial cells causes high-mobility group box 1 protein release and resultant inflammation.* Proc Natl Acad Sci U S A, 2010. **107**(28): p. 12611-6.
48. Tanaka, S., N. Choe, A. Iwagaki, D.R. Hemenway, and E. Kagan, *Asbestos exposure induces MCP-1 secretion by pleural mesothelial cells.* Exp Lung Res, 2000. **26**(4): p. 241-55.
49. Acencio, M.M., B. Soares, E. Marchi, C.S. Silva, L.R. Teixeira, and V.C. Broaddus, *Inflammatory Cytokines Contribute to Asbestos-Induced Injury of Mesothelial Cells.* Lung, 2015. **193**(5): p. 831-7.
50. Yang, H., M. Bocchetta, B. Kroczynska, A.G. Elmishad, Y. Chen, Z. Liu, C. Bubici, B.T. Mossman, H.I. Pass, J.R. Testa, G. Franzoso, and M. Carbone, *TNF-alpha inhibits asbestos-induced cytotoxicity via a NF-kappaB-dependent pathway, a possible mechanism for asbestos-induced oncogenesis.* Proc Natl Acad Sci U S A, 2006. **103**(27): p. 10397-10402.
51. Liao, D., Q. Wang, J. He, D.B. Alexander, M. Abdelgied, A.M. El-Gazzar, M. Futakuchi, M. Suzui, J. Kanno, A. Hirose, J. Xu, and H. Tsuda, *Persistent Pleural Lesions and Inflammation by Pulmonary Exposure of Multiwalled Carbon Nanotubes.* Chem Res Toxicol, 2018. **31**(10): p. 1025-1031.
52. Sekido, Y., *Molecular pathogenesis of malignant mesothelioma.* Carcinogenesis, 2013. **34**(7): p. 1413-9.
53. Benedetti, S., B. Nuvoli, S. Catalani, and R. Galati, *Reactive oxygen species a double-edged sword for mesothelioma.* Oncotarget, 2015. **6**(19): p. 16848-65.

54. Xue, J., S. Patergnani, C. Giorgi, J. Suarez, K. Goto, A. Bononi, M. Tanji, F. Novelli, S. Pastorino, R. Xu, N. Caroccia, A.U. Dogan, H.I. Pass, M. Tognon, P. Pinton, G. Gaudino, T.W. Mak, M. Carbone, and H. Yang, *Asbestos induces mesothelial cell transformation via HMGB1-driven autophagy.* Proc Natl Acad Sci U S A, 2020. **117**(41): p. 25543-25552.

55. Bueno, R., E.W. Stawiski, L.D. Goldstein, S. Durinck, A. De Rienzo, Z. Modrusan, F. Gnad, T.T. Nguyen, B.S. Jaiswal, L.R. Chirieac, D. Sciaranghella, N. Dao, C.E. Gustafson, K.J. Munir, J.A. Hackney, A. Chaudhuri, R. Gupta, J. Guillory, K. Toy, C. Ha, Y.J. Chen, J. Stinson, S. Chaudhuri, N. Zhang, T.D. Wu, D.J. Sugarbaker, F.J. de Sauvage, W.G. Richards, and S. Seshagiri, *Comprehensive genomic analysis of malignant pleural mesothelioma identifies recurrent mutations, gene fusions and splicing alterations.* Nat Genet, 2016. **48**(4): p. 407-16.

56. Hylebos, M., G. Van Camp, J.P. van Meerbeeck, and K. Op de Beeck, *The Genetic Landscape of Malignant Pleural Mesothelioma: Results from Massively Parallel Sequencing.* J Thorac Oncol, 2016. **11**(10): p. 1615-26.

57. Carbone, M., G. Gaudino, and H. Yang, *Recent insights emerging from malignant mesothelioma genome sequencing.* J Thorac Oncol, 2015. **10**(3): p. 409-11.

58. Guo, G., J. Chmielecki, C. Goparaju, A. Heguy, I. Dolgalev, M. Carbone, S. Seepo, M. Meyerson, and H.I. Pass, *Whole-exome sequencing reveals frequent genetic alterations in BAP1, NF2, CDKN2A, and CUL1 in malignant pleural mesothelioma.* Cancer Res, 2015. **75**(2): p. 264-9.

59. Hmeljak, J., F. Sanchez-Vega, K.A. Hoadley, J. Shih, C. Stewart, D. Heiman, P. Tarpey, L. Danilova, E. Drill, E.A. Gibb, R. Bowlby, R. Kanchi, H.U. Osmanbeyoglu, Y. Sekido, J. Takeshita, Y. Newton, K. Graim, M. Gupta, C.M. Gay, L. Diao, D.L. Gibbs, V. Thorsson, L. Iype, H. Kantheti, D.T. Severson, G. Ravegnini, P. Desmeules, A.A. Jungbluth, W.D. Travis, S. Dacic, L.R. Chirieac, F. Galateau-Salle, J. Fujimoto, A.N. Husain, H.C. Silveira, V.W. Rusch, R.C. Rintoul, H. Pass, H. Kindler, M.G. Zauderer, D.J. Kwiatkowski, R. Bueno, A.S. Tsao, J. Creaney, T. Lichtenberg, K. Leraas, J. Bowen, T.R. Network, I. Felau, J.C. Zenklusen, R. Akbani, A.D. Cherniack, L.A. Byers, M.S. Noble, J.A. Fletcher, A.G. Robertson, R. Shen, H. Aburatani, B.W. Robinson, P. Campbell,

and M. Ladanyi, *Integrative Molecular Characterization of Malignant Pleural Mesothelioma.* Cancer Discov, 2018. **8**(12): p. 1548-1565.

60. Lo Iacono, M., V. Monica, L. Righi, F. Grosso, R. Libener, S. Vatrano, P. Bironzo, S. Novello, L. Musmeci, M. Volante, M. Papotti, and G.V. Scagliotti, *Targeted next-generation sequencing of cancer genes in advanced stage malignant pleural mesothelioma: a retrospective study.* J Thorac Oncol, 2015. **10**(3): p. 492-9.
61. Hiltbrunner, S., Z. Fleischmann, E.S. Sokol, M. Zoche, E. Felley-Bosco, and A. Curioni-Fontecedro, *Genomic landscape of pleural and peritoneal mesothelioma tumours.* Br J Cancer, 2022. **127**(11): p. 1997-2005.
62. Sage, A.P., V.D. Martinez, B.C. Minatel, M.E. Pewarchuk, E.A. Marshall, G.M. MacAulay, R. Hubaux, D.D. Pearson, A.A. Goodarzi, G. Dellaire, and W.L. Lam, *Genomics and Epigenetics of Malignant Mesothelioma.* High Throughput, 2018. **7**(3).
63. Singhi, A.D., A.M. Krasinskas, H.A. Choudry, D.L. Bartlett, J.F. Pingpank, H.J. Zeh, A. Luvison, K. Fuhrer, N. Bahary, R.R. Seethala, and S. Dacic, *The prognostic significance of BAP1, NF2, and CDKN2A in malignant peritoneal mesothelioma.* Mod Pathol, 2016. **29**(1): p. 14-24.
64. Baldwin, D., M. Callister, A. Akram, P. Cane, J. Draffan, K. Franks, F. Gleeson, R. Graham, P. Malhotra, P. Pearson, M. Subesinghe, D. Waller, and I. Woolhouse, *British Thoracic Society quality standards for the investigation and management of pulmonary nodules.* BMJ Open Respir Res, 2018. **5**(1): p. e000273.
65. Yap, T.A., J.G. Aerts, S. Popat, and D.A. Fennell, *Novel insights into mesothelioma biology and implications for therapy.* Nat Rev Cancer, 2017. **17**(8): p. 475-488.
66. Le Stang, N., L. Burke, G. Blaizot, A.R. Gibbs, P. Lebailly, B. Clin, N. Girard, F. Galateau-Salle, Mesopath, and E. networks, *Differential Diagnosis of Epithelioid Malignant Mesothelioma With Lung and Breast Pleural Metastasis: A Systematic Review Compared With a Standardized Panel of Antibodies-A New Proposal That May Influence Pathologic Practice.* Arch Pathol Lab Med, 2020. **144**(4): p. 446-456.
67. Carbone, M., P.S. Adusumilli, H.R. Alexander, Jr., P. Baas, F. Bardelli, A. Bononi, R. Bueno, E. Felley-Bosco, F. Galateau-Salle, D. Jablons, A.S.

Mansfield, M. Minaai, M. de Perrot, P. Pesavento, V. Rusch, D.T. Severson, E. Taioli, A. Tsao, G. Woodard, H. Yang, M.G. Zauderer, and H.I. Pass, *Mesothelioma: Scientific clues for prevention, diagnosis, and therapy.* CA Cancer J Clin, 2019. **69**(5): p. 402-429.

68. Husain, A.N., T.V. Colby, N.G. Ordonez, T.C. Allen, R.L. Attanoos, M.B. Beasley, K.J. Butnor, L.R. Chirieac, A.M. Churg, S. Dacic, F. Galateau-Salle, A. Gibbs, A.M. Gown, T. Krausz, L.A. Litzky, A. Marchevsky, A.G. Nicholson, V.L. Roggli, A.K. Sharma, W.D. Travis, A.E. Walts, and M.R. Wick, *Guidelines for Pathologic Diagnosis of Malignant Mesothelioma 2017 Update of the Consensus Statement From the International Mesothelioma Interest Group.* Arch Pathol Lab Med, 2018. **142**(1): p. 89-108.
69. Sauter, J.L., S. Dacic, F. Galateau-Salle, R.L. Attanoos, K.J. Butnor, A. Churg, A.N. Husain, K. Kadota, A. Khoor, A.G. Nicholson, V. Roggli, F. Schmitt, M.S. Tsao, and W.D. Travis, *The 2021 WHO Classification of Tumors of the Pleura: Advances Since the 2015 Classification.* J Thorac Oncol, 2022. **17**(5): p. 608-622.
70. Patel, S.C. and J.E. Dowell, *Modern management of malignant pleural mesothelioma.* Lung Cancer (Auckl), 2016. **7**: p. 63-72.
71. Travis, W.D., *The 2015 WHO classification of lung tumors.* Pathologe, 2014. **35 Suppl 2**: p. 188.
72. Verma, V., C.A. Ahern, C.G. Berlind, W.D. Lindsay, J. Shabason, S. Sharma, M.J. Culligan, S. Grover, J.S. Friedberg, and C.B. Simone, 2nd, *Survival by Histologic Subtype of Malignant Pleural Mesothelioma and the Impact of Surgical Resection on Overall Survival.* Clin Lung Cancer, 2018. **19**(6): p. e901-e912.
73. Metaxas, Y., G. Rivalland, L.A. Mauti, D. Klingbiel, S. Kao, S. Schmid, A.K. Nowak, O. Gautschi, T. Bartnick, B.G. Hughes, H. Bouchaab, S.I. Rothschild, N. Pavlakis, S. Wolleb, U. Petrausch, K. O'Byrne, P. Froesch, M. Loffler-Baumann, S. Pratsch-Peter, P. Russell, W. Mingrone, S. Savic, B. Thapa, M. Fruh, M. Pless, R. von Moos, and T. John, *Pembrolizumab as Palliative Immunotherapy in Malignant Pleural Mesothelioma.* J Thorac Oncol, 2018. **13**(11): p. 1784-1791.
74. Galateau Salle, F., N. Le Stang, A.G. Nicholson, D. Pissaloux, A. Churg, S. Klebe, V.L. Roggli, H.D. Tazelaar, J.M. Vignaud, R. Attanoos, M.B. Beasley, H.

Begueret, F. Capron, L. Chirieac, M.C. Copin, S. Dacic, C. Danel, A. Foulet-Roge, A. Gibbs, S. Giusiano-Courcambeck, K. Hiroshima, V. Hofman, A.N. Husain, K. Kerr, A. Marchevsky, K. Nabeshima, J.M. Picquenot, I. Rouquette, C. Sagan, J.L. Sauter, F. Thivolet, W.D. Travis, M.S. Tsao, B. Weynand, F. Damiola, A. Scherpereel, J.C. Pairon, S. Lantuejoul, V. Rusch, and N. Girard, *New Insights on Diagnostic Reproducibility of Biphasic Mesotheliomas: A Multi-Institutional Evaluation by the International Mesothelioma Panel From the MESOPATH Reference Center.* J Thorac Oncol, 2018. **13**(8): p. 1189-1203.

75. Vigneswaran, W.T., D.Y. Kircheva, V. Ananthanarayanan, S. Watson, Q. Arif, A.D. Celauro, H.L. Kindler, and A.N. Husain, *Amount of Epithelioid Differentiation Is a Predictor of Survival in Malignant Pleural Mesothelioma.* Ann Thorac Surg, 2017. **103**(3): p. 962-966.

76. Oehl, K., B. Vrugt, I. Opitz, and M. Meerang, *Heterogeneity in Malignant Pleural Mesothelioma.* Int J Mol Sci, 2018. **19**(6).

77. de Reynies, A., M.C. Jaurand, A. Renier, G. Couchy, I. Hysi, N. Elarouci, F. Galateau-Salle, M.C. Copin, P. Hofman, A. Cazes, P. Andujar, S. Imbeaud, F. Petel, J.C. Pairon, F. Le Pimpec-Barthes, J. Zucman-Rossi, and D. Jean, *Molecular classification of malignant pleural mesothelioma: identification of a poor prognosis subgroup linked to the epithelial-to-mesenchymal transition.* Clin Cancer Res, 2014. **20**(5): p. 1323-34.

78. Tranchant, R., L. Quetel, A. Tallet, C. Meiller, A. Renier, L. de Koning, A. de Reynies, F. Le Pimpec-Barthes, J. Zucman-Rossi, M.C. Jaurand, and D. Jean, *Co-occurring Mutations of Tumor Suppressor Genes, LATS2 and NF2, in Malignant Pleural Mesothelioma.* Clin Cancer Res, 2017. **23**(12): p. 3191-3202.

79. Blum, Y., C. Meiller, L. Quetel, N. Elarouci, M. Ayadi, D. Tashtanbaeva, L. Armenoult, F. Montagne, R. Tranchant, A. Renier, L. de Koning, M.C. Copin, P. Hofman, V. Hofman, H. Porte, F. Le Pimpec-Barthes, J. Zucman-Rossi, M.C. Jaurand, A. de Reynies, and D. Jean, *Dissecting heterogeneity in malignant pleural mesothelioma through histo-molecular gradients for clinical applications.* Nat Commun, 2019. **10**(1): p. 1333.

80. Odgerel, C.O., K. Takahashi, T. Sorahan, T. Driscoll, C. Fitzmaurice, O.M. Yoko, K. Sawanyawisuth, S. Furuya, F. Tanaka, S. Horie, N.V. Zandwijk, and J. Takala,

Estimation of the global burden of mesothelioma deaths from incomplete national mortality data. Occup Environ Med, 2017. **74**(12): p. 851-858.

81. Bibby, A.C., S. Tsim, N. Kanellakis, H. Ball, D.C. Talbot, K.G. Blyth, N.A. Maskell, and I. Psallidas, *Malignant pleural mesothelioma: an update on investigation, diagnosis and treatment.* Eur Respir Rev, 2016. **25**(142): p. 472-486.
82. Rusch, V.W., K. Chansky, H.L. Kindler, A.K. Nowak, H.I. Pass, D.C. Rice, L. Shemanski, F. Galateau-Salle, B.C. McCaughan, T. Nakano, E. Ruffini, J.P. van Meerbeeck, M. Yoshimura, I. Staging, a.b. Prognostic Factors Committee, and i. participating, *The IASLC Mesothelioma Staging Project: Proposals for the M Descriptors and for Revision of the TNM Stage Groupings in the Forthcoming (Eighth) Edition of the TNM Classification for Mesothelioma.* J Thorac Oncol, 2016. **11**(12): p. 2112-2119.
83. Baas, P., A. Scherpereel, A.K. Nowak, N. Fujimoto, S. Peters, A.S. Tsao, A.S. Mansfield, S. Popat, T. Jahan, S. Antonia, Y. Oulkhouir, Y. Bautista, R. Cornelissen, L. Greillier, F. Grossi, D. Kowalski, J. Rodriguez-Cid, P. Aanur, A. Oukessou, C. Baudelet, and G. Zalcman, *First-line nivolumab plus ipilimumab in unresectable malignant pleural mesothelioma (CheckMate 743): a multicentre, randomised, open-label, phase 3 trial.* Lancet, 2021. **397**(10272): p. 375-386.
84. Treasure, T., L. Lang-Lazdunski, D. Waller, J.M. Bliss, C. Tan, J. Entwisle, M. Snee, M. O'Brien, G. Thomas, S. Senan, K. O'Byrne, L.S. Kilburn, J. Spicer, D. Landau, J. Edwards, G. Coombes, L. Darlison, J. Peto, and M. trialists, *Extra-pleural pneumonectomy versus no extra-pleural pneumonectomy for patients with malignant pleural mesothelioma: clinical outcomes of the Mesothelioma and Radical Surgery (MARS) randomised feasibility study.* Lancet Oncol, 2011. **12**(8): p. 763-72.
85. Verma, V., R.E. Wegner, E.B. Ludmir, S. Hasan, A. Colonias, S. Grover, J.S. Friedberg, and C.B. Simone, 2nd, *Management of Malignant Pleural Mesothelioma in the Elderly Population.* Ann Surg Oncol, 2019. **26**(8): p. 2357-2366.
86. Popat, S., P. Baas, C. Faivre-Finn, N. Girard, A.G. Nicholson, A.K. Nowak, I. Opitz, A. Scherpereel, M. Reck, and E.G.C.E.a. clinicalguidelines@esmo.org,

Malignant pleural mesothelioma: ESMO Clinical Practice Guidelines for diagnosis, treatment and follow-up(). Ann Oncol, 2022. **33**(2): p. 129-142.

87. Kindler, H.L., N. Ismaila, S.G. Armato, 3rd, R. Bueno, M. Hesdorffer, T. Jahan, C.M. Jones, M. Miettinen, H. Pass, A. Rimner, V. Rusch, D. Sterman, A. Thomas, and R. Hassan, *Treatment of Malignant Pleural Mesothelioma: American Society of Clinical Oncology Clinical Practice Guideline.* J Clin Oncol, 2018. **36**(13): p. 1343-1373.
88. Meyerhoff, R.R., C.F. Yang, P.J. Speicher, B.C. Gulack, M.G. Hartwig, T.A. D'Amico, D.H. Harpole, and M.F. Berry, *Impact of mesothelioma histologic subtype on outcomes in the Surveillance, Epidemiology, and End Results database.* J Surg Res, 2015. **196**(1): p. 23-32.
89. Bovolato, P., C. Casadio, A. Bille, F. Ardissone, L. Santambrogio, G.B. Ratto, G. Garofalo, A.V. Bedini, M. Garassino, L. Porcu, V. Torri, and U. Pastorino, *Does surgery improve survival of patients with malignant pleural mesothelioma?: a multicenter retrospective analysis of 1365 consecutive patients.* J Thorac Oncol, 2014. **9**(3): p. 390-6.
90. Yan, T.D., M. Boyer, M.M. Tin, D. Wong, C. Kennedy, J. McLean, P.G. Bannon, and B.C. McCaughan, *Extrapleural pneumonectomy for malignant pleural mesothelioma: outcomes of treatment and prognostic factors.* J Thorac Cardiovasc Surg, 2009. **138**(3): p. 619-24.
91. Sugarbaker, D.J., M.T. Jaklitsch, R. Bueno, W. Richards, J. Lukanich, S.J. Mentzer, Y. Colson, P. Linden, M. Chang, L. Capalbo, E. Oldread, S. Neragi-Miandoab, S.J. Swanson, and L.S. Zellos, *Prevention, early detection, and management of complications after 328 consecutive extrapleural pneumonectomies.* J Thorac Cardiovasc Surg, 2004. **128**(1): p. 138-46.
92. Ettinger, D.S., D.E. Wood, W. Akerley, L.A. Bazhenova, H. Borghaei, D.R. Camidge, R.T. Cheney, L.R. Chirieac, T.A. D'Amico, T. Dilling, M. Dobelbower, R. Govindan, M. Hennon, L. Horn, T.M. Jahan, R. Komaki, R.P. Lackner, M. Lanuti, R. Lilenbaum, J. Lin, B.W. Loo, Jr., R. Martins, G.A. Otterson, J.D. Patel, K.M. Pisters, K. Reckamp, G.J. Riely, S.E. Schild, T.A. Shapiro, N. Sharma, S.J. Swanson, J. Stevenson, K. Tauer, S.C. Yang, K. Gregory, and M. Hughes, *NCCN*

Guidelines Insights: Malignant Pleural Mesothelioma, Version 3.2016. J Natl Compr Canc Netw, 2016. **14**(7): p. 825-36.

93. Rice, D., V. Rusch, H. Pass, H. Asamura, T. Nakano, J. Edwards, D.J. Giroux, S. Hasegawa, K.H. Kernstine, D. Waller, R. Rami-Porta, C. International Association for the Study of Lung Cancer International Staging, and G. the International Mesothelioma Interest, *Recommendations for uniform definitions of surgical techniques for malignant pleural mesothelioma: a consensus report of the international association for the study of lung cancer international staging committee and the international mesothelioma interest group.* J Thorac Oncol, 2011. **6**(8): p. 1304-12.
94. Cao, C., D. Tian, J. Park, J. Allan, K.A. Pataky, and T.D. Yan, *A systematic review and meta-analysis of surgical treatments for malignant pleural mesothelioma.* Lung Cancer, 2014. **83**(2): p. 240-5.
95. Schwartz, R.M., W. Lieberman-Cribbin, A. Wolf, R.M. Flores, and E. Taioli, *Systematic review of quality of life following pleurectomy decortication and extrapleural pneumonectomy for malignant pleural mesothelioma.* BMC Cancer, 2018. **18**(1): p. 1188.
96. Vogelzang, N.J., J.J. Rusthoven, J. Symanowski, C. Denham, E. Kaukel, P. Ruffie, U. Gatzemeier, M. Boyer, S. Emri, C. Manegold, C. Niyikiza, and P. Paoletti, *Phase III study of pemetrexed in combination with cisplatin versus cisplatin alone in patients with malignant pleural mesothelioma.* J Clin Oncol, 2003. **21**(14): p. 2636-44.
97. Pasello, G., G. Marulli, V. Polo, C. Breda, L. Bonanno, L. Loreggian, F. Rea, and A. Favaretto, *Pemetrexed plus carboplatin or cisplatin as neoadjuvant treatment of operable malignant pleural mesothelioma (MPM).* Anticancer Res, 2012. **32**(12): p. 5393-9.
98. Santoro, A., M.E. O'Brien, R.A. Stahel, K. Nackaerts, P. Baas, M. Karthaus, W. Eberhardt, L. Paz-Ares, S. Sundstrom, Y. Liu, V. Ripoche, J. Blatter, C.M. Visseren-Grul, and C. Manegold, *Pemetrexed plus cisplatin or pemetrexed plus carboplatin for chemonaive patients with malignant pleural mesothelioma: results of the International Expanded Access Program.* J Thorac Oncol, 2008. **3**(7): p. 756-63.

99. van Meerbeeck, J.P., R. Gaafar, C. Manegold, R.J. Van Klaveren, E.A. Van Marck, M. Vincent, C. Legrand, A. Bottomley, C. Debruyne, G. Giaccone, R. European Organisation for, G. Treatment of Cancer Lung Cancer, and C. National Cancer Institute of, *Randomized phase III study of cisplatin with or without raltitrexed in patients with malignant pleural mesothelioma: an intergroup study of the European Organisation for Research and Treatment of Cancer Lung Cancer Group and the National Cancer Institute of Canada.* J Clin Oncol, 2005. **23**(28): p. 6881-9.

100. Di Noia, V., E. Vita, M. Ferrara, A. Strippoli, M. Basso, G. Schinzari, A. Cassano, E. Bria, C. Barone, and E. D'Argento, *Malignant Pleural Mesothelioma: Is Tailoring the Second-Line Therapy Really "Raising the Bar?".* Curr Treat Options Oncol, 2019. **20**(3): p. 23.

101. Maio, M., A. Scherpereel, L. Calabro, J. Aerts, S.C. Perez, A. Bearz, K. Nackaerts, D.A. Fennell, D. Kowalski, A.S. Tsao, P. Taylor, F. Grosso, S.J. Antonia, A.K. Nowak, M. Taboada, M. Puglisi, P.K. Stockman, and H.L. Kindler, *Tremelimumab as second-line or third-line treatment in relapsed malignant mesothelioma (DETERMINE): a multicentre, international, randomised, double-blind, placebo-controlled phase 2b trial.* Lancet Oncol, 2017. **18**(9): p. 1261-1273.

102. Alley, E.W., J. Lopez, A. Santoro, A. Morosky, S. Saraf, B. Piperdi, and E. van Brummelen, *Clinical safety and activity of pembrolizumab in patients with malignant pleural mesothelioma (KEYNOTE-028): preliminary results from a non-randomised, open-label, phase 1b trial.* Lancet Oncol, 2017. **18**(5): p. 623-630.

103. Quispel-Janssen, J., V. van der Noort, J.F. de Vries, M. Zimmerman, F. Lalezari, E. Thunnissen, K. Monkhorst, R. Schouten, L. Schunselaar, M. Disselhorst, H. Klomp, K. Hartemink, S. Burgers, W. Buikhuisen, and P. Baas, *Programmed Death 1 Blockade With Nivolumab in Patients With Recurrent Malignant Pleural Mesothelioma.* J Thorac Oncol, 2018. **13**(10): p. 1569-1576.

104. Hassan, R., A. Thomas, J.J. Nemunaitis, M.R. Patel, J. Bennouna, F.L. Chen, J.P. Delord, A. Dowlati, S.T. Kochuparambil, M.H. Taylor, J.D. Powderly, U.N. Vaishampayan, C. Verschraegen, H.J. Grote, A. von Heydebreck, K. Chin, and

J.L. Gulley, *Efficacy and Safety of Avelumab Treatment in Patients With Advanced Unresectable Mesothelioma: Phase 1b Results From the JAVELIN Solid Tumor Trial.* JAMA Oncol, 2019. **5**(3): p. 351-357.

105. Sehgal, K., *Hyperprogression in Patients With Cancer Receiving Immune Checkpoint Inhibitors.* JAMA Netw Open, 2021. **4**(3): p. e211839.
106. Zalcman, G., J. Mazieres, J. Margery, L. Greillier, C. Audigier-Valette, D. Moro-Sibilot, O. Molinier, R. Corre, I. Monnet, V. Gounant, F. Riviere, H. Janicot, R. Gervais, C. Locher, B. Milleron, Q. Tran, M.P. Lebitasy, F. Morin, C. Creveuil, J.J. Parienti, A. Scherpereel, and I. French Cooperative Thoracic, *Bevacizumab for newly diagnosed pleural mesothelioma in the Mesothelioma Avastin Cisplatin Pemetrexed Study (MAPS): a randomised, controlled, open-label, phase 3 trial.* Lancet, 2016. **387**(10026): p. 1405-1414.
107. Li, Q., S. Yano, H. Ogino, W. Wang, H. Uehara, Y. Nishioka, and S. Sone, *The therapeutic efficacy of anti vascular endothelial growth factor antibody, bevacizumab, and pemetrexed against orthotopically implanted human pleural mesothelioma cells in severe combined immunodeficient mice.* Clin Cancer Res, 2007. **13**(19): p. 5918-25.
108. Ogino, H., S. Yano, S. Kakiuchi, T. Yamada, K. Ikuta, E. Nakataki, H. Goto, M. Hanibuchi, Y. Nishioka, A. Ryan, and S. Sone, *Novel dual targeting strategy with vandetanib induces tumor cell apoptosis and inhibits angiogenesis in malignant pleural mesothelioma cells expressing RET oncogenic rearrangement.* Cancer Lett, 2008. **265**(1): p. 55-66.
109. Nutt, J.E., K. O'Toole, D. Gonzalez, and J. Lunec, *Growth inhibition by tyrosine kinase inhibitors in mesothelioma cell lines.* Eur J Cancer, 2009. **45**(9): p. 1684-91.
110. Kindler, H.L., T. Karrison, D.R. Gandara, C. Lu, T.L. Guterz, K. Nichols, H. Chen, W.M. Stadler, and E.E. Vokes, *C5-06: Final analysis of a multi-center, double-blind, placebo-controlled, randomized phase II trial of gemcitabine/cisplatin (GC) plus bevacizumab (B) or placebo (P) in patients with malignant mesothelioma.* J. Thorac. Oncol., 2007. **2**(8): p. S374.
111. Scagliotti, G.V., R. Gaafar, A.K. Nowak, T. Nakano, J. van Meerbeeck, S. Popat, N.J. Vogelzang, F. Grosso, R. Aboelhassan, M. Jakopovic, G.L. Ceresoli, P.

Taylor, F. Orlandi, D.A. Fennell, S. Novello, A. Scherpereel, K. Kuribayashi, S. Cedres, J.B. Sorensen, N. Pavlakis, M. Reck, D. Velema, U. von Wangenheim, M. Kim, J. Barrueco, and A.S. Tsao, *Nintedanib in combination with pemetrexed and cisplatin for chemotherapy-naive patients with advanced malignant pleural mesothelioma (LUME-Meso): a double-blind, randomised, placebo-controlled phase 3 trial.* Lancet Respir Med, 2019. **7**(7): p. 569-580.

112. Cantini, L., R. Hassan, D.H. Sterman, and J. Aerts, *Emerging Treatments for Malignant Pleural Mesothelioma: Where Are We Heading?* Front Oncol, 2020. **10**: p. 343.
113. Borea, F., M.A. Franczak, M. Garcia, M. Perrino, N. Cordua, R.T. Smolenski, G.J. Peters, R. Dziadziuszko, A. Santoro, P.A. Zucali, and E. Giovannetti, *Target Therapy in Malignant Pleural Mesothelioma: Hope or Mirage?* Int J Mol Sci, 2023. **24**(11).
114. Price, A., *What is the role of radiotherapy in malignant pleural mesothelioma?* Oncologist, 2011. **16**(3): p. 359-65.
115. Felmeden, D.C., A.D. Blann, and G.Y. Lip, *Angiogenesis: basic pathophysiology and implications for disease.* Eur Heart J, 2003. **24**(7): p. 586-603.
116. Belotti, D., D. Pinessi, and G. Taraboletti, *Alternative Vascularization Mechanisms in Tumor Resistance to Therapy.* Cancers (Basel), 2021. **13**(8).
117. Folkman, J., *Tumor angiogenesis: therapeutic implications.* N Engl J Med, 1971. **285**(21): p. 1182-6.
118. Gimbrone, M.A., Jr., R.H. Aster, R.S. Cotran, J. Corkery, J.H. Jandl, and J. Folkman, *Preservation of vascular integrity in organs perfused in vitro with a platelet-rich medium.* Nature, 1969. **222**(5188): p. 33-6.
119. De Palma, M., D. Biziato, and T.V. Petrova, *Microenvironmental regulation of tumour angiogenesis.* Nat Rev Cancer, 2017. **17**(8): p. 457-474.
120. Holmes, K., O.L. Roberts, A.M. Thomas, and M.J. Cross, *Vascular endothelial growth factor receptor-2: structure, function, intracellular signalling and therapeutic inhibition.* Cell Signal, 2007. **19**(10): p. 2003-12.
121. Semenza, G.L., *HIF-1 and mechanisms of hypoxia sensing.* Curr Opin Cell Biol, 2001. **13**(2): p. 167-71.

122. Folkman, J., E. Merler, C. Abernathy, and G. Williams, *Isolation of a tumor factor responsible for angiogenesis.* J Exp Med, 1971. **133**(2): p. 275-88.

123. Ferrara, N. and W.J. Henzel, *Pituitary follicular cells secrete a novel heparin-binding growth factor specific for vascular endothelial cells.* Biochem Biophys Res Commun, 1989. **161**(2): p. 851-8.

124. Dvorak, H.F., T.M. Sioussat, L.F. Brown, B. Berse, J.A. Nagy, A. Sotrel, E.J. Manseau, L. Van de Water, and D.R. Senger, *Distribution of vascular permeability factor (vascular endothelial growth factor) in tumors: concentration in tumor blood vessels.* J Exp Med, 1991. **174**(5): p. 1275-8.

125. Carmeliet, P., *VEGF as a key mediator of angiogenesis in cancer.* Oncology, 2005. **69 Suppl 3**: p. 4-10.

126. Waltenberger, J., L. Claesson-Welsh, A. Siegbahn, M. Shibuya, and C.H. Heldin, *Different signal transduction properties of KDR and Flt1, two receptors for vascular endothelial growth factor.* J Biol Chem, 1994. **269**(43): p. 26988-95.

127. Kendall, R.L. and K.A. Thomas, *Inhibition of vascular endothelial cell growth factor activity by an endogenously encoded soluble receptor.* Proc Natl Acad Sci U S A, 1993. **90**(22): p. 10705-9.

128. Karkkainen, M.J. and T.V. Petrova, *Vascular endothelial growth factor receptors in the regulation of angiogenesis and lymphangiogenesis.* Oncogene, 2000. **19**(49): p. 5598-605.

129. Tanaka, K., S. Yamaguchi, A. Sawano, and M. Shibuya, *Characterization of the extracellular domain in vascular endothelial growth factor receptor-1 (Flt-1 tyrosine kinase).* Jpn J Cancer Res, 1997. **88**(9): p. 867-76.

130. Autiero, M., J. Waltenberger, D. Communi, A. Kranz, L. Moons, D. Lambrechts, J. Kroll, S. Plaisance, M. De Mol, F. Bono, S. Kliche, G. Fellbrich, K. Ballmer-Hofer, D. Maglione, U. Mayr-Beyrle, M. Dewerchin, S. Dombrowski, D. Stanimirovic, P. Van Hummelen, C. Dehio, D.J. Hicklin, G. Persico, J.M. Herbert, D. Communi, M. Shibuya, D. Collen, E.M. Conway, and P. Carmeliet, *Role of PlGF in the intra- and intermolecular cross talk between the VEGF receptors Flt1 and Flk1.* Nat Med, 2003. **9**(7): p. 936-43.

131. Schomber, T., L. Kopfstein, V. Djonov, I. Albrecht, V. Baeriswyl, K. Strittmatter, and G. Christofori, *Placental growth factor-1 attenuates vascular endothelial*

growth factor-A-dependent tumor angiogenesis during beta cell carcinogenesis. Cancer Res, 2007. **67**(22): p. 10840-8.

132. Ferrara, N., *Vascular endothelial growth factor as a target for anticancer therapy.* Oncologist, 2004. **9 Suppl 1**: p. 2-10.
133. Xu, H.M., J.G. Zhu, L. Gu, S.Q. Hu, and H. Wu, *VEGFR2 Expression in Head and Neck Squamous Cell Carcinoma Cancer Cells Mediates Proliferation and Invasion.* Asian Pac J Cancer Prev, 2016. **17**(4): p. 2217-21.
134. Lamalice, L., F. Houle, and J. Huot, *Phosphorylation of Tyr1214 within VEGFR-2 triggers the recruitment of Nck and activation of Fyn leading to SAPK2/p38 activation and endothelial cell migration in response to VEGF.* J Biol Chem, 2006. **281**(45): p. 34009-20.
135. Claesson-Welsh, L. and M. Welsh, *VEGFA and tumour angiogenesis.* J Intern Med, 2013. **273**(2): p. 114-27.
136. Takahashi, T., S. Yamaguchi, K. Chida, and M. Shibuya, *A single autophosphorylation site on KDR/Flk-1 is essential for VEGF-A-dependent activation of PLC-gamma and DNA synthesis in vascular endothelial cells.* EMBO J, 2001. **20**(11): p. 2768-78.
137. Jiang, B.H. and L.Z. Liu, *PI3K/PTEN signaling in angiogenesis and tumorigenesis.* Adv Cancer Res, 2009. **102**: p. 19-65.
138. Wang, X., A.M. Bove, G. Simone, and B. Ma, *Molecular Bases of VEGFR-2-Mediated Physiological Function and Pathological Role.* Front Cell Dev Biol, 2020. **8**: p. 599281.
139. Bates, D.O., *Vascular endothelial growth factors and vascular permeability.* Cardiovasc Res, 2010. **87**(2): p. 262-71.
140. Matsumoto, M., S. Roufail, R. Inder, C. Caesar, T. Karnezis, R. Shayan, R.H. Farnsworth, T. Sato, M.G. Achen, G.B. Mann, and S.A. Stacker, *Signaling for lymphangiogenesis via VEGFR-3 is required for the early events of metastasis.* Clin Exp Metastasis, 2013. **30**(6): p. 819-32.
141. Apte, R.S., D.S. Chen, and N. Ferrara, *VEGF in Signaling and Disease: Beyond Discovery and Development.* Cell, 2019. **176**(6): p. 1248-1264.

142. Uthoff, S.M., M. Duchrow, M.H.H. Schmidt, R. Broll, H.P. Bruch, M.W. Strik, and S. Galandiuk, *VEGF isoforms and mutations in human colorectal cancer.* Int J Cancer, 2002. **101**(1): p. 32-6.

143. Padro, T., R. Bieker, S. Ruiz, M. Steins, S. Retzlaff, H. Burger, T. Buchner, T. Kessler, F. Herrera, J. Kienast, C. Muller-Tidow, H. Serve, W.E. Berdel, and R.M. Mesters, *Overexpression of vascular endothelial growth factor (VEGF) and its cellular receptor KDR (VEGFR-2) in the bone marrow of patients with acute myeloid leukemia.* Leukemia, 2002. **16**(7): p. 1302-10.

144. Tsourlakis, M.C., P. Khosrawi, P. Weigand, M. Kluth, C. Hube-Magg, S. Minner, C. Koop, M. Graefen, H. Heinzer, C. Wittmer, G. Sauter, T. Krech, W. Wilczak, H. Huland, R. Simon, T. Schlomm, and S. Steurer, *VEGFR-1 overexpression identifies a small subgroup of aggressive prostate cancers in patients treated by prostatectomy.* Int J Mol Sci, 2015. **16**(4): p. 8591-606.

145. Dome, B., M.J. Hendrix, S. Paku, J. Tovari, and J. Timar, *Alternative vascularization mechanisms in cancer: Pathology and therapeutic implications.* Am J Pathol, 2007. **170**(1): p. 1-15.

146. Lugano, R., M. Ramachandran, and A. Dimberg, *Tumor angiogenesis: causes, consequences, challenges and opportunities.* Cell Mol Life Sci, 2020. **77**(9): p. 1745-1770.

147. Ausprunk, D.H. and J. Folkman, *Migration and proliferation of endothelial cells in preformed and newly formed blood vessels during tumor angiogenesis.* Microvasc Res, 1977. **14**(1): p. 53-65.

148. Paku, S. and N. Paweletz, *First steps of tumor-related angiogenesis.* Lab Invest, 1991. **65**(3): p. 334-46.

149. Paku, S., K. Dezso, E. Bugyik, J. Tovari, J. Timar, P. Nagy, V. Laszlo, W. Klepetko, and B. Dome, *A new mechanism for pillar formation during tumor-induced intussusceptive angiogenesis: inverse sprouting.* Am J Pathol, 2011. **179**(3): p. 1573-85.

150. Hlushchuk, R., O. Riesterer, O. Baum, J. Wood, G. Gruber, M. Pruschy, and V. Djonov, *Tumor recovery by angiogenic switch from sprouting to intussusceptive angiogenesis after treatment with PTK787/ZK222584 or ionizing radiation.* Am J Pathol, 2008. **173**(4): p. 1173-85.

151. Semela, D., A.C. Piguet, M. Kolev, K. Schmitter, R. Hlushchuk, V. Djonov, C. Stoupis, and J.F. Dufour, *Vascular remodeling and antitumoral effects of mTOR inhibition in a rat model of hepatocellular carcinoma.* J Hepatol, 2007. **46**(5): p. 840-8.

152. Ribatti, D., *Tumor refractoriness to anti-VEGF therapy.* Oncotarget, 2016. **7**(29): p. 46668-46677.

153. Gianni-Barrera, R., M. Trani, C. Fontanellaz, M. Heberer, V. Djonov, R. Hlushchuk, and A. Banfi, *VEGF over-expression in skeletal muscle induces angiogenesis by intussusception rather than sprouting.* Angiogenesis, 2013. **16**(1): p. 123-36.

154. Rada, M., A. Lazaris, A. Kapelanski-Lamoureux, T.Z. Mayer, and P. Metrakos, *Tumor microenvironment conditions that favor vessel co-option in colorectal cancer liver metastases: A theoretical model.* Semin Cancer Biol, 2021. **71**: p. 52-64.

155. Kuczynski, E.A., P.B. Vermeulen, F. Pezzella, R.S. Kerbel, and A.R. Reynolds, *Vessel co-option in cancer.* Nat Rev Clin Oncol, 2019. **16**(8): p. 469-493.

156. Donnem, T., A.R. Reynolds, E.A. Kuczynski, K. Gatter, P.B. Vermeulen, R.S. Kerbel, A.L. Harris, and F. Pezzella, *Non-angiogenic tumours and their influence on cancer biology.* Nat Rev Cancer, 2018. **18**(5): p. 323-336.

157. Maniotis, A.J., R. Folberg, A. Hess, E.A. Seftor, L.M. Gardner, J. Pe'er, J.M. Trent, P.S. Meltzer, and M.J. Hendrix, *Vascular channel formation by human melanoma cells in vivo and in vitro: vasculogenic mimicry.* Am J Pathol, 1999. **155**(3): p. 739-52.

158. Kotiyal, S. and S. Bhattacharya, *Epithelial Mesenchymal Transition and Vascular Mimicry in Breast Cancer Stem Cells.* Crit Rev Eukaryot Gene Expr, 2015. **25**(3): p. 269-80.

159. Wesseling, P., J.A. van der Laak, M. Link, H.L. Teepen, and D.J. Ruiter, *Quantitative analysis of microvascular changes in diffuse astrocytic neoplasms with increasing grade of malignancy.* Hum Pathol, 1998. **29**(4): p. 352-8.

160. Dome, B., J. Timar, and S. Paku, *A novel concept of glomeruloid body formation in experimental cerebral metastases.* J Neuropathol Exp Neurol, 2003. **62**(6): p. 655-61.

161. Sundberg, C., J.A. Nagy, L.F. Brown, D. Feng, I.A. Eckelhoefer, E.J. Manseau, A.M. Dvorak, and H.F. Dvorak, *Glomeruloid microvascular proliferation follows adenoviral vascular permeability factor/vascular endothelial growth factor-164 gene delivery.* Am J Pathol, 2001. **158**(3): p. 1145-60.

162. Straume, O., P.O. Chappuis, H.B. Salvesen, O.J. Halvorsen, S.A. Haukaas, J.R. Goffin, L.R. Begin, W.D. Foulkes, and L.A. Akslen, *Prognostic importance of glomeruloid microvascular proliferation indicates an aggressive angiogenic phenotype in human cancers.* Cancer Res, 2002. **62**(23): p. 6808-11.

163. Asahara, T., T. Takahashi, H. Masuda, C. Kalka, D. Chen, H. Iwaguro, Y. Inai, M. Silver, and J.M. Isner, *VEGF contributes to postnatal neovascularization by mobilizing bone marrow-derived endothelial progenitor cells.* EMBO J, 1999. **18**(14): p. 3964-72.

164. Benjamin, L.E., D. Golijanin, A. Itin, D. Pode, and E. Keshet, *Selective ablation of immature blood vessels in established human tumors follows vascular endothelial growth factor withdrawal.* J Clin Invest, 1999. **103**(2): p. 159-65.

165. Hurwitz, H., L. Fehrenbacher, W. Novotny, T. Cartwright, J. Hainsworth, W. Heim, J. Berlin, A. Baron, S. Griffing, E. Holmgren, N. Ferrara, G. Fyfe, B. Rogers, R. Ross, and F. Kabbinavar, *Bevacizumab plus irinotecan, fluorouracil, and leucovorin for metastatic colorectal cancer.* N Engl J Med, 2004. **350**(23): p. 2335-42.

166. Hilberg, F., G.J. Roth, M. Krssak, S. Kautschitsch, W. Sommergruber, U. Tontsch-Grunt, P. Garin-Chesa, G. Bader, A. Zoephel, J. Quant, A. Heckel, and W.J. Rettig, *BIBF 1120: triple angiokinase inhibitor with sustained receptor blockade and good antitumor efficacy.* Cancer Res, 2008. **68**(12): p. 4774-82.

167. Popat, S., A. Mellemgaard, K. Fahrbach, A. Martin, M. Rizzo, R. Kaiser, I. Griebsch, and M. Reck, *Nintedanib plus docetaxel as second-line therapy in patients with non-small-cell lung cancer: a network meta-analysis.* Future Oncol, 2015. **11**(3): p. 409-20.

168. Richeldi, L., R.M. du Bois, G. Raghu, A. Azuma, K.K. Brown, U. Costabel, V. Cottin, K.R. Flaherty, D.M. Hansell, Y. Inoue, D.S. Kim, M. Kolb, A.G. Nicholson, P.W. Noble, M. Selman, H. Taniguchi, M. Brun, F. Le Maulf, M. Girard, S. Stowasser, R. Schlenker-Herceg, B. Disse, H.R. Collard, and I.T.

Investigators, *Efficacy and safety of nintedanib in idiopathic pulmonary fibrosis.* N Engl J Med, 2014. **370**(22): p. 2071-82.

169. Jain, R.K., *Normalizing tumor vasculature with anti-angiogenic therapy: a new paradigm for combination therapy.* Nat Med, 2001. **7**(9): p. 987-9.

170. Li, S., Q. Zhang, and Y. Hong, *Tumor Vessel Normalization: A Window to Enhancing Cancer Immunotherapy.* Technol Cancer Res Treat, 2020. **19**: p. 1533033820980116.

171. Jayson, G.C., D.J. Hicklin, and L.M. Ellis, *Antiangiogenic therapy--evolving view based on clinical trial results.* Nat Rev Clin Oncol, 2012. **9**(5): p. 297-303.

172. Mazzone, M., D. Dettori, R.L. de Oliveira, S. Loges, T. Schmidt, B. Jonckx, Y.M. Tian, A.A. Lanahan, P. Pollard, C.R. de Almodovar, F. De Smet, S. Vinckier, J. Aragones, K. Debackere, A. Luttun, S. Wyns, B. Jordan, A. Pisacane, B. Gallez, M.G. Lampugnani, E. Dejana, M. Simons, P. Ratcliffe, P. Maxwell, and P. Carmeliet, *Heterozygous deficiency of PHD2 restores tumor oxygenation and inhibits metastasis via endothelial normalization.* Cell, 2009. **136**(5): p. 839-851.

173. Nowak, A.K., S. Brosseau, A. Cook, and G. Zalcman, *Antiangiogeneic Strategies in Mesothelioma.* Front Oncol, 2020. **10**: p. 126.

174. Ohta, Y., V. Shridhar, R.K. Bright, G.P. Kalemkerian, W. Du, M. Carbone, Y. Watanabe, and H.I. Pass, *VEGF and VEGF type C play an important role in angiogenesis and lymphangiogenesis in human malignant mesothelioma tumours.* Br J Cancer, 1999. **81**(1): p. 54-61.

175. Yasumitsu, A., C. Tabata, R. Tabata, N. Hirayama, A. Murakami, S. Yamada, T. Terada, S. Iida, K. Tamura, K. Fukuoka, K. Kuribayashi, and T. Nakano, *Clinical significance of serum vascular endothelial growth factor in malignant pleural mesothelioma.* J Thorac Oncol, 2010. **5**(4): p. 479-83.

176. Kumar-Singh, S., P.B. Vermeulen, J. Weyler, K. Segers, B. Weyn, A. Van Daele, L.Y. Dirix, A.T. Van Oosterom, and E. Van Marck, *Evaluation of tumour angiogenesis as a prognostic marker in malignant mesothelioma.* J Pathol, 1997. **182**(2): p. 211-6.

177. Langerak, A.W., P.A. De Laat, C.A. Van Der Linden-Van Beurden, M. Delahaye, T.H. Van Der Kwast, H.C. Hoogsteden, R. Benner, and M.A. Versnel, *Expression*

of platelet-derived growth factor (PDGF) and PDGF receptors in human malignant mesothelioma in vitro and in vivo. J Pathol, 1996. **178**(2): p. 151-60.

178. Honda, M., T. Kanno, Y. Fujita, A. Gotoh, T. Nakano, and T. Nishizaki, *Mesothelioma cell proliferation through autocrine activation of PDGF-betabeta receptor.* Cell Physiol Biochem, 2012. **29**(5-6): p. 667-74.
179. Schelch, K., M.A. Hoda, T. Klikovits, J. Munzker, B. Ghanim, C. Wagner, T. Garay, V. Laszlo, U. Setinek, B. Dome, M. Filipits, C. Pirker, P. Heffeter, E. Selzer, J. Tovari, S. Torok, I. Kenessey, K. Holzmann, B. Grasl-Kraupp, B. Marian, W. Klepetko, W. Berger, B. Hegedus, and M. Grusch, *Fibroblast growth factor receptor inhibition is active against mesothelioma and synergizes with radio- and chemotherapy.* Am J Respir Crit Care Med, 2014. **190**(7): p. 763-72.
180. Kumar-Singh, S., J. Weyler, M.J. Martin, P.B. Vermeulen, and E. Van Marck, *Angiogenic cytokines in mesothelioma: a study of VEGF, FGF-1 and -2, and TGF beta expression.* J Pathol, 1999. **189**(1): p. 72-8.
181. Edwards, J.G., G. Cox, A. Andi, J.L. Jones, R.A. Walker, D.A. Waller, and K.J. O'Byrne, *Angiogenesis is an independent prognostic factor in malignant mesothelioma.* Br J Cancer, 2001. **85**(6): p. 863-8.
182. Robinson, B.W., A.W. Musk, and R.A. Lake, *Malignant mesothelioma.* Lancet, 2005. **366**(9483): p. 397-408.
183. Goel, S., D.G. Duda, L. Xu, L.L. Munn, Y. Boucher, D. Fukumura, and R.K. Jain, *Normalization of the vasculature for treatment of cancer and other diseases.* Physiol Rev, 2011. **91**(3): p. 1071-121.
184. Haas, G., S. Fan, M. Ghadimi, T. De Oliveira, and L.C. Conradi, *Different Forms of Tumor Vascularization and Their Clinical Implications Focusing on Vessel Co-option in Colorectal Cancer Liver Metastases.* Front Cell Dev Biol, 2021. **9**: p. 612774.
185. Percie du Sert, N., V. Hurst, A. Ahluwalia, S. Alam, M.T. Avey, M. Baker, W.J. Browne, A. Clark, I.C. Cuthill, U. Dirnagl, M. Emerson, P. Garner, S.T. Holgate, D.W. Howells, N.A. Karp, S.E. Lazic, K. Lidster, C.J. MacCallum, M. Macleod, E.J. Pearl, O.H. Petersen, F. Rawle, P. Reynolds, K. Rooney, E.S. Sena, S.D. Silberberg, T. Steckler, and H. Wurbel, *The ARRIVE guidelines 2.0: Updated guidelines for reporting animal research.* PLoS Biol, 2020. **18**(7): p. e3000410.

186. Helm, C.L., M.E. Fleury, A.H. Zisch, F. Boschetti, and M.A. Swartz, *Synergy between interstitial flow and VEGF directs capillary morphogenesis in vitro through a gradient amplification mechanism.* Proc Natl Acad Sci U S A, 2005. **102**(44): p. 15779-84.

187. Gulyas, M., M. Csiszer, E. Mehes, and A. Czirok, *Software tools for cell culture-related 3D printed structures.* PLoS One, 2018. **13**(9): p. e0203203.

188. Davis, G.E. and C.W. Camarillo, *An alpha 2 beta 1 integrin-dependent pinocytic mechanism involving intracellular vacuole formation and coalescence regulates capillary lumen and tube formation in three-dimensional collagen matrix.* Exp Cell Res, 1996. **224**(1): p. 39-51.

189. Sholl, D.A., *Dendritic organization in the neurons of the visual and motor cortices of the cat.* J Anat, 1953. **87**(4): p. 387-406.

190. Mehes, E., M. Barath, M. Gulyas, E. Bugyik, M. Geiszt, A. Szoor, A. Lanyi, and A. Czirok, *Enhanced endothelial motility and multicellular sprouting is mediated by the scaffold protein TKS4.* Sci Rep, 2019. **9**(1): p. 14363.

191. Schneider, C.A., W.S. Rasband, and K.W. Eliceiri, *NIH Image to ImageJ: 25 years of image analysis.* Nat Methods, 2012. **9**(7): p. 671-5.

192. Livak, K.J. and T.D. Schmittgen, *Analysis of relative gene expression data using real-time quantitative PCR and the 2(-Delta Delta C(T)) Method.* Methods, 2001. **25**(4): p. 402-8.

193. Mathieu, V., C. Pirker, W.M. Schmidt, S. Spiegl-Kreinecker, D. Lotsch, P. Heffeter, B. Hegedus, M. Grusch, R. Kiss, and W. Berger, *Aggressiveness of human melanoma xenograft models is promoted by aneuploidy-driven gene expression deregulation.* Oncotarget, 2012. **3**(4): p. 399-413.

194. Rozsas, A., J. Berta, L. Rojko, L.Z. Horvath, M. Keszthelyi, I. Kenessey, V. Laszlo, W. Berger, M. Grusch, M.A. Hoda, S. Torok, W. Klepetko, F. Renyi-Vamos, B. Hegedus, B. Dome, and J. Tovari, *Erythropoietin receptor expression is a potential prognostic factor in human lung adenocarcinoma.* PLoS One, 2013. **8**(10): p. e77459.

195. Chou, T.C., *Drug combination studies and their synergy quantification using the Chou-Talalay method.* Cancer Res, 2010. **70**(2): p. 440-6.

196. Garay, T., E. Juhasz, E. Molnar, M. Eisenbauer, A. Czirok, B. Dekan, V. Laszlo, M.A. Hoda, B. Dome, J. Timar, W. Klepetko, W. Berger, and B. Hegedus, *Cell migration or cytokinesis and proliferation?--revisiting the "go or grow" hypothesis in cancer cells in vitro.* Exp Cell Res, 2013. **319**(20): p. 3094-103.

197. Torok, S., M. Rezeli, O. Kelemen, A. Vegvari, K. Watanabe, Y. Sugihara, A. Tisza, T. Marton, I. Kovacs, J. Tovari, V. Laszlo, T.H. Helbich, B. Hegedus, T. Klikovits, M.A. Hoda, W. Klepetko, S. Paku, G. Marko-Varga, and B. Dome, *Limited Tumor Tissue Drug Penetration Contributes to Primary Resistance against Angiogenesis Inhibitors.* Theranostics, 2017. **7**(2): p. 400-412.

198. Yang, F., X. Tang, E. Riquelme, C. Behrens, M.B. Nilsson, U. Giri, M. Varella-Garcia, L.A. Byers, H.Y. Lin, J. Wang, M.G. Raso, L. Girard, K. Coombes, J.J. Lee, R.S. Herbst, J.D. Minna, J.V. Heymach, and Wistuba, II, *Increased VEGFR-2 gene copy is associated with chemoresistance and shorter survival in patients with non-small-cell lung carcinoma who receive adjuvant chemotherapy.* Cancer Res, 2011. **71**(16): p. 5512-21.

199. Meng, F., C.L. Speyer, B. Zhang, Y. Zhao, W. Chen, D.H. Gorski, F.R. Miller, and G. Wu, *PDGFRalpha and beta play critical roles in mediating Foxq1-driven breast cancer stemness and chemoresistance.* Cancer Res, 2015. **75**(3): p. 584-93.

200. Turner, N. and R. Grose, *Fibroblast growth factor signalling: from development to cancer.* Nat Rev Cancer, 2010. **10**(2): p. 116-29.

201. Seastedt, K.P., N. Pruett, and C.D. Hoang, *Mouse models for mesothelioma drug discovery and development.* Expert Opin Drug Discov, 2021. **16**(6): p. 697-708.

202. Brcic, L. and I. Kern, *Clinical significance of histologic subtyping of malignant pleural mesothelioma.* Transl Lung Cancer Res, 2020. **9**(3): p. 924-933.

203. Baluk, P., C.G. Lee, H. Link, E. Ator, A. Haskell, J.A. Elias, and D.M. McDonald, *Regulated angiogenesis and vascular regression in mice overexpressing vascular endothelial growth factor in airways.* Am J Pathol, 2004. **165**(4): p. 1071-85.

204. Roberts, W.G. and G.E. Palade, *Increased microvascular permeability and endothelial fenestration induced by vascular endothelial growth factor.* J Cell Sci, 1995. **108 (Pt 6)**: p. 2369-79.

205. Roberts, W.G. and G.E. Palade, *Neovasculature induced by vascular endothelial growth factor is fenestrated.* Cancer Res, 1997. **57**(4): p. 765-72.

206. Esser, S., K. Wolburg, H. Wolburg, G. Breier, T. Kurzchalia, and W. Risau, *Vascular endothelial growth factor induces endothelial fenestrations in vitro.* J Cell Biol, 1998. **140**(4): p. 947-59.
207. Batra, H. and V.B. Antony, *The pleural mesothelium in development and disease.* Front Physiol, 2014. **5**: p. 284.
208. Mutsaers, S.E. and S. Wilkosz, *Structure and function of mesothelial cells.* Cancer Treat Res, 2007. **134**: p. 1-19.
209. Wang, N.S., *Anatomy of the pleura.* Clin Chest Med, 1998. **19**(2): p. 229-40.
210. Scarpa, S., A. Giuffrida, M. Fazi, A. Coletti, C. Palumbo, H.I. Pass, A. Procopio, and A. Modesti, *Migration of mesothelioma cells correlates with histotype-specific synthesis of extracellular matrix.* Int J Mol Med, 1999. **4**(1): p. 67-71.
211. Abayasiriwardana, K.S., M.K. Wood, C.M. Prele, K.A. Birnie, B.W. Robinson, G.J. Laurent, R.J. McAnulty, and S.E. Mutsaers, *Inhibition of collagen production delays malignant mesothelioma tumor growth in a murine model.* Biochem Biophys Res Commun, 2019. **510**(2): p. 198-204.
212. Tarnoki-Zach, J., P. Stockhammer, D.G. Isai, E. Mehes, B. Szeder, I. Kovacs, E. Bugyik, S. Paku, W. Berger, S.M. Thomas, Z. Neufeld, B. Dome, B. Hegedus, and A. Czirok, *Multicellular contractility contributes to the emergence of mesothelioma nodules.* Sci Rep, 2020. **10**(1): p. 20114.
213. Bugyik, E., V. Szabo, K. Dezso, A. Rokusz, A. Szucs, P. Nagy, J. Tovari, V. Laszlo, B. Dome, and S. Paku, *Role of (myo)fibroblasts in the development of vascular and connective tissue structure of the C38 colorectal cancer in mice.* Cancer Commun (Lond), 2018. **38**(1): p. 46.
214. van Dam, P.J., E.P. van der Stok, L.A. Teuwen, G.G. Van den Eynden, M. Illemann, S. Frentzas, A.W. Majeed, R.L. Eefsen, R.R.J. Coebergh van den Braak, A. Lazaris, M.C. Fernandez, B. Galjart, O.D. Laerum, R. Rayes, D.J. Grunhagen, M. Van de Paer, Y. Sucaet, H.S. Mudhar, M. Schvimer, H. Nystrom, M. Kockx, N.C. Bird, F. Vidal-Vanaclocha, P. Metrakos, E. Simoneau, C. Verhoef, L.Y. Dirix, S. Van Laere, Z.H. Gao, P. Brodt, A.R. Reynolds, and P.B. Vermeulen, *International consensus guidelines for scoring the histopathological growth patterns of liver metastasis.* Br J Cancer, 2017. **117**(10): p. 1427-1441.

215. Carmeliet, P. and R.K. Jain, *Molecular mechanisms and clinical applications of angiogenesis.* Nature, 2011. **473**(7347): p. 298-307.
216. Kliche, S. and J. Waltenberger, *VEGF receptor signaling and endothelial function.* IUBMB Life, 2001. **52**(1-2): p. 61-6.
217. Meadows, K.L. and H.I. Hurwitz, *Anti-VEGF therapies in the clinic.* Cold Spring Harb Perspect Med, 2012. **2**(10).
218. Tsao, A.S., J. Miao, Wistuba, II, N.J. Vogelzang, J.V. Heymach, F.V. Fossella, C. Lu, M.R. Velasco, B. Box-Noriega, J.G. Hueftle, S. Gadgeel, M.W. Redman, D.R. Gandara, and K. Kelly, *Phase II Trial of Cediranib in Combination With Cisplatin and Pemetrexed in Chemotherapy-Naive Patients With Unresectable Malignant Pleural Mesothelioma (SWOG S0905).* J Clin Oncol, 2019. **37**(28): p. 2537-2547.
219. Marek, L.A., T.K. Hinz, A. von Massenhausen, K.A. Olszewski, E.K. Kleczko, D. Boehm, M.C. Weiser-Evans, R.A. Nemenoff, H. Hoffmann, A. Warth, J.M. Gozgit, S. Perner, and L.E. Heasley, *Nonamplified FGFR1 is a growth driver in malignant pleural mesothelioma.* Mol Cancer Res, 2014. **12**(10): p. 1460-9.
220. Strizzi, L., A. Catalano, G. Vianale, S. Orecchia, A. Casalini, G. Tassi, R. Puntoni, L. Mutti, and A. Procopio, *Vascular endothelial growth factor is an autocrine growth factor in human malignant mesothelioma.* J Pathol, 2001. **193**(4): p. 468-75.
221. Awasthi, N., S. Hinz, R.A. Brekken, M.A. Schwarz, and R.E. Schwarz, *Nintedanib, a triple angiokinase inhibitor, enhances cytotoxic therapy response in pancreatic cancer.* Cancer Lett, 2015. **358**(1): p. 59-66.
222. Wollin, L., E. Wex, A. Pautsch, G. Schnapp, K.E. Hostettler, S. Stowasser, and M. Kolb, *Mode of action of nintedanib in the treatment of idiopathic pulmonary fibrosis.* Eur Respir J, 2015. **45**(5): p. 1434-45.
223. Andre, F. and J. Cortes, *Rationale for targeting fibroblast growth factor receptor signaling in breast cancer.* Breast Cancer Res Treat, 2015. **150**(1): p. 1-8.
224. Abu-Hijleh, M.F., O.A. Habbal, and S.T. Moqattash, *The role of the diaphragm in lymphatic absorption from the peritoneal cavity.* J Anat, 1995. **186 (Pt 3)**: p. 453-67.
225. Shinohara, H., *Lymphatic system of the mouse diaphragm: morphology and function of the lymphatic sieve.* Anat Rec, 1997. **249**(1): p. 6-15.

226. Kindler, H.L., N. Ismaila, S.G. Armato, 3rd, R. Bueno, M. Hesdorffer, T. Jahan, C.M. Jones, M. Miettinen, H. Pass, A. Rimner, V. Rusch, D. Sterman, A. Thomas, and R. Hassan, *Treatment of Malignant Pleural Mesothelioma: American Society of Clinical Oncology Clinical Practice Guideline.* J Clin Oncol, 2018: p. JCO2017766394.

227. Jayson, G.C., R. Kerbel, L.M. Ellis, and A.L. Harris, *Antiangiogenic therapy in oncology: current status and future directions.* Lancet, 2016. **388**(10043): p. 518-29.

228. Grosso, F., N. Steele, S. Novello, A.K. Nowak, S. Popat, L. Greillier, T. John, N.B. Leighl, M. Reck, P. Taylor, D. Planchard, J.B. Sorensen, M.A. Socinski, U. von Wangenheim, A.B. Loembe, J. Barrueco, N. Morsli, and G. Scagliotti, *Nintedanib Plus Pemetrexed/Cisplatin in Patients With Malignant Pleural Mesothelioma: Phase II Results From the Randomized, Placebo-Controlled LUME-Meso Trial.* J Clin Oncol, 2017. **35**(31): p. 3591-3600.

229. Kutluk Cenik, B., K.T. Ostapoff, D.E. Gerber, and R.A. Brekken, *BIBF 1120 (nintedanib), a triple angiokinase inhibitor, induces hypoxia but not EMT and blocks progression of preclinical models of lung and pancreatic cancer.* Mol Cancer Ther, 2013. **12**(6): p. 992-1001.

230. Ackermann M., H.F., Konerding M.A., *Nintedanib inhibits tumor and vessel growth and leads to vascular normalization in A549-NSCLC-xenografts [abstract]*, in *Mol Cancer Ther*. 2015: Proceedings of the AACR Special Conference: Tumor Angiogenesis and Vascular Normalization: Bench to Bedside to Biomarkers; Mar 5-8, 2015; Orlando, FL. Philadelphia (PA): AACR; . p. Suppl. 1 Abstract nr B09.

231. Ackermann, M., Y.O. Kim, W.L. Wagner, D. Schuppan, C.D. Valenzuela, S.J. Mentzer, S. Kreuz, D. Stiller, L. Wollin, and M.A. Konerding, *Effects of nintedanib on the microvascular architecture in a lung fibrosis model.* Angiogenesis, 2017.

232. Goel, S., A.H. Wong, and R.K. Jain, *Vascular normalization as a therapeutic strategy for malignant and nonmalignant disease.* Cold Spring Harb Perspect Med, 2012. **2**(3): p. a006486.

233. Van der Veldt, A.A., M. Lubberink, I. Bahce, M. Walraven, M.P. de Boer, H.N. Greuter, N.H. Hendrikse, J. Eriksson, A.D. Windhorst, P.E. Postmus, H.M. Verheul, E.H. Serne, A.A. Lammertsma, and E.F. Smit, *Rapid decrease in delivery of chemotherapy to tumors after anti-VEGF therapy: implications for scheduling of anti-angiogenic drugs.* Cancer Cell, 2012. **21**(1): p. 82-91.

234. Irvin, C.G. and J.H. Bates, *Measuring the lung function in the mouse: the challenge of size.* Respir Res, 2003. **4**(1): p. 4.

235. Shinohara, H., *Distribution of lymphatic stomata on the pleural surface of the thoracic cavity and the surface topography of the pleural mesothelium in the golden hamster.* Anat Rec, 1997. **249**(1): p. 16-23.

236. Blanquart, C., M.-C. Jaurand, and D. Jean, *The Biology of Malignant Mesothelioma and the Relevance of Preclinical Models.* Frontiers in oncology, 2020. **10**: p. 388-388.

237. Liu, K., P.A. Newbury, B.S. Glicksberg, W.Z.D. Zeng, S. Paithankar, E.R. Andrechek, and B. Chen, *Evaluating cell lines as models for metastatic breast cancer through integrative analysis of genomic data.* Nat Commun, 2019. **10**(1): p. 2138.

238. Blanquart, C., M.C. Jaurand, and D. Jean, *The Biology of Malignant Mesothelioma and the Relevance of Preclinical Models.* Front Oncol, 2020. **10**: p. 388.

239. Pulford, E., A. Hocking, K. Griggs, J. McEvoy, C. Bonder, D.W. Henderson, and S. Klebe, *Vasculogenic mimicry in malignant mesothelioma: an experimental and immunohistochemical analysis.* Pathology, 2016. **48**(7): p. 650-659.

9. Bibliography of the candidate's publications

(Cumulative impact factor: 70.906)

9.1. List of publications that served as a basis for the current thesis

1. Kovacs I, Bugyik E, Dezso K, Tarnoki-Zach J, Mehes E, Gulyas M, Czirok A, Lang E, Grusch M, Schelch K, Hegedus B, Horvath I, Barany N, Megyesfalvi Z, Tisza A, Lohinai Z, Hoda MA, Hoetzenecker K, Pezzella F, Paku S, Laszlo V, Dome B. (2022) **Malignant pleural mesothelioma nodules remodel their surroundings to vascularize and grow** *Translational Lung Cancer Research*, 11(6), 991–1008. DOI: 10.21037/tlcr-21-828 IF: 4.0

2. Laszlo V, Valko Z, Kovacs I, Ozsvar J, Hoda MA, Klikovits T, Lakatos D, Czirók A, Garay T, Stiglbauer A, Helbich TH, Groger M, Tovari J, Klepetko W, Pirker C, Grusch M, Berger W, Hilberg F, Hegedus B, Dome B. (2018) **Nintedanib is active in malignant pleural mesothelioma cell models and inhibits angiogenesis and tumor growth in vivo** *Clinical Cancer Research*, 24(15): p. 3729-3740 DOI: 10.1158/1078-0432.CCR-17-1507. IF: 8.911

9.2. Other publications

2023

3. Valko Z, Megyesfalvi Z, Schwendenwein A, Lang C, Paku S, Barany N, Ferencz B, Horvath-Rozsas A, Kovacs I, Schlegl E, Pozonec V, Boettiger K, Rezeli M, Marko-Varga Gy, Renyi-Vamos F, Hoda MA, Klikovits T, Hoetzenecker K, Grusch M, Laszlo V, Dome B, & Schelch K. (2023) **Dual targeting of BCL-2 and MCL-1 in the presence of BAX breaks venetoclax resistance in human small cell lung cancer** *British Journal of Cancer,* 128, 1850–1861 DOI: 10.1038/s41416-023-02219-9 IF: 8.8

2021

4. Berta J, Torok S, Tarnoki-Zach J, Drozdovszky O, Tovari J, Paku S, Kovacs I, Czirok A, Masri B, Megyesfalvi Z, Oskolas H, Malm J, Ingvar C, Marko-Varga G, Dome B, Laszlo V. (2021) **Apelin promotes blood and lymph vessel formation and the growth of melanoma lung metastasis** *Scientific Reports,* 11(1): p. 5798 DOI: 10.1038/s41598-021-85162-0 IF: 4.997

5. Hegedus L, Okumus O, Livingstone E, Baranyi M, Kovacs I, Dome B, Tovari J, Bankfalvi A, Schadendorf D, Aigner C, Hegedus B. (2021) **Allosteric and ATP-Competitive MEK-Inhibition in a Novel Spitzoid Melanoma Model with a RAF- and Phosphorylation-Independent Mutation** *Cancers (Basel),* 13(4). DOI: 10.3390/cancers13040829 IF: 6.575

2020

6. Bilecz A, Stockhammer P, Theegarten D, Kern I, Jakopovic M, Samarzija M, Klikovits T, Hoda MA, Dome B, Oberndorfer F, Muellauer L, Fillinger J, Kovacs I, Pirker C, Schuler M, Plones T, Aigner C, Klepetko W, Berger W, Brcic L, Laszlo L, Hegedus B. (2020) **Comparative analysis of prognostic histopathologic parameters in subtypes of epithelioid pleural mesothelioma** *Histopathology*, 77(1): p. 55-66. DOI: 10.1111/his.14105 IF: 5.087

7. Hegedus L, Rittler D, Garay T, Stockhammer P, Kovacs I, Dome B, Theurer S, Hager T, Herold T, Kalbourtzis S, Bankfalvi A, Schmid KW, Fuhrer D, Aigner C, Hegedus B. (2020) **HDAC Inhibition Induces PD-L1 Expression in a Novel Anaplastic**

Thyroid Cancer Cell Lin *Pathology Oncology Research,* 26(4): p. 2523-2535. DOI: 10.1007/s12253-020-00834-y. IF: 3.201

8. Tarnoki-Zach J, Stockhammer P, Isai DG, Mehes E, Szeder B, Kovacs I, Bugyik E, Paku S, Berger W, Thomas SM, Neufeld Z, Dome B, Hegedus B, Czirok A, (2020) **Multicellular contractility contributes to the emergence of mesothelioma nodules** *Scientific Reports,* 10(1): p. 20114. DOI: 10.1038/s41598-020-76641-x IF: 4.380

2019

9. Laszlo V, Valko Z, Ozsvar J, Kovacs I, Garay T, Hoda MA, Klikovits T, Stockhammer P, Aigner C, Gröger M, Klepetko W, BergerW, Grusch M, TovariJ, Waizenegger IC, Dome B, Hegedus B. (2019) **The FAK inhibitor BI853520 inhibits spheroid formation and orthotopic tumor growth in malignant pleural mesothelioma** *Journal of Molecular Medicine,* 97:231–242 DOI: 10.1007/s00109-018-1725-7 IF: 4.427

2017

10. Torok S, Rezeli M, Kelemen O, Vegvari A, Watanabe K, Sugihara Y, Tisza A, Marton T, Kovacs I, Tovari J, Laszlo V, Helbich TH, Hegedus B, Klikovits T, Hoda MA, Klepetko W, Paku S, Marko-Varga G, Dome B. (2017) **Limited Tumor Tissue Drug Penetration Contributes To Primary Resistance Against Angiogenesis Inhibitors.** *Theranostics*, 7(2):400-412. DOI: 10.7150/thno.16767 IF: 8.537

2016

11. Zinngrebe J, Rieser E, Taraborrelli L, Peltzer N, Hartwig T, Ren H, Kovacs I, Endres C, Draber P, Darding M, von Karstedt S, Lemke J, Dome B, Bergmann M, Ferguson BJ, Walczak H. (2016) **--LUBAC deficiency perturbs TLR3 signaling to cause immunodeficiency and autoinflammation** *Journal of Experimental Medicine,* 213(12): p. 2671-2689. DOI: 10.1084/jem.20160041. IF: 11.991

12. Moldvay J, Hegedűs B, Kovács I, Döme B. (2016) **A mesothelioma korszerű kezelése** *KLINIKAI ONKOLÓGIA,* 3:(1) pp. 19-28. IF: 0

10. Acknowledgements

Over the past few years, I have had the opportunity to participate in several research studies in renowned laboratories in Hungary and Europe: the National Korányi Institute of Pulmonology; the Department of Experimental Pharmacology of the National Institute of Oncology; the 1st- and the 2nd Department of Pathology of the Semmelweis University; the Translational Thoracic Oncology lab in the Department of Thoracic Surgery of the Medical University of Vienna; the Department of Biomedical Engineering of Lund University and the Department of Biological Physics of Eötvös Loránd University. During these visits I've met a lot of inspiring and bright people who helped me in my PhD work and influenced me to be a better researcher. It would be impossible to list all their names here, but I'm very grateful to all of them!

I would especially like to thank my supervisor, Balázs Döme, who provided me with many opportunities to learn and always pushed me forward to progress. Also, to Zsolt Megyesfalvi, for all the useful advices he gave me, for the encouragement, and for reviewing my work.

I'm extremely grateful to Balázs Hegedűs, József Tóvári, Sándor Paku, and Katalin Dezső for all their guidance, their time, and for the opportunities to participate in their research projects.

I would like to thank Viktória László for allowing me to take part in the preclinical testing of nintedanib, which eventually became the basis for this PhD thesis.

I'm genuinely grateful to my colleagues, Erzsébet Schlegl, Erzsébet Nagy, Szilvia Török, Judit Berta, Edina Bugyik, Anna Tisza, Anita Rózsás, Anita Hidvégi and Violetta Lénert for their much-much appreciated support and friendship. I know I can always count on them!

I also would like to show my gratitude towards my entire family. A special thanks to my son Vince, who was always very enthusiastic to "help" me in the writing of this thesis, and to my husband Ádám, who actually helped me by keeping Vince busy. Without him, this work could not have been finished.